PERFORMANCE ANALYSIS OF RELAY ASSISTED CONVERGENT FREE SPACE OPTICAL - UNDERWATER WIRELESS OPTICAL COMMUNICATION SYSTEM

Thesis

Submitted in partial fulfillment of the requirements for the degree of

DOCTOR OF PHILOSOPHY

by

L BHARGAVA KUMAR

DEPARTMENT OF ELECTRONICS & COMMUNICATION ENGINEERING

NATIONAL INSTITUTE OF TECHNOLOGY KARNATAKA

SURATHKAL, MANGALORE - 575025

DECEMBER 2022

DECLARATION

I hereby *declare* that the Research Thesis entitled **PERFORMANCE ANAL-YSIS OF RELAY ASSISTED CONVERGENT FREE SPACE OPTICAL - UNDERWATER WIRELESS OPTICAL COMMUNICATION SYSTEM** which is being submitted to the *National Institute of Technology Karnataka, Surathkal* in partial fulfillment of the requirement for the award of the Degree of *Doctor of Philosophy* in **Department of Electronics and Communication Engineering** is a *bonafide report of the research work carried out by me*. The material contained in this Research Thesis has not been submitted to any University or Institution for the award of any degree.

L BHARGAVA KUMAR
Reg. No. 187109/187EC015
Department of ECE.

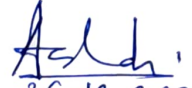Place: NITK, Surathkal.
Date: 22.12.2022

3

CERTIFICATE

This is to certify that the Research Thesis entitled **PERFORMANCE ANAL-YSIS OF RELAY ASSISTED CONVERGENT FREE SPACE OPTICAL - UNDERWATER WIRELESS OPTICAL COMMUNICATION SYSTEM** submitted by **Mr. L BHARGAVA KUMAR** (Register Number: 187109/187EC015) as the record of the research work carried out by him, is accepted as the *Research Thesis submission* in partial fulfillment of the requirements for the award of degree of **Doctor of Philosophy.**

Research Guide

(Dr. PRABU K)

Chairman-DRPC

26-12-2022

(Prof. ASHVINI CHATURVEDI)

प्राध्यापक एवं विभागाध्यक्ष / PROF & HEAD
ई एवं सी विभाग / E & C Department
एन आई टी के, सुरतकल/N I T K, Surathkal
मंगलूर / MANGALORE - 575 025

Acknowledgements

I would like to thank my parents L Siva Basaiah and Vijaya Sri, brother L Harish Kumar, sister-in-law Tejaswini, Dhruvan Sai and other family members, friends for their continuous support, love, and encouragement.

I express my gratitude to my wife, Prathima for her continuous support, motivation, and love during my research work.

I am thankful to my co-scholars, G Pradeep, N Vijaya Ratnam, R Vignesh, Abhishek Kumar, T L Purushottama, B Parthasaradhi, G Srinath, M Ashoka Chakravarthi, G Polaiah, A J Santosh, M Deeksha, T N Mahesh for their support, motivation to prepare for the course work, the comprehension exam and other research related aspects.

I am deeply indebted to all my teachers throughout life, who have guided, encouraged, and inspired me to grow in both technical and personal aspects. Finally, I would like to thank god for giving me good health, strength, and ecstasy during my research work.

<div align="right">L BHARGAVA KUMAR</div>

Place: NITK, Surathkal
Date: 22.12.2022

Dedicated to
My Parents & Family

Abstract

The growth in mobile networks from the second generation (2G) to the fifth generation (5G) and the evolution of broadband Internet access increased the services of communication systems. Hence, there is a requirement for ultra-wideband and ultra-highspeed wireless networks to support people's ever-increasing needs. Wireless optical communication (WOC) systems accomplish these requirements with high bandwidth, high security, cost-effectiveness, license-free operation, simple deployment, and free from interference. WOC is mostly used in the terrestrial applications that is named as free space optical (FSO) system.

Most of the part of the earth is filled with water, and oceans hold around 97% of this water. Oceans play a crucial role in human life because people use these oceans for traveling, edibles, and communication. Humans have explored only 5% of the oceans, and discovering the large parts of the oceans is possible with the advanced communication systems. Underwater communication requires high speed and high bandwidth, similar to terrestrial communication, to establish communication links between remotely operated vehicles (ROVs) and underwater wireless sensor networks (UWSNs). These ROVs collect the information and transfer it to a nearby offshore base station. Suitable technologies are acoustic, wired (fiber optic), and WOC systems for underwater communications. The underwater wireless optical communication (UWOC) system is attractive and highly preferred among these methods. UWOC has several advantages over acoustic and RF communications regarding data rate, latency, and cost. It is also helpful to recover, offload, download, or exchange a more massive collection of information in real-time while minimizing loss of energy and traffic congestion. The UWOC system has several applications such as environmental monitoring, oceanography, maritime archaeology, imaging, port security, live video streaming, disaster preparedness, offshore oil field exploration, high-performance UWSNs, IoUT, and military operations

In this thesis, we proposed relay-assisted convergent FSO-UWOC systems. Even though the WOC systems have substantial advantages, the link range, reliability, and data rate are affected by atmospheric/underwater

scintillation, attenuation, and pointing errors. This thesis considers pointing errors and turbulence as significant limitations and reviews the average bit error rate (ABER) performance of the end-to-end convergent FSO-UWOC systems. Under strong turbulence conditions, the dual-hop single input single output (SISO) system gives an ABER of 10^{-2} at 25dB of average signal to noise ratio (SNR). Using the multiple-input multiple-output (MIMO) technique, we improved the end-to-end system's ABER performance to 10^{-5} over strong turbulence with pointing errors at an average SNR of 25dB.

We proposed multi-hop FSO-UWOC convergent systems for island communication, Internet of underwater things (IoUT), and underwater optical wireless sensor networks (UOWSN) applications. We analyzed the outage performance of the multi-hop FSO-UWOC systems. We also proposed multi-hop FSO convergent with the UWOC system for navy applications. Here we assumed (n-1) FSO links and one UWOC link to perform the ABER and outage performances. We did a case study for the proposed system with real-time values of the Arabian Sea (GPS coordinates: N 13^0 0'38.0988', E 74^0 47'17.4876') near Surathkal, located in Mangalore, Karnataka, India.

We proposed a multi-hop UWOC convergent with an FSO system with an 'n' number of links for navy applications and identifying the item of the wrecked cargo ship. We analyzed the outage performance of the end-to-end system by considering the turbulence, attenuation, and pointing losses. We used the decode and forward (DF) relaying technique in all the proposed works. In this thesis, we considered the coherent and non-coherent modulation schemes, such as binary phase-shift keying (BPSK), binary frequency-shift keying (BFSK), and differential phase-shift keying (DPSK).

Keywords: Free-Space Optical; Underwater wireless optical communication; Intensity modulation/direct detection; Internet of Underwater Things; underwater wireless sensor networks.

Contents

List of Figures

xiii

List of Tables

Abbreviations

4G	Fourth-Generation
5G	Fifth-Generation
ABER	Average Bit Error Rate
AM-SIM	Amplitude Modulation - Subcarrier Intensity Modulation
ASK	Amplitude Shift Keying
ASNR	Average Signal to Noise Ratio
AUVs	Autonomous Underwater Vehicles
AWGN	Additive White Gaussian Noise
BER	Bit Error Rate
BPOLSK	Binary Polarization Shift Keying
CDF	Cumulative Distribution Function
CPOLSK	Circular Polarization Shift Keying
DF	Decode-and-Forward
DPIM	Digital Pulse Interval Modulation
DPSK	Differential Phase Shift Keying
FM-SIM	Frequency Modulation - Subcarrier Intensity Modulation
FSO	Free Space Optical
GG	Gamma-Gamma
HD	Heterodyne Detection
IM/DD	Intensity Modulation / Direct Detection
IoUT	Internet of Underwater Things
LAUV	Light Autonomous Underwater Vehicle
LOS	Line-Of-Sight
LPOLSK	Linear Polarization Shift Keying
MIMO	Multiple-Input Multiple-Output
MPOLSK	Multilevel Polarization Shift Keying
NLOS	Non-Line-Of-Sight
NRZ-OOK	Non Return to Zero - On Off Keying
OFDM	Orthogonal Frequency Division Multiplexing
OOK	On Off Keying
OP	Outage Probability

PAM	Pulse Amplitude Modulation
PDF	Probability Density Function
PD	Photo Detector
PFM	Pulse Frequency Modulation
PM	Phase Modulation
POLSK	Polarization Shift Keying
PPM	Pulse Position Modulation
PSK	Phase Shift Keying
PSK-SIM	Phase Shift Keying - Subcarrier Intensity Modulation
PWM	Pulse Width Modulation
RF	Radio Frequency
ROVs	Remotely Operated Vehicles
RZ-OOK	Return to Zero - On Off Keying
SNR	Signal-to-Noise Ratio
SISO	Single-Input Single-Output
SIM	Subcarrier Intensity Modulation
SIMO	Single-Input Multiple-Output
UAVs	Unmanned Aerial Vehicles
UOWSNs	Underwater Optical Wireless Sensor Networks
UWSNs	Underwater Wireless Sensor Networks
UWOC	Underwater Wireless Optical Communication
UWAV	Underwater Wireless Autonomous Vehicle
WOC	Wirless Optical Communication

Notations

η	Responsivity
λ	Wavelength
$a(\lambda)$	Absorption coefficient
$b(\lambda)$	Scattering coefficient
$c(\lambda)$	Extinction coefficient
L	Link length
h	Over all channel effect
h_l	Path loss
h_a	Atmospheric turbulence
h_p	Pointing error
$\Gamma(\cdot)$	Gamma function
$K_v(.)$	Modified Bessel function of second kind
$G_{\cdot\cdot}^{\cdot\cdot}(\cdot)$	Meijer G function
A_{avg}	Aperture averaging factor
$\bar{\gamma}$	Average SNR
γ_{th}	Threshold SNR
n	AWGN noise
σ_I^2	Scintillation index
σ_R	Rytov variance
α	Large scale turbulent eddies
β	Small scale turbulent eddies

Chapter 1

INTRODUCTION

1.1 Background of WOC

Wireless optical communication (WOC) is an advanced laser-based communication technology that exchanges information from one entity to other using the atmosphere as a medium. Ancient people used to communicate with the fire beacons during 800 BC, and later at about 150 BC, the people used smoke signaling for information exchange. Later in the 18th century, navigators used semaphores to communicate. Alexander Graham Bell was the first human to experimentally transfer a voice signal modulated by Sun radiation for about 200 meters in 1880. In the early 1930s, Mr. Sony was involved in research on modulated light communication system prototypes. These systems with high security and high directivity provided the military before the microwave hardware became available. Later in the 1930s, German, Australian, and Japanese armies did several communication experiments obtained from recording optical soundtracks on motion picture films using modulated electric light sources. However, the non-accurate tracking & pointing systems and unreliable optical components make communication difficult. In addition, the energy losses involved in the laser beam propagating over the atmospheric channel due to the atmospheric turbulence and attenuation. With the advancements in opto-electronic devices in the market and the increasing demand for larger bandwidth, there was a growing research activity in WOC technology in the early 1960s. Several WOC experiments in history are:

1. 1962: Gallium Arsenide (GaAs) light-emitting diode-based television (TV) signal transmission @ MIT Lincoln Laboratory for about 30 miles [Goodwin (1970)].

2. 1963: Duntley proposed that the attenuation in seawater is relatively low at 450nm-550nm wavelengths of light which corresponds to the blue and green spectrum. Gilbert et al. experimentally approved this in the year 1965 [Goodwin (1970)].

3. 1963: A He-Ne laser modulated by voice signals transmitted over 118 miles between Panamint Ridge and San Gabriel Mountain, USA [Goodwin (1970)].

4. 1963: The first TV-over laser demonstration @ North American Aviation [Goodwin (1970)].

5. 1970: The first full-duplex FSO transceiver was built using a 0.6328-micrometer He-Ne laser and demonstrated @ Nippon Electric Company (NEC), Japan. Also verified the same over 14 km of distance between Yokohama and Tamagawa [Goodwin (1970)].

6. 1970: Hayashi et al. demonstrated the first semiconductor laser that required no cooling, which operates at room temperature [Popoola (2009)].

7. 1976: Karp et al. evaluated the feasibility of WOC systems between underwater and above the surface (satellite) terminals [Karp (1976)].

8. 1977: The researchers proposed a one-way WOC system from shore to submarine @ the Lawrence Livermore Laboratory - University of California [Callaham (1981)].

9. The 1980s: Development of military and commercial WOC devices.

10. The 1990s: Many companies from the USA, Europe, and Japan were involved in laser-based long-range WOC systems.

Free Spcae Optical (FSO) communications have seen rapid development in commercial, military operations, and deep space applications. With the invention of the newer optical devices, namely, the laser, in 1960, there is an enormous growth in FSO communications.

The German Aerospace Center researchers, Deutsches Zentrum für Luft- und Raumfahrt (DLR) and ADd VAlue (ADVA - Optical company) set a record data transmission rate of 1.72 Tbps in 2016 [D.Messier (2016)]. It happened from the DLR again in 2018, a new record FSO transmission data rate of 13.16 Tbps [DLR (2018)].

1.2　Research Motivation

The development of fourth-generation (4G) and fifth-generation (5G) wireless communication networks are witnessing the evolution of communication and information technologies, such as ultra-high-speed broadband Internet access, voice over WiFi (VoWiFi) internet protocol telephony, video calling, high-definition television (HDTV) service for mobile phone, online meetings, and gaming services, streaming movies & music and other streamed multimedia applications. Cisco report says that there will be 5.7 billion mobile users by 2023, i.e., 71% of the global population. Also, there will be 14.7 billion machine-to-machine connections by 2023. The average mobile network connection speed was 13.2 Mbps in 2018 and will be 43.9 Mbps by 2023. Nowadays, users expect internet services that provide the content on a snap/flash. Soon, the required bandwidth for the users may be more than 500Mbps [Cisco (2020)].

All the services mentioned earlier require high bandwidth with low latency. The ever-growing bandwidth requirement of modern and emerging communication systems is the driving force behind research in wireless optical communications. Also, the existing RF-based links have limitations of low data rate, limited bandwidth, security, and prone to interference. WOC is one such technology that can offer colossal bandwidth (practically 400 THz), long operational range (up to several kilometers). WOC also provides license-free operation, re-usability in terms of equipment, and wavelengths, high security, and immune to electromagnetic interference [Ghassemlooy *et al.* (2016)].

The term WOC refers to optical transmission, which uses guided visible light (VL), infrared (IR), or ultra-violet (UV) spectrum as propagation media. WOC has been an innovative technology for the last four decades and is gaining more attention. Terrestrial WOC is also known as FSO communication system. Terrestrial point-to-point FSO communication systems operate at IR, VL, and UV frequencies. WOC has got significant research in the water and is known as underwater wireless optical communication (UWOC).

WOC is suitable for many applications such as offices, industry, shopping malls, surveillance, healthcare, railway stations, transportation, disaster recovery, homes, underwater, and space. For these application platforms, all types of communication, such as device-to-device (D2D); machine-to-machine (M2M); chip-to-chip; device/ machine-to-user; user-to-device /machine; vehicle-to-infrastructure, vehicle-to-vehicle, and infrastructure-to-vehicle (V2X); ground/ satellite-to-satellite /ground; ground/ vehicle-to-vehicle /ground; point-to-point; point-to-multi-point, and multi-point-to-

point; can be performed using WOC technologies. Based on the application type, required data speed, and platform, various WOC technologies can be applied.

1.3   Research Objectives

This research investigates the performance of relay-assisted convergent FSO-UWOC systems over the combined channel model (attenuation, turbulence and misalignment induced fading). Initially, the research interest was on the dual-hop convergent system. Later, the research extended to the multi-hop convergent system and to enhance the performance of FSO-UWOC systems using multiple-input multiple-output (MIMO), relay and diversity techniques. To analyze the end-to-end system performance, different terrestrial weather conditions (clear air, rain, fog, haze, etc.), different types of water (clear, coastal, turbid harbor), turbulences (weak, moderate, strong), and pointing loss (weak, moderate, strong) were considered. Several research objectives outlined are as follows:

- To analyse the performance of a dual-hop convergent FSO-UWOC system over combined channel model for various weather, turbulence, and pointing error conditions.

- To enhance the performance of a dual-hop convergent FSO-UWOC system using multiple input multiple output (MIMO) technique and compare the results with single input single output (SISO) mode of communication.

- To analyze the performance of a multi-hop convergent FSO-UWOC system to establish reliable communication link between the islands.

- To analyze the performance of a multi-hop FSO convergent with UWOC system, with a case study near by NITK, Surathkal, in the Arabian sea (GPS coordinates: N 13°0'38.0988', E 74°47'17.4876'), Karnataka, India.

- To analyze the performance of a multi-hop UWOC convergent with FSO system that suits for Internet of underwater things (IoUT) and underwater optical wireless sensor networks (UOWSN) applications.

1.4   Original Research Contributions

This research resulted in the following contributions:

- We investigated the performance of an FSO-UWOC convergent system in terms of average bit error rate (ABER) for the differential phase shift keying (DPSK) modulation scheme using the end-to-end channel probability density function (PDF). We derived the closed-form ABER expressions in terms of the Meijer G function using Malaga and Gamma-Gamma (GG) distribution for the FSO and UWOC channels. The corresponding numerical results are plotted for different turbulence, pointing errors, and weather conditions in Chapter Three.

- The ABER performance of the FSO-UWOC system is enhanced using a MIMO technique in Chapter Four. A closed-form ABER expression is derived for the relay-assisted end-to-end system using DPSK modulation. We have analyzed the proposed system ABER performance under various turbulence and PE regimes (weak and strong) for various oceanic and free-space weather conditions of both UWOC and FSO links. The results show a performance enhancement of the end-to-end system from SISO to MIMO system for specific conditions.

- The outage performance of a multi-hop FSO-UWOC convergent system using the DPSK modulation scheme under the effect of atmospheric turbulence and pointing errors are reported in Chapter Five. Using the cumulative distribution function (CDF), we derived a closed-form outage probability (OP) expression for the DPSK modulation scheme. Malaga distribution is considered for modeling the FSO link, and GG distribution is assumed for modeling the UWOC link. Numerical results for OP are analyzed and presented for the proposed system.

- The performance of the multi-hop FSO convergent with the UWOC system in terms of ABER and outage is analyzed. The results are plotted for various atmospheric turbulence conditions and water types in Chapter Six.

- The outage performance of the multi-hop UWOC convergent with the FSO system is analyzed in chapter Seven. The FSO channel was modeled using GG distribution, and the UWOC channel was hyper tangent log-normal (HTLN) distributed. New CDF and outage expressions were acquired using the Meijer G function. The results are plotted for different weather conditions such as clear air, haze, etc., and various water types, including turbulence and pointing errors.

Fig.1.1 shows the summary of the contributions of the study mentioned earlier.
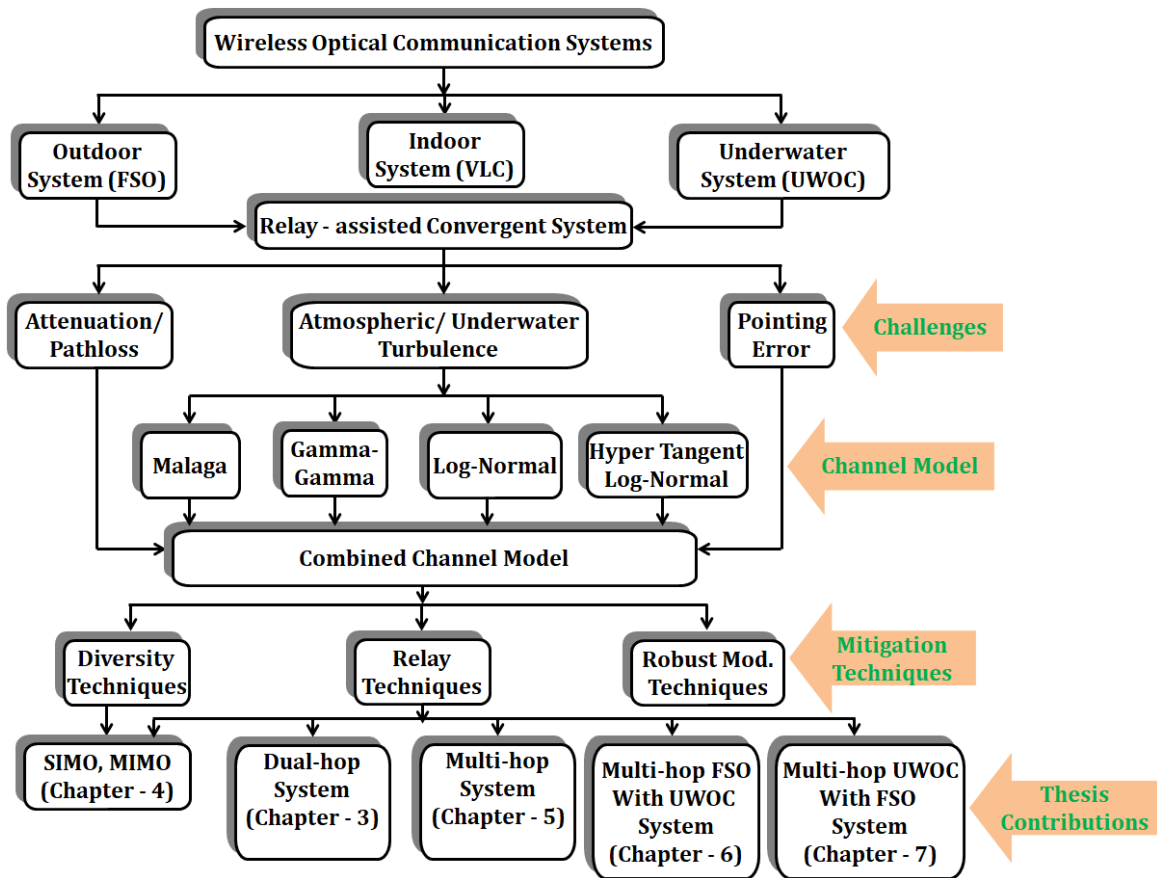
Figure 1.1: Research Contributions

1.5 Organization of Thesis

This thesis propose & presents the performance analysis of relay-assisted and convergent communication systems. This thesis presents the performance of dual-hop as well as multi-hop FSO-UWOC convergent systems. The thesis is organized as follows.

- Chapter 2 presents the FSO & UWOC communication systems, relay-assisted systems, and convergent communication systems. Chapter 2 also presents the literature, applications of convergent systems, limitations and challenges involved in the FSO & UWOC systems and various mitigation techniques.

- Chapter 3 proposes and presents the performance analysis of a dual-hop FSO - UWOC convergent communication system over atmospheric/underwater turbulence, attenuation, and pointing errors.

- Chapter 4 presents the performance enhancement of the dual-hop FSO - UWOC convergent system using the mitigation techniques such as SIMO and MIMO.

- Chapter 5 proposes and presents the performance of a multi-hop FSO-UWOC convergent system for the reliable communication between islands.

- Chapter 6 proposes and presents the performance of a multi-hop $(n-1$ hops$)$ FSO convergent with single-hop UWOC system. End-to-end performance is evaluated with DF relaying. Proposed system performance is evaluated under different channel parameters.

- Chapter 7 proposes and presents the performance of a multi-hop $(n-1$ hops$)$ UWOC convergent with single-hop FSO system. End-to-end performance is evaluated with DF relaying. Proposed system performance is evaluated under different channel parameters.

- Chapter 8 We concluded the thesis by identifying future directions that an interested researcher could pursue.

Chapter 2

Wireless Optical Communication Systems

This chapter discusses the relay-assisted and convergent communication system. Mathematical modeling is critical in the performance analysis of relay-assisted communication systems. It enables the prognosis of the abilities of the end-to-end system before actual deployment. Mainly, we first present individual Free Space Optical (FSO) and Underwater Wireless Optical Communication (UWOC) system channel models. Then, we discuss the combined channel models. We also describe optical atmospheric and underwater turbulence channels, pointing error, and attenuation impairments.

2.1 WOC Systems

The past decade has seen a renewed importance in wireless technology with the invention of fourth-generation long-term evolution services. The recent development in wireless communications leads toward the fifth-generation networks and ultrahigh-speed applications. In the literature, wireless communications often refer to radio frequency (RF) communications because of the vast establishment and usage of RF devices and systems. With the exponential increase in the high-speed mobile wireless communication users, the RF spectrum demand also increases. Also, the RF electromagnetic (EM) spectrum is limited in capacity, licensed, and costly. Wireless optical communication (WOC) is one technology that supports EM interference-free, license-free optical spectrum, highly secure, highly energy-efficient, and low-cost communications.[Khalighi and Uysal (2014)]

WOC utilizes the available three different optical regions of the EM spectrum, i.e., ultraviolet (UV), visible light, and infrared (IR). Figure 1 of Ref. [Al-Kinani *et al.* (2018)] illustrates the optical spectrum window. The visible light spectrum finds its applications in visible light communication systems and uses the entire visible

light wavelength region. The IR spectrum is useful for both indoor and outdoor communications depending on the distance and application [Al-Kinani *et al.* (2018)].
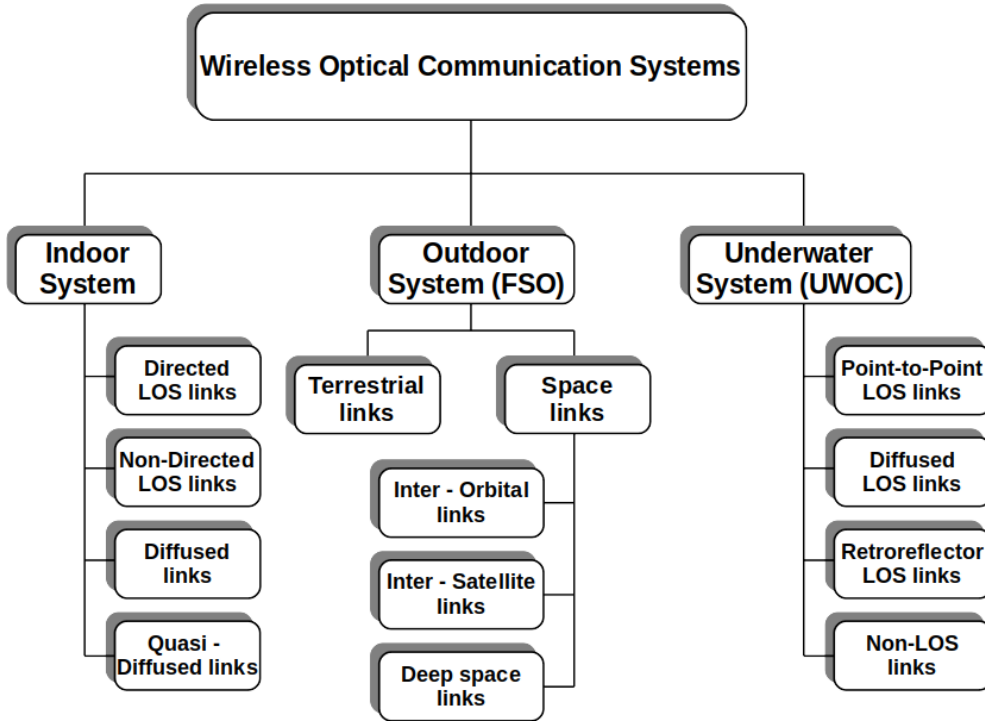
Figure 2.1: Classification of Wireless Optical Communication systems

The wireless optical communication systems are classified into three different categories depending on the environment in which they are embedded. Fig. 2.1 depicts the various types of links available under each category of the WOC systems.

1. Indoor system - visible light communication (VLC), light fidelity (Li-Fi).

2. Outdoor system - FSO.

3. Underwater system - UWOC.

This thesis concentrates on the FSO and the UWOC channels. The significant parameters that affect the received signal power are atmospheric/underwater turbulence, attenuation, and pointing loss. The following sections discuss these parameters and their combined effect of them. The block diagram of WOC system is shown in figure 2.2. The major blocks include transmitter, receiver and the terrestrial/underwater channel. The transmitter sends the modulated information through the optical source. The receiver collects the faded optical signal from the channel and converts it into the

electrical signal, amplifies and demodulates the signal to extract the original information sent.
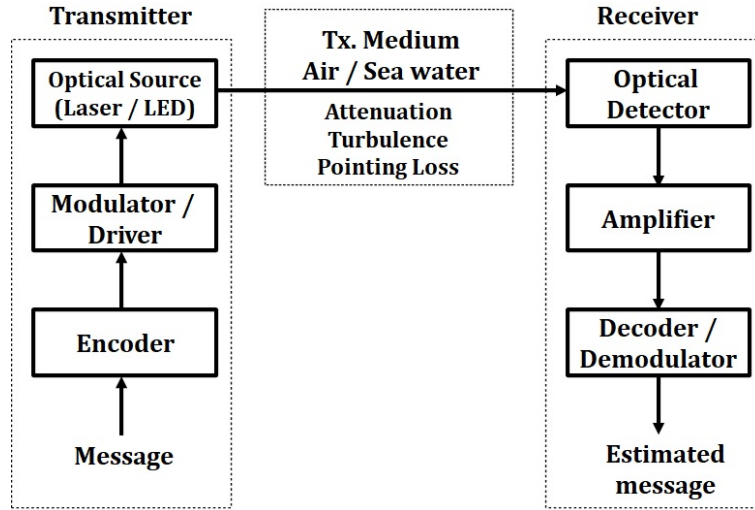
Figure 2.2: Block diagram of Wireless Optical Communication systems

2.1.1 FSO System
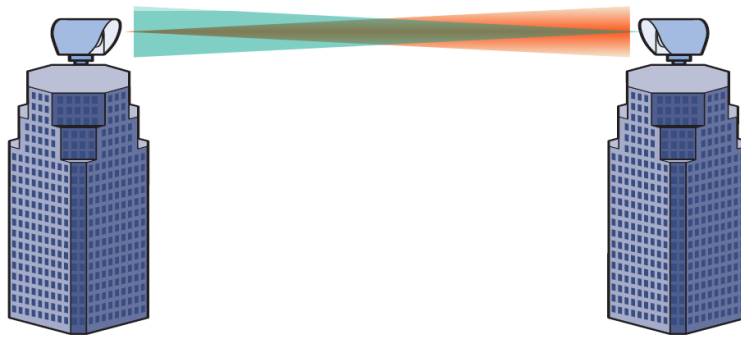
Figure 2.3: General terrestrial FSO System

Terrestrial point-to-point WOC system is named as FSO communication system. FSO systems are suitable and alternative for any fiber optical cable connections. Through FSO once can realize dedicated point-point links, high-speed broadband connectivity, inter base station connections, and network communications. Figure 2.3 shows the general terrestrial communication between two towers using FSO transceivers.
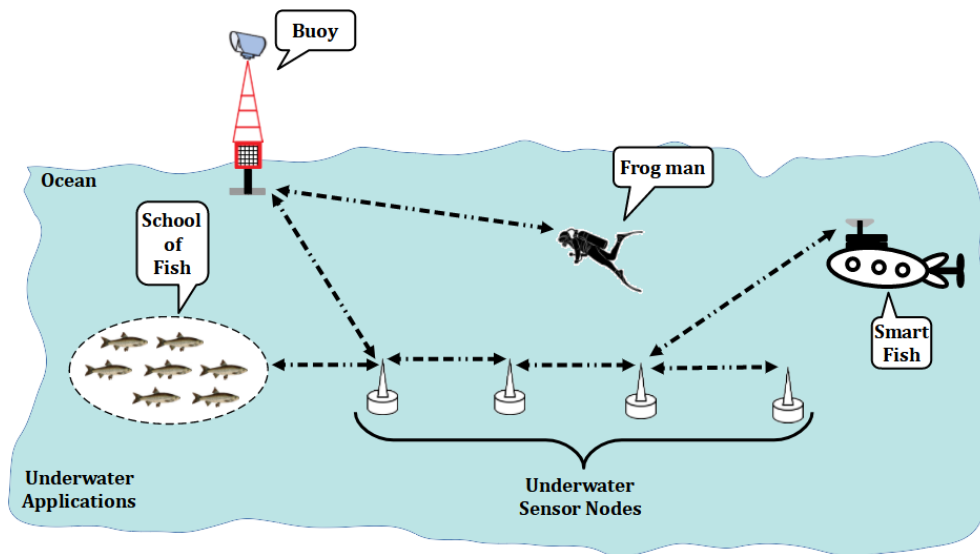
Figure 2.4: General UWOC System

2.1.2 UWOC System

WOC system with an underwater channel is named as UWOC system. UWOC systems can replace the existing underwater RF communication links as well as acoustic links with its high data rate and relative shorter delay links. Figure 2.4 shows the general UWOC system in various applications.

2.1.3 Applications of WOC Systems

Wireless optical communications have a wide range of applications, such as indoor, terrestrial/outdoor, and underwater communications. WOC finds its applications in various fields, such as healthcare, smart homes, offices, industries, transportation, railway stations, shopping malls, space, and underwater. Depending on the platform, communication range, application type, and the data transfer rate required, the WOC can apply for the following communications: [Chowdhury *et al.* (2018)]

- Point-to-point

- Point/multipoint-to-multipoint/point

- Device-to-device

- Chip-to-chip

- Machine-to-machine
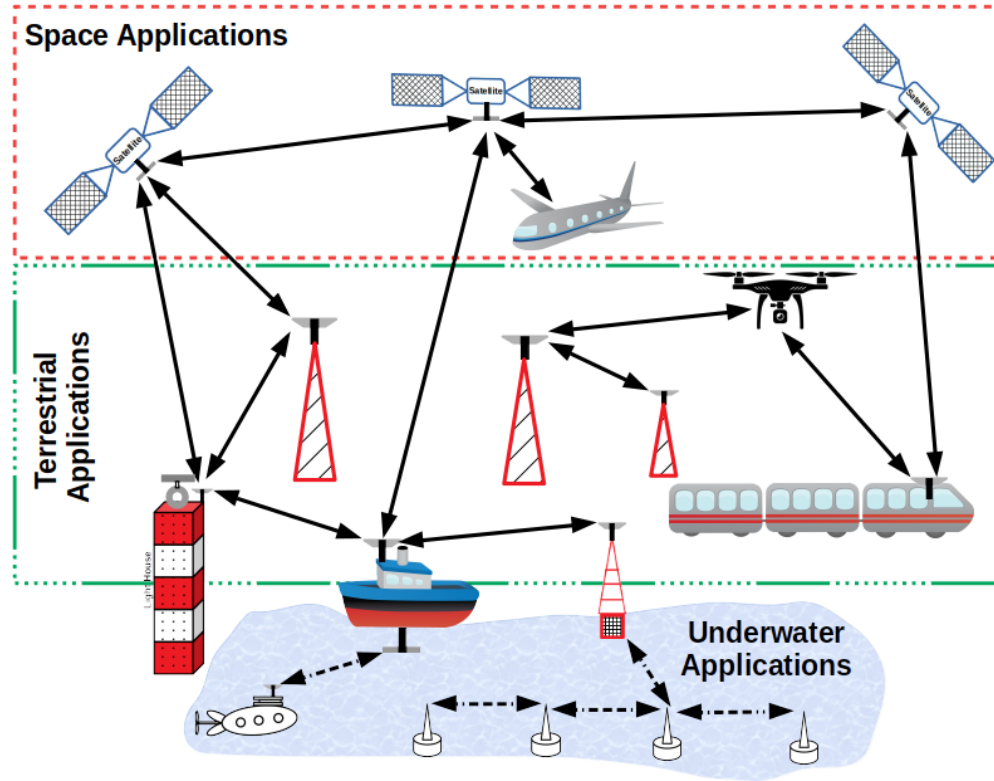
Figure 2.5: Applications of WOC systems

- Device/user-to-user/device

- Vehicle/infrastructure-to-infrastructure/vehicle (V2X)

This thesis concentrates on the FSO-UWOC systems. Fig. 2.5 shows the applications of FSO and UWOC systems. The FSO systems find their applications in last-mile connectivity, backhaul connectivity, disaster recovery, wireless local area network (WLAN), wireless personal area network (WPAN), wireless body area network (WBAN), inter-building connections, inter-satellite and deep space links [Prabu (2014), Khalighi and Uysal (2014)]. The UWOC systems find their applications in oceanography, ocean observation, sensor tracking, seismic events, seabed geodesy, oil & gas explorations, search & relocation, maritime archaeology, imaging, port security, live video streaming, disaster preparedness, high-performance underwater wireless optical sensor networks (UWOSNs), optical Internet of underwater things (O-IoUT), and military operations and shallow water tracking [Online (-), Zeng *et al.* (2016), Xu *et al.* (2016)].

13

2.1.4   WOC Channel: Turbulence

The medium is highly vulnerable to scattering, attenuation, and turbulence in FSO communication with a link range of more than 1km. The earth absorbs the sunlight; due to this, the surface near the earth gets heated up. This random phenomenon creates unexpected changes in the atmospheric temperature and pressure along the propagation path resulting in the formation of turbulent cells called eddies of different sizes with different refractive indices. Similarly, for an underwater channel, the fluctuations in the water density, salinity, and temperature variations cause changes in the refraction index along the propagation path, leading to oceanic turbulence and resulting in significant changes in the intensity of the light signal at the receiver [Kaushal and Kaddoum (2016a,b)].

The interaction between the turbulent medium and the laser beam produces random variations in amplitude and phase of the transmitted optical signal. The turbulence-induced fading in the transmitted optical signal is called scintillation. Turbulence depends on pressure, wind speed, altitude, and refraction index variation due to temperature inhomogeneity. The effects of atmospheric turbulence include beam spreading, beam steering, beam scintillation, image dancing, polarization fluctuation, and spatial coherence degradation [Killinger (2002)]. The scintillation index (SI) gives the measure of turbulence strength in the atmosphere, such as weak (SI $\ll$ 1), moderate (SI $\approx$ 1), strong (SI $>$ 1), and extremely strong (SI $\gg$ 1). Various turbulent channel models that describe the irradiance fluctuation in terms of probability density function (PDF) are lognormal, Malaga, gamma-gamma [Andrews and Phillips (2005)].

2.1.4.1   lognormal turbulence channel model

The statistics of the irradiance fluctuations in this channel model follow the lognormal distribution. This model is best suited for weak turbulence regimes. The PDF of the lognormal channel can be given as

$$f(h) = \frac{1}{\sqrt{2\pi\sigma_h^2}} \frac{1}{h} \exp\left(-\frac{\left(\ln\left(\frac{h}{h_0}\right) - E[h]\right)^2}{2\sigma_h^2}\right), h \geq 0 \qquad (2.1)$$

Where h_0 is the received mean irradiance, also represented as $E[h]$.

2.1.4.2   Gamma-Gamma turbulence channel model

In this model, the atmospheric turbulence follows a gamma-gamma (GG) distribution with scintillation parameters α and β, indicated as the Rytov variance functions and a geometry factor. The PDF of the gamma-gamma turbulence channel model is given as [Andrews and Phillips (2005)]

$$f_h(h) = \frac{2(\alpha\beta)^{(\alpha+\beta)/2}}{\Gamma(\alpha)\Gamma(\beta)} \; h^{(\alpha+\beta)/2-1} \; \mathrm{K}_{(\alpha-\beta)}\left(2\sqrt{\alpha\beta h}\right) \tag{2.2}$$

Where α and β represent the adequate number of large-scale and small-scale turbulent eddies. $\Gamma(\cdot)$ represents the gamma function and $\mathrm{K}_{(\alpha-\beta)}$ is the modified Bessel function of the second kind of order $(\alpha-\beta)$. The effective number of large-scale and small-scale eddies varies for a plane wave and a spherical wave.

2.1.4.3   Malaga turbulence channel model

Many irradiance pdf models such as lognormal and gamma-gamma were proposed with different degrees of success until now. Perhaps the lognormal and gamma-gamma channel models are exceptional cases of the newly proposed Malaga distribution model. The Malaga channel model is validated by comparing its PDF with the most published irradiance statistical channel models proposed in the literature by the researchers over the last six decades. Some exceptional cases of the Malaga distribution are gamma, Rice-Nakagami, shadowed-Rician, K-distribution, homodyned-K, exponential or Gamma-Rician. The Malaga turbulence channel PDF is given as [Jurado-Navas et al. (2012), Ansari et al. (2015), Vellakudiyan et al. (2019)]

$$f_h(h) = A \sum_{m=1}^{\beta} a_m \; h \; \mathrm{K}_{\alpha-m}\left(2\sqrt{\frac{\alpha\,\beta\,h}{g\,\beta+\Omega'}}\right), \quad h > 0 \tag{2.3}$$

Where

$$
\begin{aligned}
A &\triangleq \frac{2\,\alpha^{\alpha/2}}{g^{1+\alpha/2}\Gamma(\alpha)}\left(\frac{g\,\beta}{g\,\beta+\Omega'}\right)^{\beta+\alpha/2}, \\
a_m &\triangleq \binom{\beta-1}{m-1}\frac{(g\,\beta+\Omega')^{1-m/2}}{(m-1)!}\left(\frac{\Omega'}{g}\right)^{m-1}\left(\frac{\alpha}{\beta}\right)^{m/2}
\end{aligned}
\tag{2.4}
$$

2.1.5 WOC Channel: Attenuation/Path Loss

Attenuation is a critical propagation effect that makes the transmitted optical signal power unstable as it propagates to longer distances [Ghassemlooy *et al.* (2019)]. Attenuation is a function of distance and is modeled using the Beer Lambert law. It also depends on the attenuation coefficient, the summation of absorption, and scattering coefficients. The atmospheric channel consists of various gases such as oxygen, methane, carbon dioxide, nitrous oxide, ozone, and tiny air particles - aerosols. The other showers, such as fog, haze, and rain, are also present in the atmosphere. The quantity of precipitation in the atmosphere varies from one location to another and one season to another. When the optical signal passes through the atmosphere, it is absorbed or scattered by the particles present in the atmosphere and results in power loss. The general Beer-Lambert is given as [Andrews and Phillips (2005)]

$$h_l = \exp\left(-\sigma\ L\right) \tag{2.5}$$

Where σ represents the attenuation coefficient for atmospheric/underwater channel, and L is the link distance between the source and destination. The attenuation coefficient for atmospheric and underwater channels are given in table 2.1 and table 2.2, respectively. The parameters $a(\lambda), b(\lambda)$ represent absorption and scattering coefficients, $c(\lambda)$ represents the attenuation coefficient for underwater channel.

Table 2.1: Attenuation coefficient for 1550nm wavelength [(Balaji and Prabu, 2018*b*, Prabu, 2019)].

Weather condition	σ (dB/km)
Very clear air	0.0647
Drizzle	0.2208
Haze	0.7360
Mean rain	0.8793
Strong rain	0.5554
Light Fog	4.2850
Moderate fog	25.5160

Table 2.2: Typical values of absorption, scattering and extinction coefficients for 530nm wavelength [(Hanson and Radic, 2008)]

Water type	$a(\lambda)(m^{-1})$	$b(\lambda)(m^{-1})$	$c(\lambda)(m^{-1})$
Clear ocean	0.114	0.037	0.151
Coastal ocean	0.179	0.220	0.399
Turbid harbor	0.366	1.829	2.195

2.1.6 WOC Channel: Pointing Errors

In wireless optical communication systems, the alignment between transmitter and receiver plays a crucial role in determining the link performance and reliability. Pointing loss in FSO could arise due to beam wander, building sway, or errors in the tracking system. Pointing loss in the UWOC link occurs due to the movement caused by underwater vehicles, ocean currents, giant fishes, and other turbulent sources. The other sources that cause the pointing errors are thermal expansion and weak earthquakes that fade the signals at the receiver. We consider a circular detection aperture with radius and a Gaussian beam, the PDF is given by

$$f_{h_p}(h_p) = \frac{g^2}{A_0^{g^2}} \, h_p^{g^2-1}, \quad 0 \le h_p \le A_0 \tag{2.6}$$

Where $A_0 = [erf(v)]^2$ represents the fraction of the power collected at $r = 0$. $erf(\cdot)$ represents the gauss error function defined as $erf(\mathrm{x}) = \frac{2}{\sqrt{\pi}} \int_0^{\mathrm{x}} e^{-\mathrm{t}^2} d\mathrm{t}$. The parameter r denotes the radial distance, and g is the ratio of the equivalent beam radius and the pointing error displacement (jitter) standard deviation at the receiver.

2.1.7 WOC Channel: Combined Channel Model

The block diagram of the WOC system with a transmitter, receiver, and the channel effects is shown in fig. 2.2. The random variable associated with the combined channel (turbulence, pointing errors and path loss) is $h = h_l \, h_a \, h_p$, can be derived as [Ansari et al. (2015)]

$$
\begin{aligned}
f_h(h) &= \int_{h/(h_l \, A_0)}^{\infty} f_h(h_a) \, f_{h|h_a}(h|h_a) \, dh_a \\
&= \int_{h/(h_l \, A_0)}^{\infty} f_h(h_a) \, \frac{h}{h_a \, h_l} f_p\left(\frac{h}{h_a \, h_l}\right) \, dh_a.
\end{aligned}
\tag{2.7}
$$

The lognormal channel PDF of the irradiance intensity, h for weak atmospheric turbulence conditions expressed as

$$f_h(h) = \frac{\xi^2}{(A_0 \ h_l)^{\xi^2}} \ h^{\xi^2-1} \times \int_{h/A_0 \ h_l}^{\infty} \frac{1}{h_s^{\xi^2+1}\sigma_I(D)\sqrt{2\pi}} \exp\left(-\frac{[\ln(h_s) + 0.5\sigma_I^2(D)]^2}{2\sigma_I^2(D)}\right) dh_s \tag{2.8}$$

Where $\sigma_I^2(D)$ represents the average aperture scintillation index, $\xi = W_{z_{eq}}/\sigma_s$ represents the ratio of the equivalent beam radius and the pointing errors displacement standard deviation at the receiver, and A_0 represents the received power fraction at zero radial distance.

The GG channel PDF for strong atmospheric turbulence conditions is given as

$$f_h(h) = \frac{2\xi^2(\alpha\beta)^{(\alpha+\beta)/2}}{(A_0 \ h_l) \ \xi^2\Gamma(\alpha)\Gamma(\beta)} h^{\xi^2-1} \times \int_{h/A_0 \ h_1}^{\infty} h_s^{(\alpha+\beta)/2-1-\xi^2} \ K_{(\alpha-\beta)}\left(2\sqrt{\alpha\beta h_s}\right) dh_s \tag{2.9}$$

Where α and β represent the effective number of large and small scale turbulent eddies. $K_{(\alpha-\beta)}$ represents the modified Bessel function of the second kind of order $(\alpha - \beta)$, and $\Gamma(\cdot)$ represents the gamma function. The modified Bessel function is converted into the Meijer G function using Eq. 14 of [Adamchik and Marichev (1990)], and the combined GG channel model is integrated using [Research (2021)]. The closed-form expression obtained for the GG channel model is

$$f_h(h) = \frac{\alpha\beta\xi^2}{A_0 \ h_l\Gamma(\alpha)\Gamma(\beta)} G_{1,3}^{3,0}\left(\frac{\alpha\beta h}{A_0 \ h_l}\left|\begin{array}{c} \xi^2 \\ \xi^2 - 1, \ \alpha - 1, \ \beta - 1 \end{array}\right.\right) \tag{2.10}$$

By applying the simple random variable transformation on 2.3 and using 2.7, the PDF of the receiver irradiance intensity h undergoing Malaga turbulence in the presence of pointing error is given as [Ansari et $al.$ (2015)]

$$f_h(h) = \frac{\xi^2 A}{2 \ h} \sum_{m=1}^{\beta} b_m \ G_{1,3}^{3,0}\left[\frac{\alpha \ \beta}{(g \ \beta + \Omega')} \frac{h}{h_l \ A_0}\left|\begin{array}{c} \xi^2 + 1 \\ \xi^2, \alpha, m \end{array}\right.\right] \tag{2.11}$$

Where $b_m = a_m \left[\frac{\alpha\beta}{g\beta+\Omega'}\right]^{-\frac{\alpha+m}{2}}$

2.2 Limitations and Challenges

The significant challenges involved in FSO and UWOC systems are as follows:

- Atmospheric/underwater turbulence

- Atmospheric/underwater attenuation

- Pointing errors

- Acquisition and tracking

- Communication range in the underwater environment

- Line-of-sight obstructions

- Laser safety

2.3 Mitigation Techniques

Modern FSO and UWOC systems must be potential & seamless, provide high bandwidth with good quality of service to both communication entities in various atmospheric conditions. The FSO and UWOC systems need improved reliability when operating in adverse atmospheric conditions. Atmospheric conditions eventually determine the FSO and UWOC system performance for terrestrial, space, and underwater applications because the atmospheric/underwater channel always includes scattering and turbulence media.

Various detrimental features of the atmospheric channel may lead to severe signal fading and even cause complete signal loss. Exciting and challenging research is going on towards FSO and UWOC systems and the mitigation methods to reduce the turbulence fading. The important performance parameter measured in these FSO and UWOC systems is bit error rate (BER). The atmospheric/underwater turbulence affects the BER parameter. Another performance parameter determining channel fading is outage probability (OP). Fading can be significant for long-distance communication and transmissions with a mobile platform. Eventually, the system's reliability gets reduced due to the atmospheric effects available in the channel. One can achieve improved performance using the mitigation techniques such as aperture averaging, adaptive optics, diversity techniques, optimum modulation scheme, and relay-assisted systems as shown in Fig. 2.6.
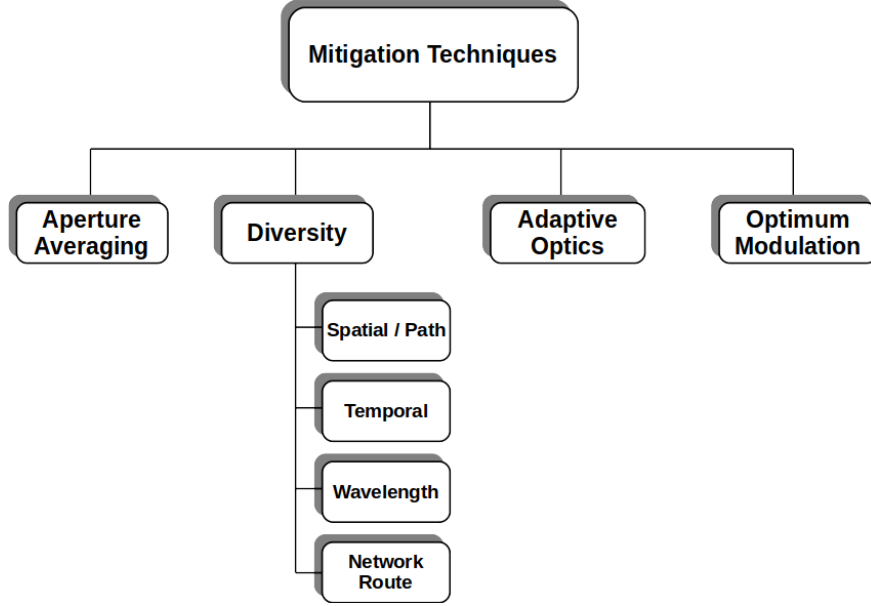
Figure 2.6: Mitigation Techniques used in WOC systems

2.3.1 Aperture Averaging

The modern WOC systems use the laser beam, and the averaging aperture effects are studied in terms of the laser beam propagation over the channel. The simple mitigation technique to reduce the turbulence fading is to increase the effective receive aperture. The aperture averaging method does not need additional bandwidth, power, and size/weight overhead to the overall design. The aperture averaging factor is the parameter used to quantify the fading reduction by aperture averaging, and it is estimated as

$$A_{avg} = \frac{\sigma_I^2(D)}{\sigma_I^2(D=0)} = \left[1 + 1.062 \left(\frac{kD^2}{4L}\right)^{7/6}\right]^{-1} \tag{2.12}$$

Where $k = \frac{2\pi}{\lambda}$ is the wave number, $\sigma_I^2 = 1.23\ C_n^2\ k^{7/6}\ L^{11/6}$ is the scintillation index, D is the receiver diameter, and L is the propagation distance.

2.3.2 Diversity Methods

Increasing the diameter of the receiver aperture is not always possible above a particular level; it will increase background noise and may not be an optimum solution. Diversity techniques such as wavelength, spatial, and temporal diversity improve the channel performance in the WOC links.

The turbulence effect is practically the same for all wavelengths, and hence wave-

length diversity method is less effective for WOC systems. Temporal diversity requires a longer signal processing time.

An array of small apertures replaces a single large aperture at the transmitter or receiver to achieve a similar performance as aperture averaging. The spatial diversity method employs multiple apertures at either side of the transmitter or receiver, both the transmitter and receiver.

2.3.3 Adaptive Optics

The applied optics technique provides an additional wavefront to decrease the data losses and increase the signal-to-noise ratio (SNR). The applied optics technique was earlier developed to mitigate wavefront distortions rendered by atmospheric turbulence in astronomical observations. WOC systems use the same applied optics technology to mitigate wavefront distortions by applying real-time wavefront control to decrease signal fading.

2.3.4 Optimum Modulation
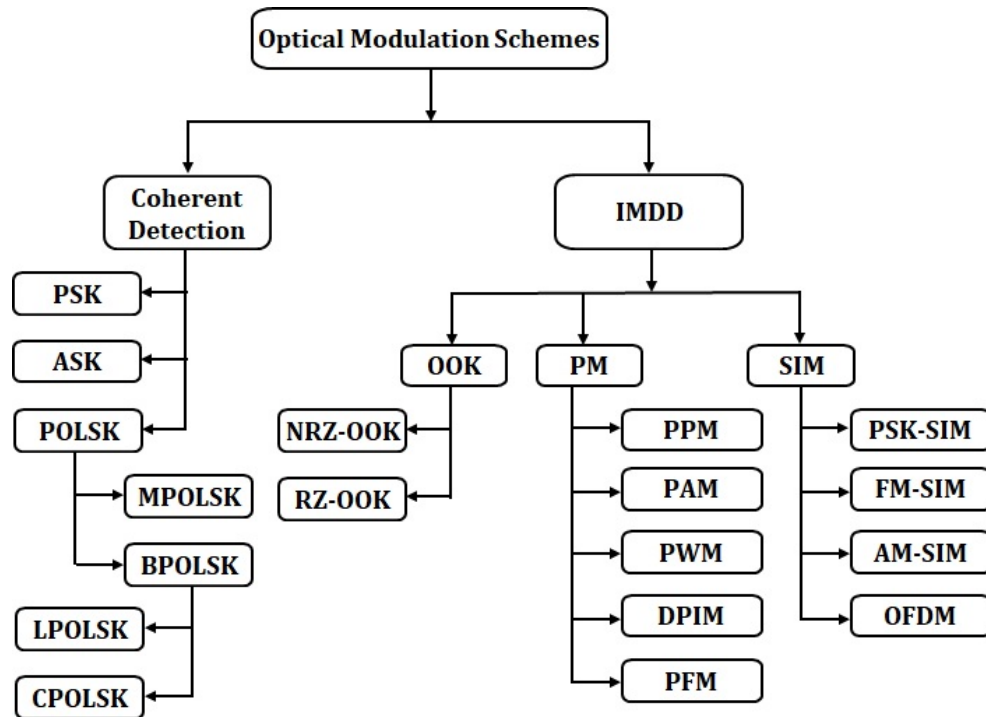
Figure 2.7: Modulation schemes used in WOC systems

The modulation schemes play a vital role in WOC systems. The modulation

21

scheme decides the system's performance, signal processing, and compatibility. The modulation schemes suitable for WOC systems are shown in Fig. 2.7. Among all the modulation schemes, OOK is the simplest and most widely used. OOK is very sensitive to atmospheric turbulence and requires an adaptive threshold for optimal performance. To overcome the drawbacks of OOK modulation, one can use PPM; however, it suffers from poor bandwidth efficiency and requires a complex transceiver design. The modulation schemes, such as DPSK and BPSK, are susceptible to the phase noise effects. The SIM mixed with different PSK modulations was employed over the channels with different atmospheric turbulence. PolSK has high immunity toward the laser phase noise and is an effective alternative modulation technique for OOK and PSK. The PolSK modulated signals propagating through the atmosphere are unaffected by the atmospheric turbulence.

2.4 Relay-assisted Systems and Convergent Systems

Relaying technology in WOC is introduced to overcome the atmospheric turbulence and enhance the communication range by strengthening the network and reliability of the communication link with a high data rate. The two standard relay protocols are amplify and forward (AF) and decode and forward (DF). The AF relaying protocol commonly works in analog signal processing mode. In an AF scheme, the relay does not decode the received signal; simply, it estimates the received signal and sends the amplified signal to the destination. In the DF scheme, the relay detects, estimates the received signals, and retransmits the encoded signal to the destination, working in a digital signal process mode [Liu *et al.* (2020)].

Relaying technology is embraced to realize better WOC systems for information transmission in the environments such as indoor, outdoor, and underwater. Fig. 2.8 shows the block diagram for the classification of relaying technology in outdoor and underwater WOC systems and also shows the equipment suitable for the relay. Relaying technology uses buildings, posters, and street lamps as a fixed relay and UAVs or vehicles as a relay in establishing a communication link between the source and destination. Introducing the relay between the source and destination strengthens the communication link quality by shortening the communication link between source-relay and relay-destination.

The relaying technology used in the UWOC systems overcomes significant limita-
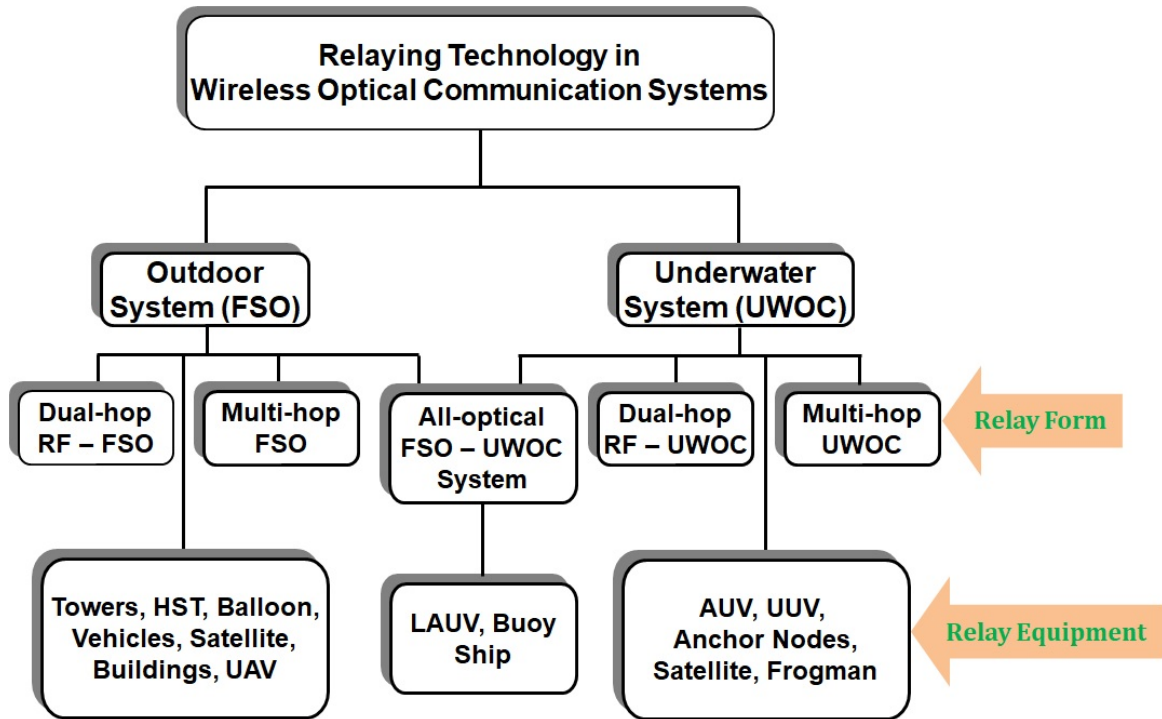
Figure 2.8: Relaying techniques and equipment in WOC systems [Liu *et al.* (2020)].

tions: communications range and large attenuation. Ships sailing at sea, AUVs, ROVs, and buoys are used as relay terminals to establish a communication link between the offshore base station and the underwater equipment.

Converging two different communication systems such as RF-FSO, RF-UWOC, FSO-UWOC, and FSO-mmwave brings the advantages of both systems. It makes the entire communication system efficient and reliable. It requires relaying technology to converge the two different communication systems. The convergent systems are different from hybrid systems. In convergent/hybrid systems, there will be two different communication systems, but in hybrid systems, only one mode of communication is possible when the other mode is not possible in the only communication link. Whereas when the two systems converge, it will have two hops in between source and destination with a relay. This thesis concentrates on the convergence of the FSO and UWOC systems. The UWOC integration with FSO provides long-range communication with underwater links.

2.5 Previous Works

Researchers started working on relay-assisted RF-FSO, RF-UWOC, and FSO-UWOC systems a few years ago. The dual-hop and multi-hop systems have recently received much attention as they simultaneously achieve the advantages of different technologies. In Refs. [Vellakudiyan *et al.* (2016)] and [Vellakudiyan *et al.* (2019)], the authors proposed a dual-hop RF/FSO system and analyzed the end-to-end system's performance. The RF link was Rayleigh distributed, and the FSO link was M-distributed. Results are plotted in the presence of turbulence as well as PEs using analytical equations. In Ref. [Li *et al.* (2020*b*)], the authors examined an RF-UWOC system's performance in terms of the outage, capacity, and BER.

Li et al. [Li *et al.* (2019)] worked on an FSO-plastic optical fiber-UWOC connecting system with a range of 50 m, 30 m, and 2 m, respectively, and achieved the data transfer rate of 9 Gbps. Jurado-Navas et al. [Jurado-Navas *et al.* (2019)] proposed a merged FSO-UWOC system for offering a high data rate optical affinity between aground and submerge systems, also derived equations for bit error rate (BER) by assuming amplify and forward relay. Christopoulou et al. [Christopoulou *et al.* (2019)] proposed a multisensor mixed UWOC-FSO setup and verified the performance of a UWSN with several sensors communicating with a terrestrial destination with reference to the outage probability. Most recently, Naik et al. [Naik *et al.* (2020)] analyzed the performance of a cooperative RF-UWOC link over hyperbolic tangent log-normal distribution channel with pointing errors. The authors proposed an analytical model and determined the outage probability and asymptotic bit error rate (ABER) for the end-to-end system.

Li et al. proposed and demonstrated a wavelength-division-multiplexing and four-level pulse amplitude modulation (PAM4) FSO–UWOC convergent system. Using 405- and 450-nm laser diodes with 500-m FSO links and 5-m UWOC links, they achieved a 100-Gb/s channel capacity [Li *et al.* (2020*a*)]. In Ref. [Tsai *et al.* (2020)], the authors proposed and experimentally demonstrated a 500-Gb/s PAM4 FSO–UWOC converging system over 100-m free-space transmission with either 10-m piped underwater link or 5-m turbid underwater link. They employed a five-wavelength red/green/blue (R/G/B) polarization-multiplexing scheme to demonstrate and achieve an aggregate data rate of 500 Gb/s.

Recently, in Ref. [Yang *et al.* (2021)], the authors proposed a dual-hop FSO–UWOC communication system and studied its performance considering a clear ocean environ-

ment. In particular, the authors analyzed the outage probability, average bit error rate (ABER), and average capacity for both HD and IM/DD detection schemes considering an AF relay in the presence of misalignment fading. Sarma et al. proposed a DF-based triple-hop RF–FSO–UWOC communication system in Ref. [Sarma *et al.* (2020)] and analyzed BER and outage probability performance with closed-form expressions.

2.6 Performance Metrics

The performance analysis is essential for WOC system design, and It provides the designers with standard systems performance metrics, such as BER and outage probability. This thesis shows the performance analysis of an IM/DD WOC system. The received signal at the detector is given as

$$y = x\ h + n \tag{2.13}$$

Where x represents the transmit data intensity, h represents the channel state, and n is the additive white gaussian noise (AWGN) with zero mean and variance σ_n^2. The instantaneous SNR of the on off keying (OOK) modulated system is given as

$$\gamma = \bar{\gamma}h^2 \tag{2.14}$$

Where $\bar{\gamma} = \frac{2P_t^2}{\sigma_n^2}$ represents the average SNR, P_t represents the average optical transmit power.

2.6.1 BER Performance

The average bit error rate (ABER) of the system with a particular modulation scheme is given as

$$P_e = \int_0^\infty P_{ec}(e|\gamma)\ f_\gamma(\gamma)\ d\gamma \tag{2.15}$$

Where $P_{ec}(e|\gamma)$ gives the conditional BER probability of a modulation scheme and $f_\gamma(\gamma)$ is the channel PDF. The average bit error rate (ABER) of the system for digital modulation schemes using CDF is given as

$$P_e = \frac{q^p}{2\Gamma(p)} \int_0^\infty \exp(-q\gamma)\ \gamma^{p-1} F_\gamma(\gamma)\ d\gamma \tag{2.16}$$

Where p, and q represent the type of modulation schemes.

2.6.2 Outage Probability

The outage probability is defined as the output SNR drops more petite than a specified threshold. A threshold is the least SNR value exceeding which the quality of service is good [Prabu *et al.* (2014*b*)].

$$P_{out} = P \ (SNR(h) \ \leq \ SNR_{TH}) = F_h(SNR_{TH}) \qquad (2.17)$$

Here SNR_{TH} represents the threshold SNR.

2.7 Summary

This chapter summarized the outline and introduction of FSO and UWOC systems. The previous research on convergent RF-FSO, RF-UWOC, and FSO-UWOC systems is discussed. The features, limitations, and applications of FSO and UWOC systems are highlighted. With a neat block diagram, the essential operation of the WOC system is discussed. Also, various modulation schemes suitable for the WOC systems have been discussed. The different turbulence models have been outlined for weak, moderate, and strong regimes. The combined channel model is introduced, and its mathematical model and the effects are described. Also, various mitigation techniques used to improve the reliability of WOC systems are discussed.

Chapter 3

ABER analysis of Dual-hop convergent FSO-UWOC system

3.1 Introduction

Recently, wireless optical communication (WOC) has attracted attention and has become an imperative technology for high-speed underwater data transfer operations. Underwater wireless optical communication (UWOC) proffers a large bandwidth with optical carriers. Due to this, it has become an alternative for underwater radio frequency (RF) and acoustic communication systems [Fei *et al.* (2018)]. UWOC systems provide the prospect for the envisaged sensor nodes and marine vehicles to convene and transmit huge data in a shorter duration compared with the underwater acoustic communication system [Diamant *et al.* (2017)]. UWOC systems have several applications such as environmental monitoring, oceanography, maritime archaeology, imaging, port security, live video streaming, disaster preparedness, offshore oil field exploration, high-performance underwater wireless sensor networks (UWSNs), and military operations [Zeng *et al.* (2016), Xu *et al.* (2016)]. UWOC is an alternative and attractive technology to RF because of its high data rates, low latency, and power consumption. Therefore, it is highly preferred to establish networks between remotely operated vehicles (ROVs) and UWSNs, and it is also helpful to recover, offload, download, or exchange more massive collection of information in real time while minimizing loss of energy and traffic congestion [Xu *et al.* (2016)].

Free-space optical (FSO) communication system is expeditiously becoming a part of the ever-growing technology. In view of its advantages, including high security, high bandwidth, license-free spectrum, and cost-effectiveness compared to the long-

established RF communication systems, it has indoor applications such as line-of-sight (LOS) systems, non-LOS systems, and diffused and tracked systems. Outdoor applications include terrestrial, deep-space, inter-satellite, and inter-orbital links [Kaushal and Kaddoum (2016a), Khalighi and Uysal (2014)]. FSO is also useful in many cases, such as high-speed trains, unmanned aerial vehicles (UAVs), satellites, indoor and outdoor local area networks, wide area networks, and building-to-building and deep-space communications [Chan (2006)]. Recently, FSO is used in indoor wireless optical power transfer to smart cells during the low-light hours [Fakidis et al. (2016)]. A remotely operated mobile power source with laser transmitter-based wireless power transmission to the UAVs to reduce the weight of the batteries carried by the vehicles has been investigated in Refs. [Duncan (2016) and Lu et al. (2018)].

The combination of UWOC and FSO is a fascinating alternative to solve the connectivity barriers. It is an auspicious confluent system that possesses various advantages, such as an unlicensed optical spectrum, thin laser beam size, ease of construction, high transmission capacity, and the reuse of atmospheric or underwater functional bandwidths. Because of the rapid evolution of UWOC-FSO convergent systems, its emerging demand increases the necessity for high-speed WOC systems. To meet the demand for high data rate WOC systems, building a high-transmission-rate UWOC-FSO combined system is needed [Tsai et al. (2019)].

UWOC-FSO system also finds the applications in Internet of Underwater Things (IoUT) such as in aquariums, fish farms, pipeline monitoring, and harbor security [Domingo (2012)]. IoUT works with UWSN systems, which have different sensors to sense the quality of the water, pressure level, temperature, metals, organic elements, and chemical properties, ROVs, sinks [buoys, ships, or autonomous surface vehicles (ASVs)]. The sinks accumulate the data and forward it to the remote monitoring center at the seashore to analyze the data and perform the necessary operations [Kao et al. (2017a)].

Jurado-Navas et al. [Jurado-Navas et al. (2019)] proposed a merged FSO-UWOC system for offering a high data rate optical affinity between aground and submerge systems, also derived equations for bit error rate (BER) by assuming amplify and forward relay. Christopoulou et al. [Christopoulou et al. (2019)] proposed a multisensor mixed UWOC-FSO setup and verified the performance of a UWSN with several sensors communicating with a terrestrial destination with reference to the outage probability. Most recently, Naik et al. [Naik et al. (2020)] analyzed the performance of a coop-

erative RF-UWOC link over hyperbolic tangent log-normal distribution channel with pointing errors. The authors proposed an analytical model and determined the outage probability and asymptotic bit error rate (ABER) for the end-to-end system. Also, Kumar and Krishnan [Kumar and Krishnan (2020)] proposed a decode-and-forward multihop convergent FSO-UWOC system to establish a reliable communication link between the islands. The authors performed outage analysis for differential phase-shift keying (DPSK)-based multi-hop system using closed form expressions.

3.2 Major contributions

In this chapter, we propose a UWOC-FSO convergent system and derive a new ABER expression for the DPSK modulation scheme using the probability density function (PDF). Because of the benefits of DPSK, such as 3-dB sensitivity, less bandwidth requirement, long-haul applicability, and simplified receiver circuit as the carrier, are not required at the receiving end, they are exploited in WOC systems [Gnauck and Winzer (2005)]. Among the available channel distributions, log-normal is used for weak turbulence (WT), and negative exponential is valid for strong turbulence (ST) and gamma–gamma (GG) distribution is applicable for both modest and ST regimes. Malaga distribution is a generalized distribution that is suitable for all turbulence regimes [Krishnan (2018)]. In this chapter, we considered GG [Gappmair (2011)] and Malaga [Jurado-Navas *et al.* (2011*b*)] turbulent channels for the UWOC and the FSO links. Numerical results also provided for the proposed system.

3.3 System and Channel model

The proposed system model is illustrated in Fig. 3.1, which consists of dual-hop UWOC and FSO links. A dual hop decode-and-forward relay is used to connect the source and destination. UWOC link is considered from source to relay and is GG distributed, whereas FSO link is considered from relay to destination and is Malaga distributed.

3.3.1 UWOC Link

The optical signal propagated through the underwater channel is affected by absorption, scattering, and turbulence. Also, the attenuation and fading add to the signal that is transmitted while propagating through the UWOC medium. In such cases, the light intensity of the received signal becomes $I_r = I_t \cdot P_l^U \cdot I_c$. Here I_t is the intensity of the transmitted signal, P_l^U is the path loss caused by absorption/scattering effects
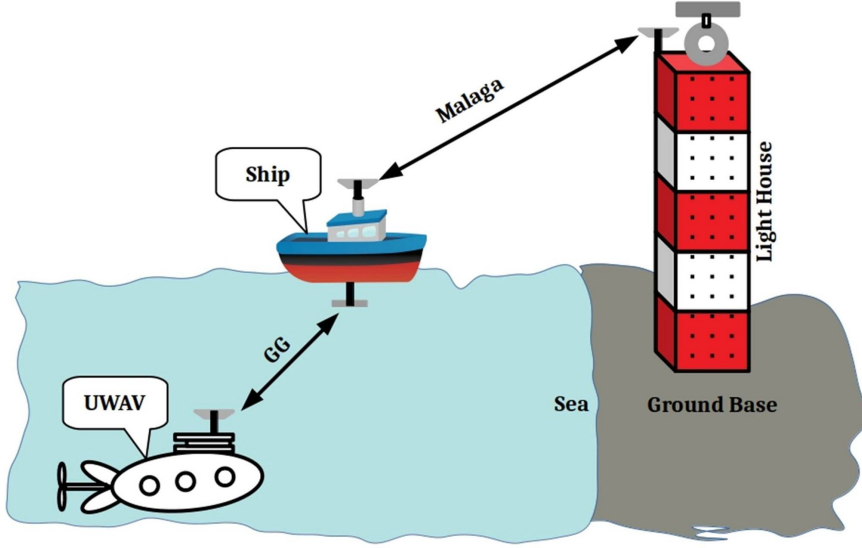
Figure 3.1: System model

and beam enlargement, which reduces the average irradiance of the light beam, and I_c signifies the turbulence-induced fading of the normalized channel and satisfies a PDF.

The photons of the light propagating may collide with the water molecules and particles. As a result, each photon loses its energy thermally and is observed as absorption and is determined by the absorption coefficient $a(\lambda)$. In the same collision, every photon may change its direction, which is considered as scattering and is characterized by the scattering coefficient $b(\lambda)$. The total energy loss of the light signal due to scattering and absorption effects describe the extinction coefficient $c(\lambda) = a(\lambda) + b(\lambda)$. The typical values of the extinction coefficient are given in Table 3.1 [Hanson and Radic (2008)]. Where λ is the wavelength of the transmitted signal; these coefficient values can vary with water types and source wavelength λ [Tang *et al.* (2013)]. The path loss of underwater channel P_l^U is represented in terms of wavelength λ and link distance L as [Kaushal and Kaddoum (2016*b*)]

$$P_l^U(\lambda, L) = e^{-c(\lambda)L}$$

In this chapter, we considered the gamma-gamma distribution for the UWOC link as the atmospheric and underwater optical turbulence caused by the random variations of the temperature and pressure of the channel. As the scattering and absorption effects do not affect the fading property, the gamma-gamma distribution can be used for the UWOC channel [Liu *et al.* (2015)]. Also, the variation of light

Table 3.1: The values of absorption, scattering and extinction coefficients (λ=530nm).[Hanson and Radic (2008)]

Water type	$a(\lambda)(m^{-1})$	$b(\lambda)(m^{-1})$	$c(\lambda)(m^{-1})$
Clear ocean	0.114	0.037	0.151
Coastal ocean	0.179	0.220	0.399
Turbid harbor	0.366	1.829	2.195

radiation can be described by the gamma-gamma model when the light is transmitted through an underwater strong turbulent environment [Jamali *et al.* (2016*a*)]. The PDF of gamma-gamma channel model is given as [Prabu *et al.* (2013)]

$$f_{\gamma_1}(\gamma) = \frac{\alpha_1\beta_1 g^2}{A_0 P_l^U \Gamma(\alpha_1)\Gamma(\beta_1)} \; G_{1,3}^{3,0}\left(\frac{\alpha_1\beta_1\gamma}{A_0 P_l^U}\middle|\begin{array}{l} g^2 \\ g^2-1, \; \alpha_1-1, \; \beta_1-1 \end{array}\right) \quad (3.1)$$

$A_0 = [erf(v)]^2$ is the fraction of the received optical power, $v = \frac{a_r}{w_z}\sqrt{(\frac{\pi}{2})}$. The parameter g indicates pointing errors caused by the misalignment between the transmitter and receiver. The cumulative distribution function (CDF) of Eq. (3.1) is expressed as

$$F_{\gamma_1}(\gamma) = \frac{\alpha_1\beta_1 g^2}{A_0 P_l^U \Gamma(\alpha_1)\Gamma(\beta_1)} \; \gamma \; G_{2,4}^{3,1}\left(\frac{\alpha_1\beta_1\gamma}{A_0 P_l^U}\middle|\begin{array}{l} g^2, \; 0 \\ g^2-1, \; \alpha_1-1, \; \beta_1-1, \; -1 \end{array}\right) \quad (3.2)$$

3.3.2 FSO Link

The generalized M - distribution is used for FSO link. The M - distributed channel forms on a physical model which includes three terms namely, LOS component U_L with power $\Omega = E[|U_L|^2]$ due to the eddies on propagation axis, the other two components are, coupled to LOS component U_S^C with power $E[|U_S^C|^2] = 2\rho b_0$ and the independent scatter component U_S^G with power $E[|U_S^G|^2] = 2(1-\rho)b_0$ due to the off-axis eddies. The scattered components will give a total average power as $E[|U_S^C|^2 + |U_S^G|^2] = 2b_0$. The parameter ρ relates the scattered components, also represents the amount of

scattering power coupled to the LOS component and varies from 0 to 1 [Balaji and Prabu (2018b)]. The PDF of the Malaga distributed channel is given by [Balaji and Prabu (2018a)]

$$f_{\gamma_2}(\gamma) = \frac{g^2 A}{2\gamma} \sum_{m=1}^{\beta_2} a_m B^{-\left(\frac{\alpha_2+m}{2}\right)} \mathrm{G}_{1,3}^{3,0}\left(\frac{B\,\gamma}{A_0 P_l^F}\,\middle|\,\begin{matrix} g^2+1 \\ g^2,\ \alpha_2,\ m \end{matrix}\right) \tag{3.3}$$

where

$$B = \frac{\alpha_2 \beta_2}{\xi\beta_2 + \Omega'}$$

P_l^F is the path loss of FSO channel and is determined by Beer-Lambert's law as

$$P_l^F = e^{-\sigma L}$$

The parameter σ is the attenuation coefficient, and L is the link distance. The path loss for the UWOC link and FSO link for different atmospheric conditions are given in Table 3.2 and Table 3.3. The parameter R in Table 3.3 represents the rainfall rate in mm/hr. The attenuation coefficient calculation for rain is mentioned in Table 3.4 [Soni (2018)].

Table 3.2: Path loss of 20m UWOC link (λ=530nm).

Water type	$c(\lambda)(m^{-1})$	P_l^U (dB)
Clear ocean	0.151	0.4989
Coastal ocean	0.399	0.1592
Turbid harbor	2.195	4.0738×10^{-5}

$$A \triangleq \frac{2\alpha_2^{\frac{\alpha_2}{2}}}{\xi^{1+\frac{\alpha_2}{2}}\Gamma(\alpha_2)}\left(\frac{\xi\beta_2}{\xi\beta_2+\Omega'}\right)^{\beta_2+\frac{\alpha_2}{2}}$$

$$a_m \triangleq \binom{\beta_2-1}{m-1}\frac{(\xi\beta_2+\Omega')^{1-\frac{m}{2}}}{(m-1)!}\left(\frac{\Omega'}{\xi}\right)^{m-1}\left(\frac{\alpha_2}{\beta_2}\right)^{\frac{m}{2}}$$

The parameter α_2 is a positive value related to the number of enlarged scattering cells in the atmosphere, β_2 is a natural number, which signifies the measure of fading suffered by the signal. The parameter g in Eq. (3.3) represents the pointing error

Table 3.3: Path loss of 2Km FSO link (λ=1550nm).

Atmosphere condition	Attenuation coefficient, σ (dB/Km)	P_l^F (dB)
Very clear air	0.0647	0.9706
Drizzle	0.2208	0.9033
Haze	0.7360	0.7125
Light Fog	4.2850	0.1390
Moderate fog	25.5160	7.885×10^{-6}
Mean rain (R=4)	0.7639	0.7034
Mean rain (R=5)	0.8793	0.6670
Strong rain (R=7)	0.5554	0.7743

Table 3.4: Attenuation coefficient of Rain for FSO link (λ=1550nm) Soni (2018)

Types of rain	Relationship
Light (R < 3.8mm/hr)	0.509 $R^{0.63}$
Mean (3.8 < R < 7.6mm/hr)	0.319 $R^{0.63}$
Strong (R < 7.6mm/hr)	0.163 $R^{0.63}$

and is defined as $g = \frac{w_{zeq}}{2\sigma}$. Here $w_{zeq} = \left[\frac{\sqrt{\pi}erf(v)w_z^2}{2ve^{-v^2}}\right]^{\frac{1}{2}}$ and w_z of w_{zeq} is the beam width at a distance L. The parameter $\xi = E[|U_S^G|^2] = 2(1-\rho)b_0$ and $\Omega' = \Omega + 2\rho b_0 + 2\sqrt{2b_0\rho\Omega}cos(\phi_A - \phi_B)$ which represents the average power from the coherent contributions. The angles ϕ_A and ϕ_B are, the deterministic phases of the LOS and the coupled-to-LOS components. $\Gamma(.)$ is the Gamma function and is defined in [Jeffrey and Zwillinger (2007), Eq. (8.310)]. The CDF of Eq. (3.3) is

$$F_{\gamma_2}(\gamma) = \frac{g^2 A}{2} \sum_{m=1}^{\beta_2} a_m B^{-\left(\frac{\alpha_2+m}{2}\right)} \mathrm{G}_{2,4}^{3,1}\left(\frac{B\,\gamma}{A_0 P_l^F}\,\middle|\,\begin{array}{c} g^2+1,\ 1 \\ g^2,\ \alpha_2,\ m,\ 0 \end{array}\right) \tag{3.4}$$

3.4 Statistical Analysis

The PDF of the end-to-end system can be expressed in terms of the equivalent signal-to-noise ratio (SNR), γ as [Vellakudiyan *et al.* (2019)]

$$f_\gamma(\gamma) = f_{\gamma_1}(\gamma) + f_{\gamma_2}(\gamma) - f_{\gamma_1}(\gamma)F_{\gamma_2}(\gamma) - F_{\gamma_1}(\gamma)f_{\gamma_2}(\gamma) \tag{3.5}$$

after substituting Eqs. (3.1) - (3.4) in Eq. (3.5) the PDF of the end-to-end system can be expressed as

$$
\begin{aligned}
f_\gamma(\gamma) = {} & \frac{\alpha_1\beta_1 g^2}{A_0 P_l^U \Gamma(\alpha_1)\Gamma(\beta_1)} \; \mathrm{G}_{1,3}^{3,0}\left(\frac{\alpha_1\beta_1\gamma}{A_0 P_l^U}\;\middle|\; \begin{matrix} g^2 \\ g^2-1,\; \alpha_1-1,\; \beta_1-1 \end{matrix}\right) \\
& + \frac{g^2 A}{2\gamma}\sum_{m=1}^{\beta_2} a_m B^{-\left(\frac{\alpha_2+m}{2}\right)}\mathrm{G}_{1,3}^{3,0}\left(\frac{B\,\gamma}{A_0 P_l^F}\;\middle|\; \begin{matrix} g^2+1 \\ g^2,\; \alpha_2,\; m \end{matrix}\right) \\
& - \frac{\alpha_1\beta_1 g^2}{A_0 P_l^U \Gamma(\alpha_1)\Gamma(\beta_1)} \; \mathrm{G}_{1,3}^{3,0}\left(\frac{\alpha_1\beta_1\gamma}{A_0 P_l^U}\;\middle|\; \begin{matrix} g^2 \\ g^2-1,\; \alpha_1-1,\; \beta_1-1 \end{matrix}\right) \\
& \frac{g^2 A}{2}\sum_{m=1}^{\beta_2} a_m B^{-\left(\frac{\alpha_2+m}{2}\right)}\mathrm{G}_{2,4}^{3,1}\left(\frac{B\,\gamma}{A_0 P_l^F}\;\middle|\; \begin{matrix} g^2+1,\; 1 \\ g^2,\; \alpha_2,\; m,\; 0 \end{matrix}\right) \\
& - \frac{\alpha_1\beta_1 g^2}{A_0 P_l^U \Gamma(\alpha_1)\Gamma(\beta_1)} \; \gamma \; \mathrm{G}_{2,4}^{3,1}\left(\frac{\alpha_1\beta_1\gamma}{A_0 P_l^U}\;\middle|\; \begin{matrix} g^2,\; 0 \\ g^2-1,\; \alpha_1-1,\; \beta_1-1,\; -1 \end{matrix}\right) \\
& \frac{g^2 A}{2\gamma}\sum_{m=1}^{\beta_2} a_m B^{-\left(\frac{\alpha_2+m}{2}\right)}\mathrm{G}_{1,3}^{3,0}\left(\frac{B\,\gamma}{A_0 P_l^F}\;\middle|\; \begin{matrix} g^2+1 \\ g^2,\; \alpha_2,\; m \end{matrix}\right) \tag{3.6}
\end{aligned}
$$

3.5 Asymptotic Bit Error Rate

The ABER of the overall system can be expressed as [Fu and Du (2018)]

$$P_e = \int_0^\infty f_\gamma(\gamma)\; P_{ec}(\gamma)\; d\gamma \tag{3.7}$$

For DPSK modulation, probability of conditional BER is represented as [Kiasaleh (2006)]

$$P_{ec}(\gamma) = 0.5 \ \exp\left(-\frac{\eta A_d T}{P\nu}\gamma\right) \tag{3.8}$$

where η denotes the quantum efficiency of the detector, A_d is the area of the detector in m^2, T is the DPSK symbol duration rate in seconds, P is the Planck's constant, and ν is the received signal frequency in Hz.

On substituting Eqs. (3.6) and (3.8) in (3.7) and solving the equation using the formula of integration by parts and [Adamchik and Marichev (1990), Eqs. 22 and 26], we get

$$
\begin{aligned}
P_e = \ &\frac{\alpha_1 \beta_1 g^2 P\upsilon}{2 \ A_0 \ P_l^U \ \Gamma(\alpha_1)\Gamma(\beta_1)\eta A_d T} \ \mathrm{G}_{2,3}^{3,1}\left(\frac{\alpha_1 \beta_1 P\upsilon}{A_0 \ P_l^U \ \eta A_d T}\ \middle|\ \begin{matrix} g^2, \ 0 \\ g^2 - 1, \ \alpha_1 - 1, \ \beta_1 - 1 \end{matrix}\right) \\
&+ \frac{g^2 \ A}{4}\sum_{m=1}^{\beta_2} a_m B^{-\left(\frac{\alpha_2 + m}{2}\right)}\mathrm{G}_{2,3}^{3,1}\left(\frac{B P\upsilon}{A_0 \ P_l^F \ \eta A_d T}\ \middle|\ \begin{matrix} g^2 + 1, 1 \\ g^2, \ \alpha_2, \ m \end{matrix}\right)
\end{aligned} \tag{3.9}
$$

3.6 Results and Discussion

In this section, we illustrate the analytical results derived in the previous sections.We evaluate the ABER performance of the proposed system in terms of SNR for different values of turbulence parameters α and β, pointing error parameter g, and link distance L. The analytical results are validated with Monte carlo simulations. Some of the important used simulation parameters are outlined as follows. The path loss of UWOC and FSO links is considered with the normalized transmitted power, i.e., $\Omega + 2b_0 = 1$. We considered these parameters as $\Omega = 0.5$, $b_0 = 0.25$ and $\rho = 0.25$. The values of these parameters are considered based on the results of [Jurado-Navas et al. (2011a)]. The normalized jitter $\frac{\sigma}{a} = 3$ and normalized beam width $\frac{w_z}{a} = 20$ [Balaji and Prabu (2018a)]. The parameters α and β are associated with the atmospheric turbulence of the channel. Lower values of α and β indicate the strong turbulence and greater values indicate the weak turbulence [Uysal et al. (2006), Popoola and Ghassemlooy (2009)]. Always the relationship $\alpha > \beta$ is to be maintained [Wang and Cheng (2010)]. The different turbulence conditions like weak turbulence (WT), moderate turbulence (MT), and strong turbulence (ST) are considered based on the values of α

and β for both UWOC and FSO links as shown in Table 3.5.

Table 3.5: Turbulence cases

Turbulence Condition	Parameters
WT	$\alpha = 10,\ \beta = 5$
MT	$\alpha = 4.1,\ \beta = 2$
ST	$\alpha = 2,\ \beta = 1$
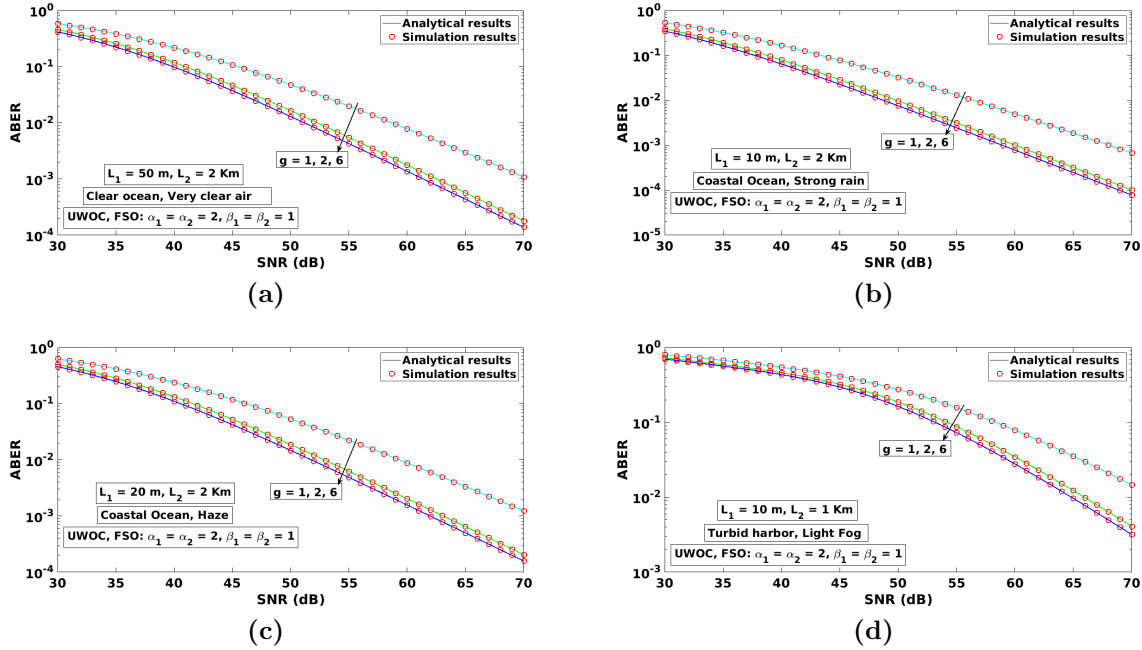
Figure 3.2: ABER versus SNR for different weather conditions based on pointing errors for (a) clear ocean and very clear air conditions; (b) coastal ocean and strong rain conditions; (c) coastal ocean and haze conditions; and (d) turbid harbor and light fog conditions.

Fig. 3.2 depicts the end-to-end ABER performance of the proposed system. The different underwater and FSO environments considered in this analysis are (clear ocean, very clear air), (coastal ocean, strong rain), (coastal ocean, haze), (turbid harbor, light fog) as depicted in figures 3.2a to 3.2d respectively. Figures 3.2a and 3.2b show the ABER performance of the end-to-end system for 2 km of FSO link length and varying UWOC link length. We varied the pointing error parameter from

strong to weak considering the strong turbulence scenario. From the Fig. 3.2 it can be observed that, from weak to strong pointing errors, clear to turbid harbor and very clear air to fog, the ABER decreases. For example, the ABER of 10^{-2} is achieved at SNR of 50 dB for $g = 6$ in clear ocean environment. An additional SNR of 15 dB is required to achieve the same ABER in the turbid harbor environment.
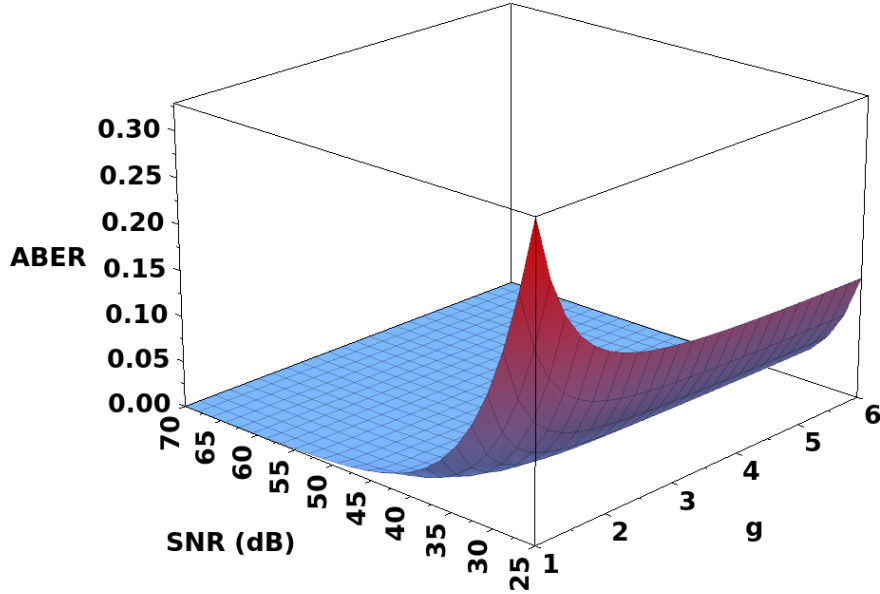
Figure 3.3: ABER versus SNR versus g for clear ocean and very clear air conditions

Fig. 3.3 illustrates a 3-dimensional plot for ABER with the variation of SNR and pointing error parameter g. The SNR is varied from 25 dB to 70 dB. The parameter g is varied from 1 to 6. With an increase in SNR and g, there is a decrease in ABER. For the least values of g and SNR, the ABER is at peak.

Fig. 3.4 presents the ABER analysis of the convergent UWOC-FSO system for clear ocean (a,b), coastal ocean (c,d) and turbid harbor (e,f) scenarios by considering the strong turbulence over FSO link. Fig. 3.4a shows the performance of the end-to-end system for the clear ocean and very clear air conditions. The path losses and link distances of UWOC and FSO links are considered as 0.4989 dB, 0.9706 dB and 20 m, 2 Km respectively. In this case, the ABER is analyzed by varying the turbulence parameters of the UWOC link with pointing error parameter g. As the α_1, β_1, and g increases, the ABER is decreasing. Fig. 3.4b gives ABER analysis for 50 m of clear ocean and 1 Km of light fog conditions. The path loss values are 0.1758 and 0.3728 for UWOC and FSO links. Here also we varied the turbulence parameters of UWOC
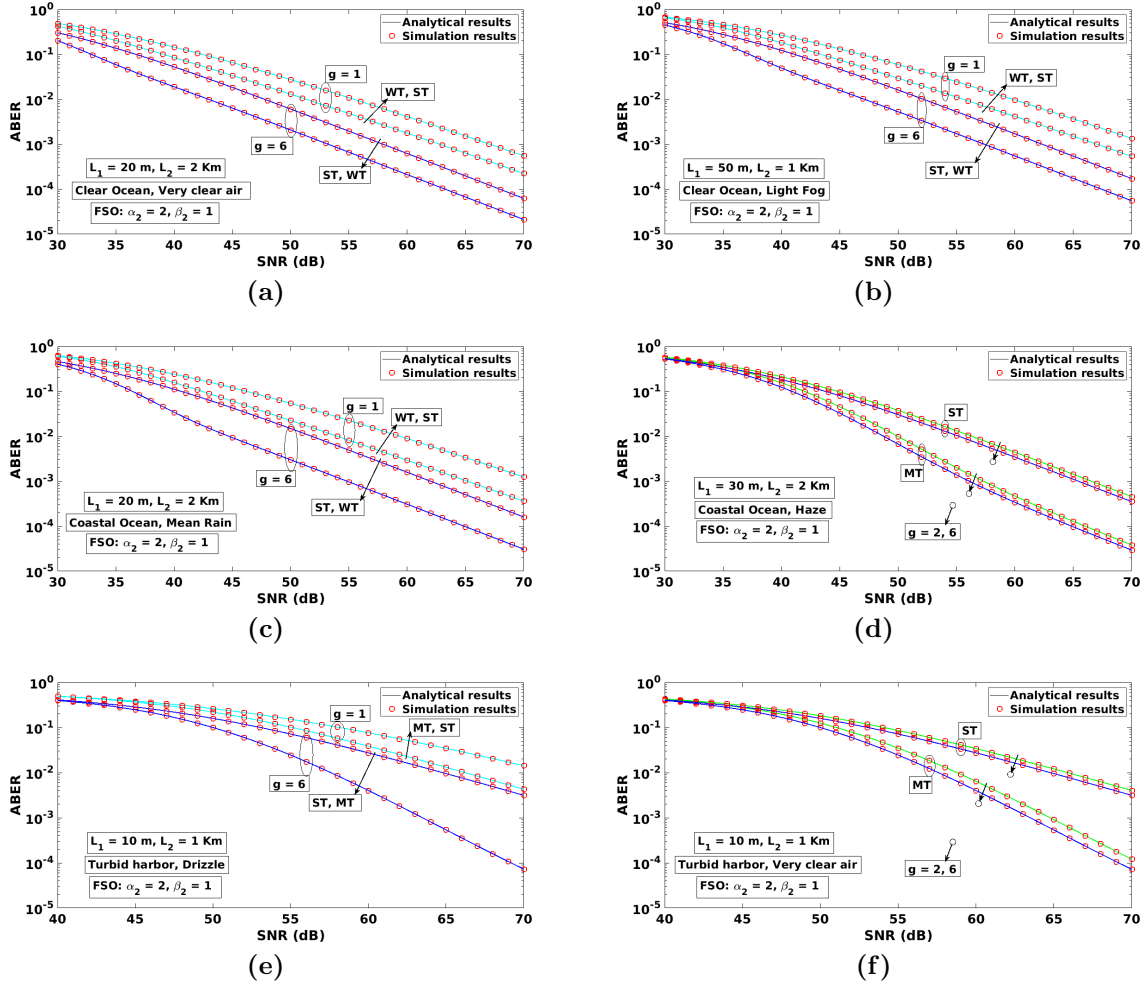
Figure 3.4: ABER versus SNR for different UWOC turbulence conditions along with pointing errors for (a) clear ocean and very clear air conditions; (b) clear ocean and light fog conditions; (c) coastal ocean and mean rain conditions; (d) coastal ocean and haze conditions; (e) turbid harbor and drizzle conditions; and (f) turbid harbor and very clear air conditions.

with pointing errors. Under weak turbulence condition, for $g = 1$ case, it is observed that the ABER is greater than 10^{-2} at 55dB of SNR. In the same environment, for $g = 6$, the ABER is approximately equal to 10^{-3}.

Figs. 3.4c and 3.4d show the ABER performance of the proposed system for the coastal ocean; moderate rain and haze conditions of FSO link over the strong turbulence case. The figure shows that with a change in the pointing error parameter g and UWOC turbulence parameters, there is a considerable change in the ABER performance of the end-to-end system. The figures also show that, during moderate rain, the performance is slightly better than that of haze conditions.

Figs. 3.4e and 3.4f illustrate the ABER performance of the proposed FSO-UWOC system for the UWOC link having turbid harbor water, drizzle, and clear air scenarios of FSO link. We consider the strong turbulence over the FSO link, varying the pointing error parameter and UWOC turbulence. The results show that larger SNR values are required to improve the system's performance under the turbid harbor scenario.
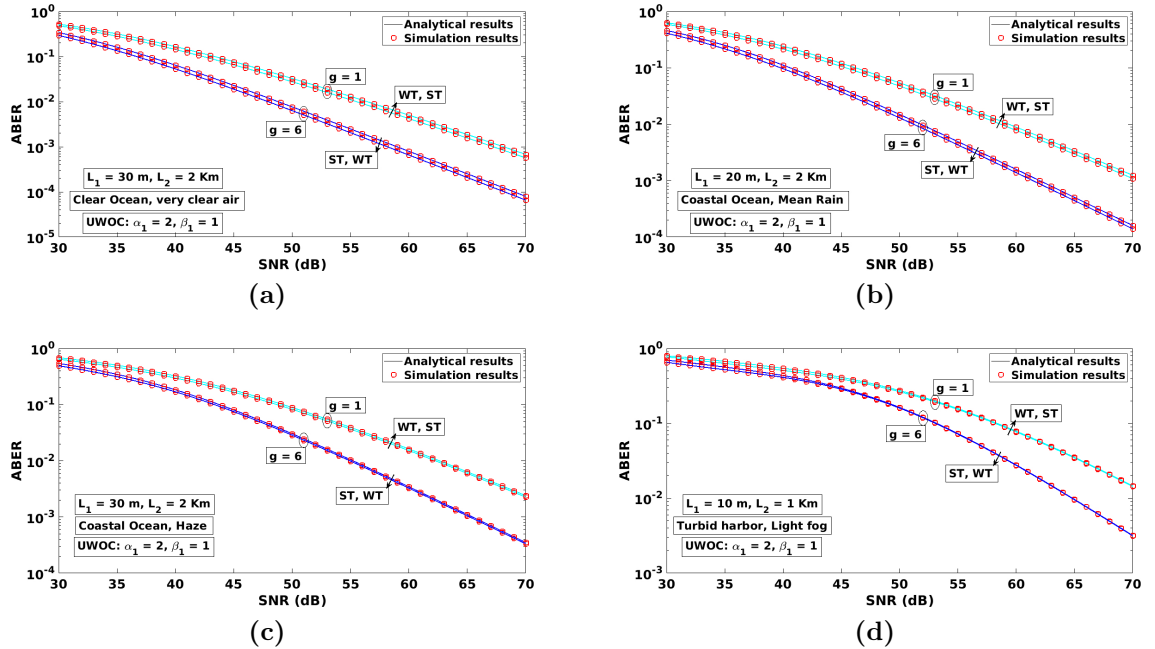
Figure 3.5: ABER versus SNR for different FSO turbulence conditions along with pointing errors for (a) clear ocean and very clear air conditions; (b) coastal ocean and mean rain conditions; (c) coastal ocean and haze conditions; and (d) turbid harbor and light fog conditions.

The ABER analysis of the proposed convergent UWOC-FSO system is analyzed for

strong UWOC turbulence conditions with the variations of different FSO turbulence conditions, pointing errors. The different underwater and FSO environments considered in this analysis are like (clear ocean, very clear air), (coastal ocean, mean rain), (coastal ocean, haze), (turbid harbor, light fog) as depicted in figures 3.5a to 3.5d respectively. Fig. 3.5a portrays ABER analysis for 30 m clear ocean with path loss of $P_l^U = 0.3524$ dB and 2 Km FSO link in very clear air with path loss of $P_l^F = 0.9706$ dB. At 30 dB of SNR, the ABER is almost equal for all the variations in g, α_2, and β_2. At 70 dB of SNR, ABER is lesser than 10^{-4}.

Figs. 3.5b and 3.5c depicts the ABER performance of the end-to-end system over coastal ocean water. We consider the 2 Km FSO link length and 20 m and 30 m UWOC link lengths in this case. These figures show that the ABER of 10^{-3} is achieved at SNR of 60 dB in a mean rain FSO link environment. An additional 5 dB of SNR is required to achieve the same ABER performance in a haze FSO link environment. The results also show that the weak pointing error scenario improves system performance compared to the strong pointing error.
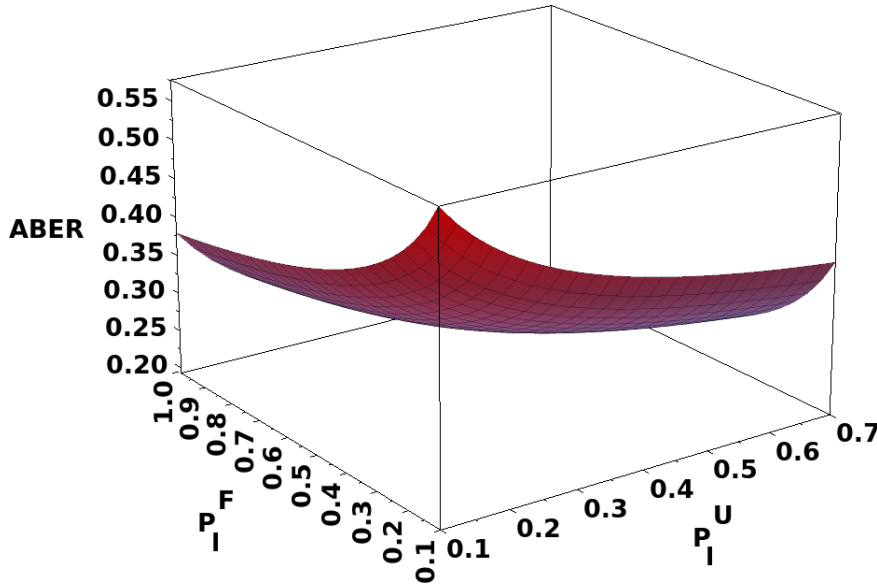
Figure 3.6: ABER versus P_l^F versus P_l^U for all oceanic and free-space weather conditions.

Fig. 3.5d depicts the ABER performance of end-to-end system in turbid harbor environment. The link ranges of UWOC and FSO are considered as 10 m and 1 Km, the corresponding path losses are 0.0064 dB and 0.3728 dB respectively. From this figure, it is observed that the ABER is greater than 10^{-2} for $g = 1$, and decreases as

g increases.

Fig. 3.6 shows the performance of the overall system when the turbulence parameters of UWOC and FSO links made constant. The P_l^U is varied from 0.1 dB to 0.7 dB, and P_l^F is varied from 0.1 dB to 1.0 dB. The ABER is at a peak when the path loss of both UWOC and FSO links is minimum, and it decreases as the path loss increases.

3.7 Summary

This chapter uses a novel closed-form ABER expression for the proposed convergent UWOC-FSO system. The simulation results are plotted and analyzed for weak, moderate, and ST regimes with the various levels of scatterings for both UWOC and FSO links. The results were further analyzed for different environments of UWOC and FSO links with the different levels of pointing errors. The results also show the performance degradation of the system in the case of turbid harbors compared to clear and coastal ocean scenarios. The proposed convergent UWOC-FSO system can be helpful in UWSN, oceanography, disaster precaution, and military applications.

Chapter 4

ABER Analysis of Dual-hop convergent FSO-UWOC System Using MIMO

4.1 Introduction

Free-space optical (FSO) communication and underwater wireless optical communication (UWOC) fall under the wireless optical communication (WOC) technology and are useful for indoor, outdoor terrestrial, space communications, and underwater communications. Recently in Ref. [Chowdhury *et al.* (2020)], hybrid wireless optical networks were proposed. A hybrid network forms by converging one network/communication link with another, such as an RF link with an optical link or an optical link with another optical link. These convergent/hybrid systems (RF/FSO, RF/UWOC, RF-UWOC, and UWOC-FSO) with single-hop, dual-hop, and multi-hops were proposed by many researchers all over the world.

Water on planet Earth is fantastic, without which people cannot survive. Also, oceans are doing an excellent job, such as providing oxygen, food, transportation, mineral resources, etc. Hence, people started researching oceanic things. Marine research is happening underwater on ocean observation, shallow water tracking, search and relocation, oil and gas explorations, ocean currents, and seismic events.[Online (-)]

Without a communication system or human interaction, the gathered underwater information will not reach the base station or research center. For this, a convergent UWOC-FSO communication system is a better platform to transfer the data. Convergent UWOC-FSO systems find the applications in the research areas as mentioned earlier as well as internet of underwater things (IoUT) such as fish farms, aquari-

ums, oceanography, and defense [Domingo (2012)]. IoUT works with different sensors to sense water quality, temperature, pressure level, chemical properties, and organic elements. Remotely operated vehicles, light autonomous underwater vehicles, sinks (ships, buoys, or autonomous surface vehicles) are also part of IoUTs. The data accumulated by the sinks are forwarded to the remote monitoring center at the seashore to analyze and perform the necessary operations that are needed [Kao *et al.* (2017*a*)].

Several techniques have been proposed to diminish the fading effect over the years, such as spatial diversity and multi-hop relaying transmission. As link distance and turbulence strength are proportional to each other, using relays will be a solution to reduce the fading. Multiple-input multiple-output (MIMO) is considered a promising technology to mitigate the effects of fading and has been proven to improve the channels' communication reliability through spatial diversity. Researchers are motivated toward the MIMO technology because of its advantages in incorporating multiple transmit and receiving apertures in FSO communication systems. Over several years, the literature shows many statistical models to describe the FSO fading channels, which are used with a specific range of turbulence conditions. Gamma–Gamma (GG) fading model has proven under moderate to strong turbulence (ST) conditions and is widely adopted for FSO channels [Pham *et al.* (2018), Niu *et al.* (2013)].

During the last decade, there is a considerable amount of research toward the MIMO-based WOC links over terrestrial and underwater channels. In Ref. [Jamali *et al.* (2016*b*)], the authors investigated MIMO-based UWOC systems' performance with on-off keying using a lognormal fading channel. Ramavath et al. evaluated the end-to-end bit error rate (BER) performance of an RS-coded MIMO-based UWOC system [Ramavath *et al.* (2020)]. Authors in Ref. [Song *et al.* (2017)] showed an experimental demonstration on the MIMO-OFDM 2-m UWOC system and achieved a data rate of 33.691 Mb/s using low-cost blue light-emitting diodes, 10-MHz PIN photodiodes. UWOC systems' performance using MIMO channel models has been thoroughly studied in Refs. [Jamali *et al.* (2018)] and [Nezamalhosseini and Chen (2020)].

Prabu et al. performed a detailed analysis of end-to-end system performance in terms of average BER over spatially diversified-FSO links using differential phase shift keying-subcarrier intensity modulation, coherent binary polarization shift keying, binary phase shift keying-subcarrier intensity modulation in GG fading channel with pointing errors (PE) [Prabu and Kumar (2014), Prabu *et al.* (2014*a*), Prabu and

Kumar (2015)]. In Ref. [Jaiswal *et al.* (2019)], the authors proposed a generalized LASER-based MIMO setup employing differential optical spatial modulation (DOSM) with R-ary PAM called DOSM-PAM scheme, over different turbulence conditions. The instantaneous symbol error rate and diversity order are analytically derived for the proposed system over GG and negative exponential channel models using Monte–Carlo simulations. The authors also investigated a special case of DOSM, called differential optical space shift keying.

Researchers started working on relay-assisted RF-FSO, RF-UWOC, and FSO-UWOC systems a few years ago. The dual-hop and multi-hop systems have recently received much attention as they simultaneously achieve the advantages of different technologies. In Refs. [Vellakudiyan *et al.* (2016)] and [Vellakudiyan *et al.* (2019)], the authors proposed a dual-hop RF/FSO system and analyzed the end-to-end system's performance. The RF link was Rayleigh distributed, and the FSO link was M-distributed. Results are plotted in the presence of turbulence as well as PEs using analytical equations. In Ref. [Li *et al.* (2020*b*)], the authors examined an RF-UWOC system's performance in terms of the outage, capacity, and BER. In contrast, using both decode-and-forward (DF) and amplify-and-forward (AF) relaying, mixed RF-UWOC systems' performance was investigated in Ref. [Naik *et al.* (2020)].

An AF-based FSO-UWOC system provides high-speed optical connectivity between onshore and submerge systems proposed and investigated [Jurado-Navas *et al.* (2019)]. A DF-based multisensor mixed UWOC-FSO system was considered in Ref. [Christopoulou *et al.* (2019)] and analyzed the end-to-end system's outage performance. The authors in Ref. [Levidala and Krishnan (2020)] recently proposed a convergent UWOC–FSO system. GG distribution was employed for describing the UWOC link and Malaga distribution for the FSO link. Such a model considered attenuation, turbulence, and PE effects into account to analyze the asymptotic BER. A multihop convergent FSO–UWOC system establishes communication between islands with a DF relay based on the proposed Malaga and GG distributions [Kumar and Krishnan (2020)].

Li et al. proposed and demonstrated a wavelength-division-multiplexing and four-level pulse amplitude modulation (PAM4) FSO–UWOC convergent system. Using 405- and 450-nm laser diodes with 500-m FSO links and 5-m UWOC links, they achieved a 100-Gb/s channel capacity [Li *et al.* (2020*a*)]. In Ref. [Tsai *et al.* (2020)], the authors proposed and experimentally demonstrated a 500-Gb/s PAM4 FSO–UWOC

converging system over 100-m free-space transmission with either 10-m piped underwater link or 5-m turbid underwater link. They employed a five-wavelength red/green/blue (R/G/B) polarization-multiplexing scheme to demonstrate and achieve an aggregate data rate of 500 Gb/s.

Recently, in Ref. [Yang *et al.* (2021)], the authors proposed a dual-hop FSO–UWOC communication system and studied its performance considering a clear ocean environment. In particular, the authors analyzed the outage probability, average bit error rate (ABER), and average capacity for both HD and IM/DD detection schemes considering an AF relay in the presence of misalignment fading. Sarma et al. proposed a DF-based triple-hop RF–FSO–UWOC communication system in Ref. [Sarma *et al.* (2020)] and analyzed BER and outage probability performance with closed-form expressions. All channel impairments such as weather conditions, atmospheric turbulence, and PEs for FSO and oceanic turbulence and PE cases for UWOC links are not considered in the literature's dual-hop FSO underwater optical links-related works. For the first time in UWOC, we examined the impact of all of these effects on end-to-end system performance and mitigated them using MIMO techniques.

Varshney et al. performed research on cognitive DF MIMO-RF/FSO cooperative relay systems. The authors proposed a dual-hop RF/FSO system, where the MIMO-RF link is Rayleigh faded between the source and relay, and the FSO link is GG faded between the relay and destination. The performance analysis is made in terms of BER, outage probability, and ergodic capacity [Varshney and Jagannatham (2017), Varshney and Puri (2017), Varshney *et al.* (2018)].

The contributions of this chapter are as follows:

- We proposed a novel MIMO based dual-hop convergent UWOC - FSO communication system and derived the expressions for ABER.

- Closed-form expressions for the ABER of both UWOC and FSO links individually derived using the cumulative distribution function (CDF).

- The performance of the proposed system is analyzed under different turbulence, and weather conditions, along with pointing error effects.

- The analysis is carried out with different oceanic conditions such as the clear ocean, coastal ocean, turbid harbor for the UWOC link, and various atmospheric effects such as very clear air, fog, rain, drizzle haze for the FSO link.

- The ABER performance of the end-to-end system is evaluated by varying the number of paths of the individual links.

- A comparison was shown for the single input single output (SISO) based UWOC-FSO convergent system with proposed MIMO based system.

4.2 System model

The proposed dual-hop MIMO-based convergent UWOC-FSO system model is shown in Fig. 4.1. The underwater wireless autonomous vehicle (UWAV) acts as a source, the buoy is considered relaying equipment, and the terrestrial base station is considered a destination. The UWOC and the FSO links are GG distributed.
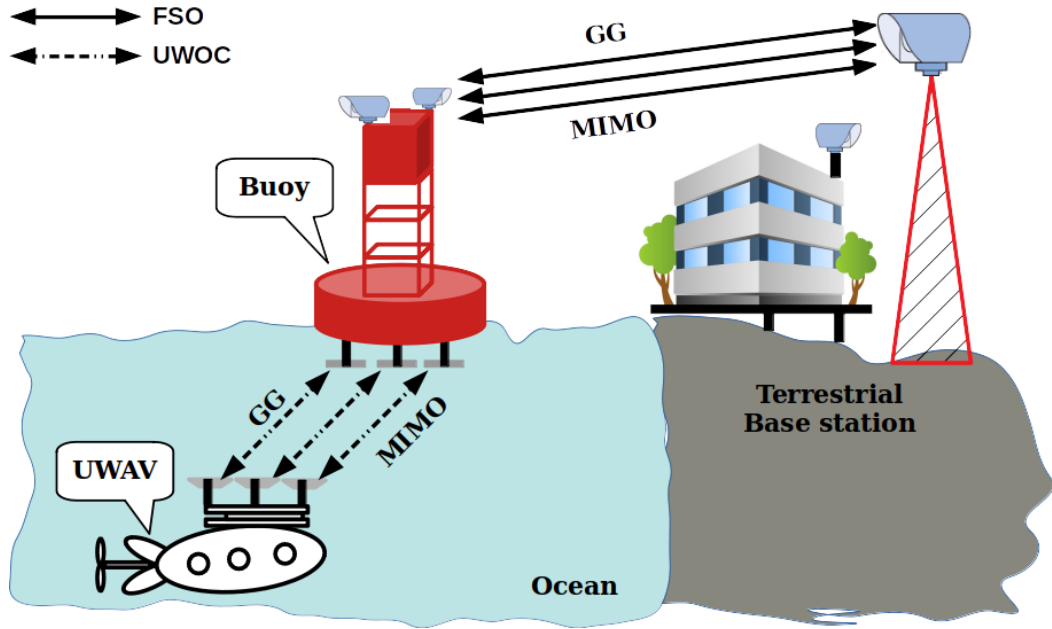
Figure 4.1: System Model

Proposed system consists of M transmitting sources and N detectors. At the receiver, the N optical signals are combined using the equal gain combining (EGC) technique. The data received from the ith source to the jth detector is given as,

$$Y = \sum_{i=1}^{M} \sum_{j=1}^{N} H_{ij}S + n(t) \tag{4.1}$$

where H_{ij} is channel coefficient due to the turbulence, pointing errors and path loss due to attenuation, S is data given from the source and $n(t)$ is additive White

Gaussian noise of zero mean and σ_N^2 variance, which is mainly due to the shot noise [Ramavath *et al.* (2020)].

4.3 Statistical Characteristics

UWOC and FSO channel models realization using SISO and MIMO systems are presented in this Section.

4.3.1 SISO channel models: UWOC and FSO

The generalized turbulence perturbing to UWOC and FSO channels under the influence of pointing errors and path loss is obtained using Gamma-Gamma (GG) CDF is obtained from [Sandalidis *et al.* (2009)], and modified as follows.

$$F_\gamma(\gamma) = \frac{g^2}{\Gamma(\alpha)\Gamma(\beta)} G_{2,4}^{3,1}\left(\begin{smallmatrix} 1,g^2+1 \\ g^2,\alpha,\beta,0 \end{smallmatrix} \middle| \frac{\alpha\beta g^2}{h_l\bar\gamma(g^2+1)}\right) \tag{4.2}$$

where, g is the pointing error parameter, α and β are the scintillation parameters given below, $\Gamma(.)$ is the gamma function, h_l is the path loss produced by the attenuation coefficients of UWOC and FSO channels given in Eqs. (4.4) and (4.5), $\bar\gamma$ is the average received SNR and scintillation index parameters are,

$$\alpha = \left[\exp\left(\frac{0.49\sigma_R^2}{\left(1+1.11\sigma_R^{12/5}\right)^{7/6}}\right) - 1\right]^{-1}$$

$$\beta = \left[\exp\left(\frac{0.51\sigma_R^2}{\left(1+0.69\sigma_R^{12/5}\right)^{5/6}}\right) - 1\right]^{-1}$$

σ_R^2 is the Rytov variance and is calculated as,

$$\sigma_R^2 = 1.23 \; C_n^2(Z) \; k^{7/6} \; L^{11/6} \tag{4.3}$$

where $k = \frac{2\pi}{\lambda}$ is the wave number, λ is wavelength, and $C_n^2(Z)$ is refractive-index structure parameter dependent on height of the transmitter or receiver (Z) typically varies from $10^{-13}m^{-2/3}$ to $10^{-17}m^{-2/3}$ for strong turbulence to weak turbulence regimes [Kaushal and Kaddoum (2016a)].

The path loss value of UWOC system can be obtained as [Eq. (10) of Kaushal

and Kaddoum (2016b)],

$$h_u = \exp\left(-c(\lambda)\ L\right) \tag{4.4}$$

where $c(\lambda)$ is the extinction coefficient due to the absorption and scattering losses of the underwater channel and are given in Table 1 of [Levidala and Krishnan (2020)]. The path loss of 30 m for different waters of underwater channel is given in Table 4.1

Table 4.1: Path loss of 30m UWOC link (λ=530nm).

Water type	$c(\lambda)(m^{-1})$	h_u (dB)
Clear ocean	0.151	0.3524
Coastal ocean	0.399	0.0635
Turbid harbor	2.195	2.6002×10^{-7}

The path loss value of FSO system can be obtained as [Eq. (1) of Prabu and Kumar (2015)],

$$h_f = \exp\left(-\sigma\ L\right) \tag{4.5}$$

The parameter σ in Eq. (4.5) is the attenuation coefficient of FSO channel. Table 3 of [Levidala and Krishnan (2020)] gives the path loss of 2 Km FSO link.

4.3.2   MIMO channel models: UWOC and FSO

The CDF of MIMO based UWOC and/or FSO system is,

$$F_\gamma(\gamma) = \frac{g^2}{\Gamma\left(\bar{\alpha}\right)\Gamma\left(\bar{\beta}\right)} \mathrm{G}_{2,4}^{3,1}\left(\begin{matrix} 1,g^2+1 \\ g^2,\bar{\alpha},\bar{\beta},0 \end{matrix}\middle|\frac{\bar{\alpha}\bar{\beta}g^2}{h_l\bar{\gamma}\left(g^2+1\right)}\right) \tag{4.6}$$

where $\bar{\alpha} = h\alpha$, $\bar{\beta} = h\beta$, $h = K\left(1+\frac{2}{K}\rho\right)^{-1}$ [Pham et al. (2018)], $K = MN$ is number of transmit-receive paths, ρ is correlation coefficient.

4.3.3   ABER Analysis

The ABER for the proposed system can be calculated using the following equation [Anees and Deka (2019)],

$$P_e = P_e^U(1 - P_e^F) + P_e^F(1 - P_e^U), \tag{4.7}$$

where P_e^U is the ABER of the UWOC channel and P_e^F is the ABER of the FSO

channel. The ABER of FSO and/or UWOC channel can be calculated as

$$P_e = \frac{q^p}{2\,\Gamma(p)} \int\limits_0^\infty \exp\left(-q\gamma\right)\; \gamma^{p-1}\; F_\gamma(\gamma)\; d\gamma \qquad (4.8)$$

Where

$$p = \begin{cases} 0.5 & \text{for coherent detection} \\ 1 & \text{for non-coherent or differentially,} \end{cases} \qquad (4.9)$$

$$q = \begin{cases} 0.5 & \text{for FSK} \\ 1 & \text{for PSK.} \end{cases} \qquad (4.10)$$

To calculate the ABER of the end-to-end system, individual link ABERs are to be calculated first. The integral value of the Eq. (4.8) is calculated using the Eqs. (21) and (22) of [Adamchik and Marichev (1990)]. Hence the ABER of UWOC communication link is calculated using the following equation.

$$P_e^U = \frac{g_u^2}{2\Gamma(p)\Gamma\left(\bar{\alpha}_u\right)\Gamma\left(\bar{\beta}_u\right)} \mathrm{G}_{3,4}^{3,2} \left(\left. \begin{smallmatrix} 1,1-p,g_u^2+1 \\ g_u^2,\bar{\alpha}_u,\bar{\beta}_u,0 \end{smallmatrix} \right| \frac{\bar{\alpha}_u\bar{\beta}_u g_u^2}{\bar{\gamma}q h_u\left(g_u^2+1\right)} \right) \qquad (4.11)$$

Since the channel model used for the FSO link is also same as UWOC link, the ABER of the FSO channel can be calculated using the Eq. (4.12)

$$P_e^F = \frac{g_f^2}{2\Gamma(p)\Gamma\left(\bar{\alpha}_f\right)\Gamma\left(\bar{\beta}_f\right)} \mathrm{G}_{3,4}^{3,2} \left(\left. \begin{smallmatrix} 1,1-p,g_f^2+1 \\ g_f^2,\bar{\alpha}_f,\bar{\beta}_f,0 \end{smallmatrix} \right| \frac{\bar{\alpha}_f\bar{\beta}_f g_f^2}{\bar{\gamma}q h_f\left(g_f^2+1\right)} \right) \qquad (4.12)$$

After substituting Eqs. (4.11) and (4.12) in (4.7), obtained end-to-end ABER is

given as,

$$
\begin{aligned}
P_e &= \left(\frac{g_u^2}{2\Gamma(p)\Gamma\left(\bar{\alpha}_u\right)\Gamma\left(\bar{\beta}_u\right)} \mathrm{G}_{3,4}^{3,2} \left({}_{g_u^2,\bar{\alpha}_u,\bar{\beta}_u,0}^{1,1-p,g_u^2+1} \, \middle| \, \frac{\bar{\alpha}_u\bar{\beta}_u g_u^2}{\bar{\gamma}qh_u\left(g_u^2+1\right)} \right) \right) \\
&\times \left(1 - \frac{g_f^2}{2\Gamma(p)\Gamma\left(\bar{\alpha}_f\right)\Gamma\left(\bar{\beta}_f\right)} \mathrm{G}_{3,4}^{3,2} \left({}_{g_f^2,\bar{\alpha}_f,\bar{\beta}_f,0}^{1,1-p,g_f^2+1} \, \middle| \, \frac{\bar{\alpha}_f\bar{\beta}_f g_f^2}{\bar{\gamma}qh_f\left(g_f^2+1\right)} \right) \right) \\
&+ \left(\frac{g_f^2}{2\Gamma(p)\Gamma\left(\bar{\alpha}_f\right)\Gamma\left(\bar{\beta}_f\right)} \mathrm{G}_{3,4}^{3,2} \left({}_{g_f^2,\bar{\alpha}_f,\bar{\beta}_f,0}^{1,1-p,g_f^2+1} \, \middle| \, \frac{\bar{\alpha}_f\bar{\beta}_f g_f^2}{\bar{\gamma}qh_f\left(g_f^2+1\right)} \right) \right) \\
&\times \left(1 - \frac{g_u^2}{2\Gamma(p)\Gamma\left(\bar{\alpha}_u\right)\Gamma\left(\bar{\beta}_u\right)} \mathrm{G}_{3,4}^{3,2} \left({}_{g_u^2,\bar{\alpha}_u,\bar{\beta}_u,0}^{1,1-p,g_u^2+1} \, \middle| \, \frac{\bar{\alpha}_u\bar{\beta}_u g_u^2}{\bar{\gamma}qh_u\left(g_u^2+1\right)} \right) \right) \quad (4.13)
\end{aligned}
$$

4.4 Results and Discussions

This section presents the numerical results for the ABER derived in the previous sections. We considered the DPSK modulation scheme and the number of apertures as two in both the UWOC and FSO links to analyze the system performance. The turbulence parameters α and β are considered as 2, 1 for strong turbulence (ST) and 10, 5 for weak turbulence (WT) regimes respectively [Levidala and Krishnan (2020)]. Fig. 4.2 to 4.4 show the results for SIMO system over i.e., for $K = 2$ ($M = 1, N = 2$). Fig. 4.2, illustrates the ABER of strong turbulence (ST) end-to-end system for varying link range, underwater and free space weather conditions, pointing errors (PE) (for ease of analysis we have considered $g_f = g_u = g$, which is 1 for strong PE and 6 for weak PE) and correlation coefficient (ρ, which is 0.2 for highly un-correlated and 0.8 for less un-correlated) conditions with respect to average SNR. The link distance for the clear ocean link is 30 m, for coastal ocean is 20 m, and for turbid harbor is 10 m. Similarly, the FSO link distance is considered as 2 Km for the performance analysis.

The ABER of the proposed end-to-end system for clear oceanic link and FSO link with clear air surface is shown in Fig. 4.2a. Similar to Fig. 4.2a, we have presented various ABER plots for varying link range, ocean water and free space environment type. For a coastal ocean link, free space link with moderate rain is given in Fig. 4.2b. Fig. 4.2c is ABER plot of turbid harbor and light fog free space weather condition. From the Fig. 4.2a and 4.2c, the average SNR requires to reach ABER of 10^{-4} is varies from 32 dB to 49 dB for the systems with the clear ocean and clear air to turbid harbor and light fog system. This is due to the beam attenuation (more specifically scattering) is more in turbid harbor and less visibility in foggy environments compared with the
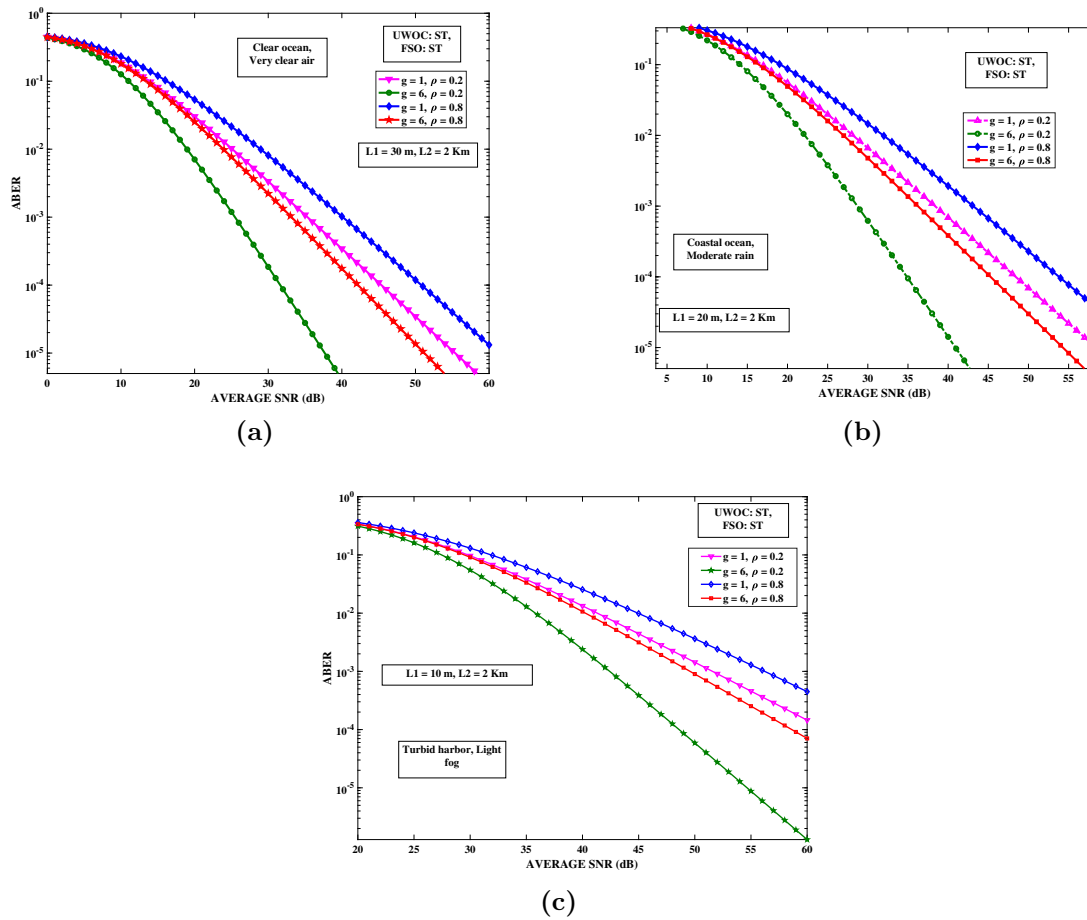
Figure 4.2: ABER versus average SNR for ST conditions of UWOC and FSO with different PEs. (a) For clear ocean and very clear air, (b) for coastal ocean and moderate rain, and (c) for turbid harbor and light fog.

clear ocean and air environments. However, the attenuation effect is less for the free space haze environment, so the average SNR of the end-to-end system is nearer to the clear air environments at a specified ABER value. From Figs. 2a and 2b, the average SNR of the system are 32 dB and 35 dB at ABER of 10^{-4} respectively.
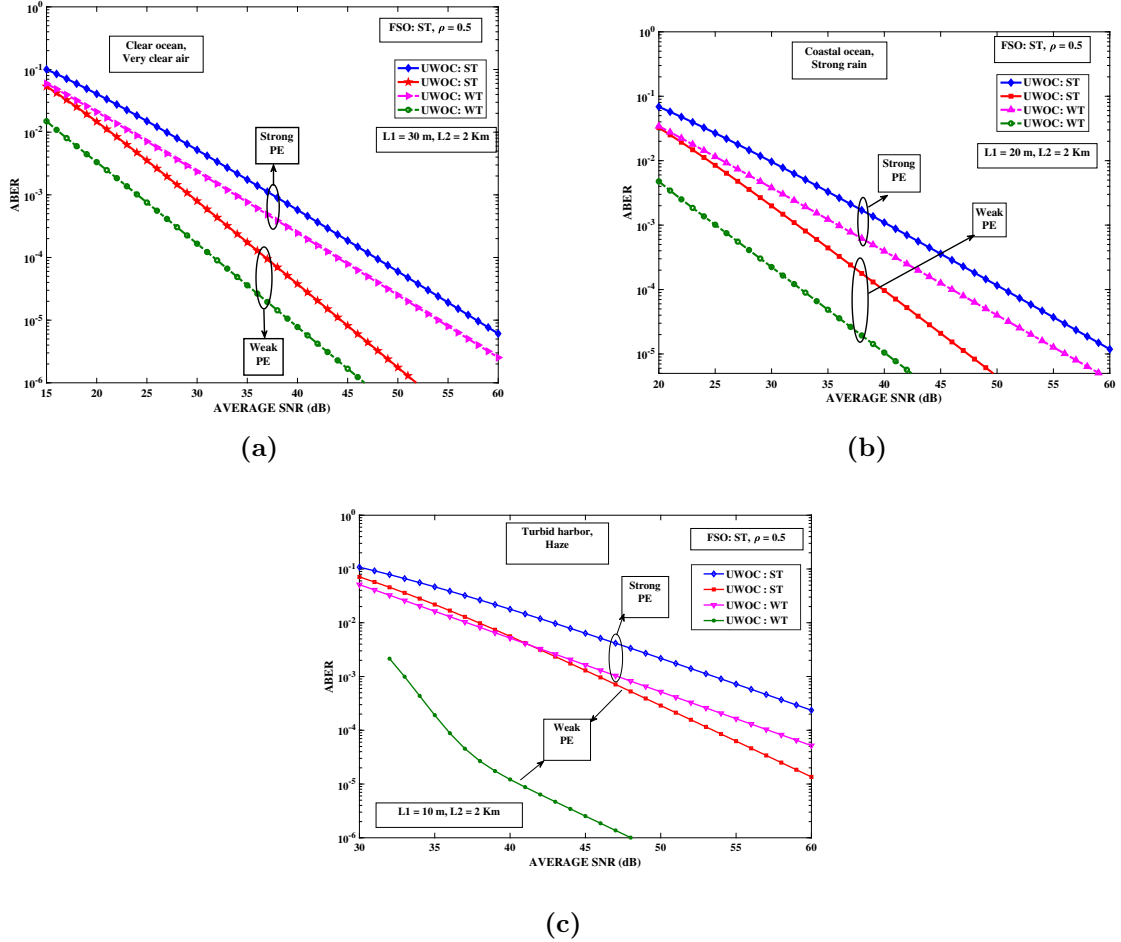
Figure 4.3: ABER versus average SNR for ST FSO conditions with different UWOC turbulence and PEs. (a) For clear ocean and very clear air, (b) for coastal ocean and strong rain, and (c) for turbid harbor and haze.

Fig. 4.3 shows the ABER of proposed end-to-end system for strong turbulence FSO link and varying turbulence UWOC link from weak to strong under the influence of weak and strong pointing errors. Figs. 4.3a and 4.3b are ABER plots for clear ocean UWOC–clear air FSO and coastal ocean UWOC–free space strong rain environments respectively. Average SNR of 32 dB and 35 dB seen from Figs. 4.3a to 4.3b (clear ocean UWOC–clear air FSO to clear ocean UWOC–strong rain FSO system) at ABER

of 10^{-4} respectively. Fig. 4.3c shows the ABER plots for turbid harbor and Haze weather conditions. The ABER of 10^{-3} is achieved with strong pointing errors, and the average SNR varies from 47 dB to 54 dB with respect to the variation in turbulence of UWOC link.
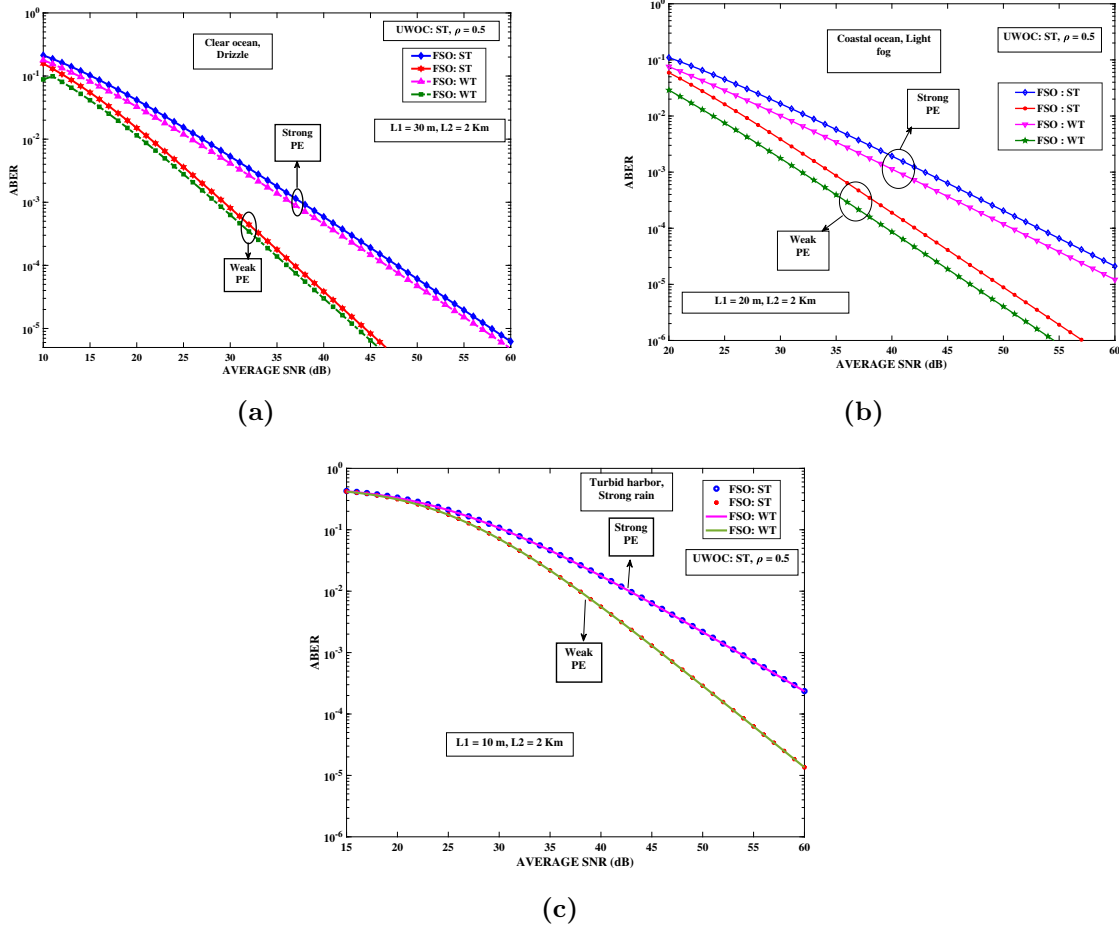
Figure 4.4: ABER versus average SNR for ST UWOC conditions with different FSO turbulence and PEs. (a) For clear ocean and drizzle, (b) for coastal ocean and light fog, and (c) for turbid harbor and strong rain.

Fig. 4.4, shows the ABER for strong turbulence UWOC; weak and strong turbulence FSO system under the influence of varying pointing errors. Average SNR of 0.5 dB difference observed from weak to strong turbulence FSO system. From Figs. 4.4a and 4.4b, the average SNR of 10 dB difference have been observed from clear ocean UWOC–drizzle FSO to coastal ocean UWOC–light fog FSO at ABER of 10^{-4} respectively. Fig. 4.4c depicts the ABER for the turbid harbor and haze weather conditions.

An average SNR of 53 dB is required to achieve an ABER of 10^{-4} in case of UWOC strong turbulence with weak pointing error.
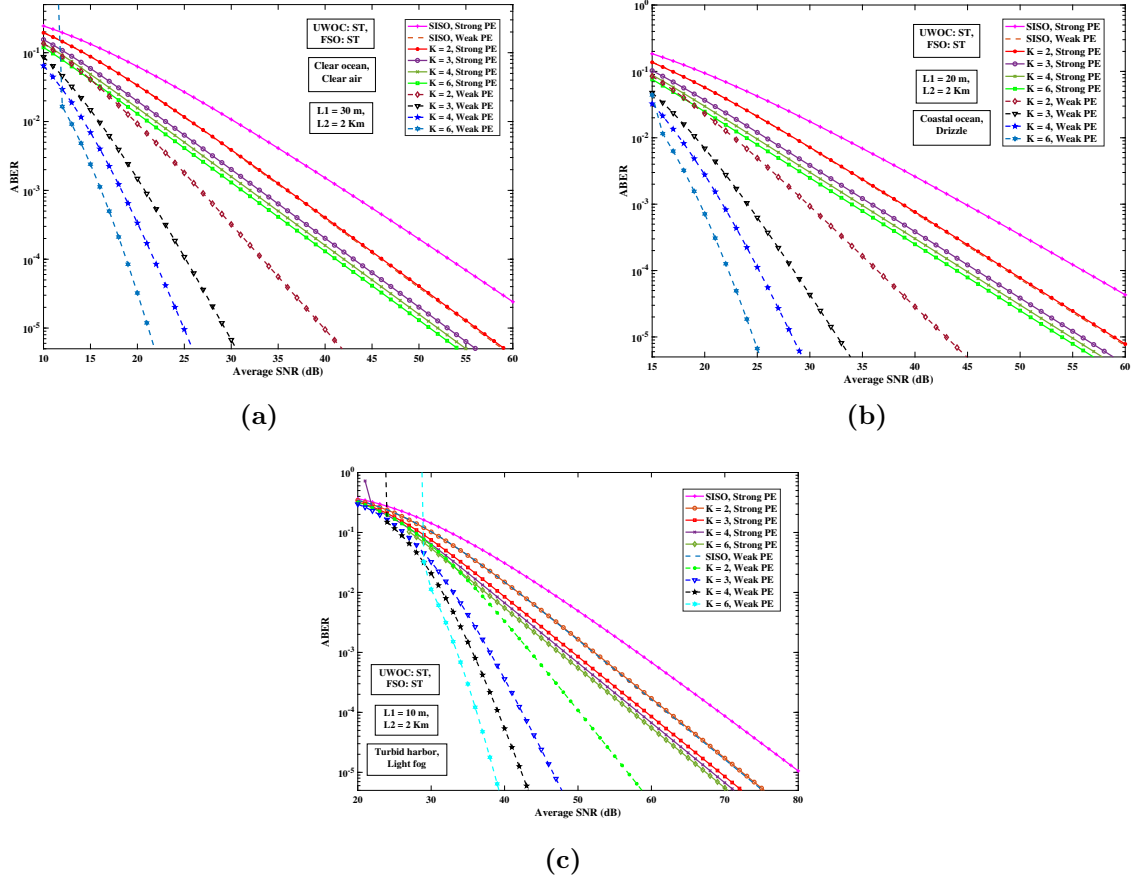
Figure 4.5: Comparison of dual-hop convergent UWOC-FSO system under ST with strong and weak PEs: SISO and MIMO cases: (a) for clear ocean and very clear air, (b) for coastal ocean and drizzle, and (c) for turbid harbor and light fog.

Fig. 4.5, portrays a comparison in the performance of the proposed system with single communication links (SISO) in as well as multiple links (MIMO) both the hops. Strong turbulence case is considered for UWOC and FSO links; pointing error is varied along with the number of links. In all the Figs. 4.5a to 4.5c the better performance is achieved with the increase in number of links. Fig. 4.5a shows ABER analysis of the end-to-end system for clear ocean and very clear air conditions. For weak pointing error, the ABER of 10^{-4} is a achieved at average SNR of 46 dB for SISO. And to achieve the same ABER with two links average SNR of 33 dB is required. Similarly, for coastal ocean and drizzle weather conditions, to achieve 10^{-4} ABER with two links

under weak pointing error, 13 dB less average SNR is required. For turbid harbor case additional 19 dB average SNR is required to achieve ABER of 10^{-4} for SISO system.
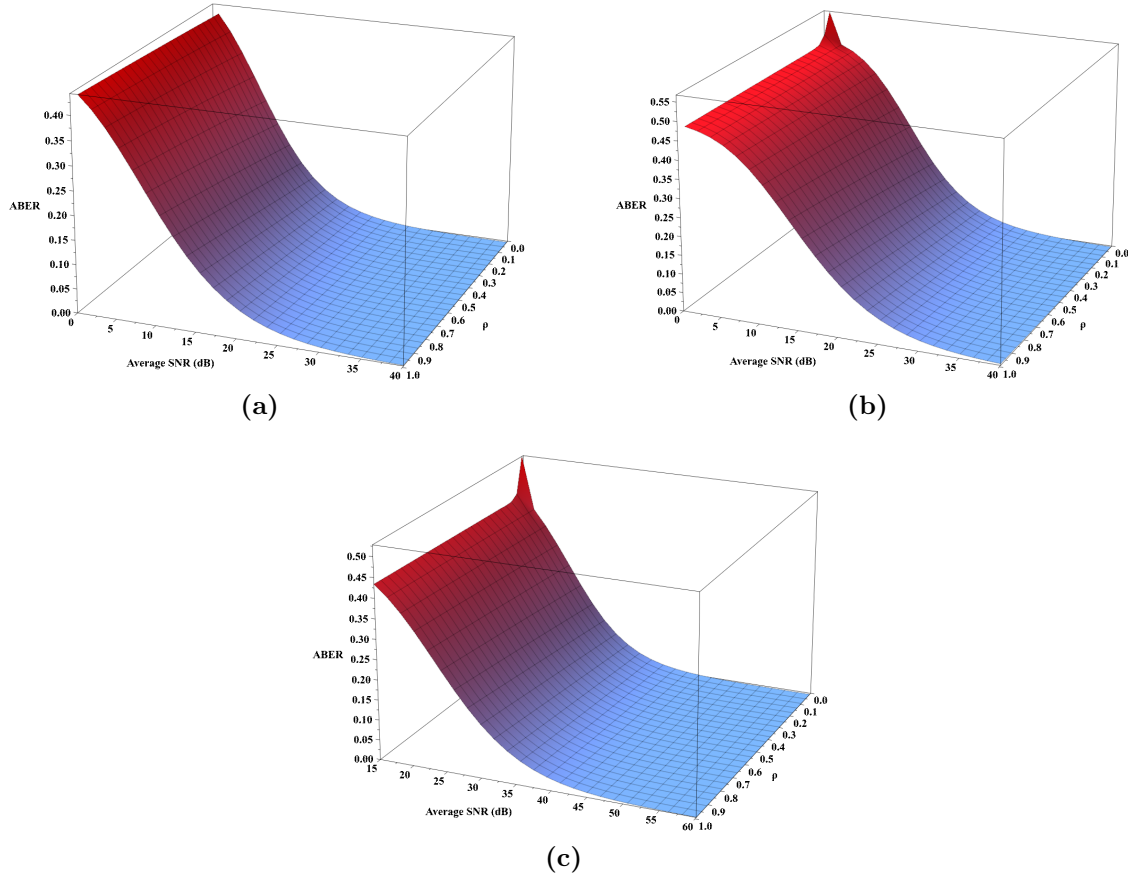
Figure 4.6: ABER versus ρ versus average SNR in ST conditions with strong PEs (a) for clear ocean and very clear air conditions, (b) for coastal ocean and light fog conditions, and (c) for turbid harbor and haze weather conditions.

Fig. 4.6 shows the 3-D plots of ABER with respect to correlation coefficient (ρ) and average SNR for strong turbulence and strong pointing errors respectively. Figs. 4.6a to 4.6c depict the ABER under various oceanic and free space weather conditions. The ρ value is varied from 0.01 to 0.99. The performance of the proposed UWOC-FSO system is given for two apertures. As the average SNR increases, the ABER is decreasing. There is a remarkable degradation in the end-to-end system performance from clear ocean to turbid harbor waters. Also with the increase in correlation coefficient, there is degradation in ABER of proposed MIMO-based system.

The ABER comparison of the proposed MIMO based convergent UWOC - FSO

system with SISO over strong turbulence (for both FSO and UWOC) with weak pointing errors is given in Table 4.2. The performance comparison is analyzed at the average SNR of 25 dB for different weather conditions and water types of FSO and UWOC links such as (clear ocean, clear air), (costal ocean, drizzle) and (turbid harbor, light fog). From the table, it can be noticed that the proposed MIMO system improves the ABER performance compared with SISO system. For example, in costal ocean, drizzle conditions, we can reduce the ABER from 10^{-1} to 10^{-5} using MIMO (2×3) systems under weak pointing error scenario. The communication is not possible in turbid harbor and light fog conditions due to very high attenuation.

Table 4.2: Comparison of ABER of SISO and MIMO systems at an average SNR of 25 dB in the presence of weak pointing error.

UWOC & FSO conditions	ABER of SISO system	ABER of MIMO system
Clear ocean, clear air	10^{-2}	$< 10^{-5}$
Coastal ocean, drizzle	$> 10^{-2}$	$< 10^{-5}$
Turbid harbor, light fog	communication is difficult ($> 10^{-1}$)	communication is difficult ($> 10^{-1}$)

4.5   Summary

This chapter proposes a MIMO-based convergent UWOC-FSO system. A Novel closed-form ABER expression is derived for the end-to-end system. We have analyzed the proposed system ABER performance under various turbulence and pointing error regimes (weak and strong) for various oceanic and free space weather conditions of both UWOC and FSO links. The results show that 35 dB performance enhancement of the end-to-end system from SISO to 2×3 MIMO system for the clear ocean and clear air conditions under weak turbulence case at ABER of 10^{-5}. In a turbid harbor environment, a higher average SNR is required due to high attenuation. Hence, an additional 17.5 dB of average SNR is required to achieve better performance in the case of turbid harbor compared to clear and coastal ocean scenarios. The results also depict the more ABER values with the increase in correlation coefficient ρ. The proposed MIMO-based dual-hop convergent UWOC-FSO system gives improved performance compared to the SISO system. This study will be helpful for design engineers to establish reliable high-speed connectivity in ocean monitoring applications.

Chapter 5

Multi-hop convergent FSO-UWOC system to establish a reliable communication link between the islands

5.1 Introduction

Wireless optical communication (WOC) has received much attention over the last two decades. Terrestrial WOC is also known as Free space optical (FSO) communications. FSO has several advantages over existing RF and microwave communication systems such as unregulated spectrum, huge bandwidth, long operational range, high data rate, license-free operation, re-usability in terms of equipment and wavelengths, high security, and immunity to electromagnetic interference [Mahdy and Deogun (2004), Smyth *et al.* (1993)]. FSO is highly suitable for many applications such as unmanned aerial vehicles (UAVs), high-speed trains, satellites, building-to-building, indoor, outdoor local- and wide-area networks, and deep-space communications [Kaymak *et al.* (2018)]. It supports higher data transfer rate from giga bits per second (Gbps) to tera bits per second (Tbps). WOC plays a significant role in next generation wireless optical networks such as optical wireless satellite networks (OWSN), optical wireless terrestrial networks (OWTN) and optical wireless home networks (OWHN) [Son and Mao (2017), D.Messier (2016)].

WOC has considerable research in the water and is known as underwater wireless optical communication (UWOC). It transfers the information in the military, industry and scientific community. It plays a prominent role in pollution monitoring, environmental monitoring, offshore exploration, live video streaming, maritime archaeology, imaging, oceanography, port security, oil control and maintenance, disaster precau-

tion, tactical surveillance, and high performance underwater optical wireless sensor networks (UOWSN). Because of its high data rates, low latency, short-range wireless links, and low power consumption UWOC has become attractive and alternative technology for traditional RF and acoustic in underwater communication systems [Kaushal and Kaddoum (2016b), Zeng *et al.* (2016)].

UWOC finds its use in difficult-access locations and in deep sea for remotely-operated vehicles (ROVs) and autonomous underwater vehicles (AUVs) as they will limit the range and maneuverability of the underwater vehicle [Khalighi *et al.* (2014)]. UWOC is also applicable to internet of underwater things (IoUT). IoUT has received much attention in the past decade. IoUT was first discussed in 2012 and is defined as "the network of intelligent interconnected underwater entities". The digital entities could be underwater wireless autonomous vehicles (UWAV), ships, buoys, and different types of underwater sensors. These devices hear, interpret, and respond to the atmosphere because of the incorporation of the Internet, tracking technologies, and embedded underwater sensors. IoUT is classified under internet of things (IoT) [Ramavath *et al.* (2020), Kao *et al.* (2017a)].

A multi-hop communication can enhance the reliability of the communication link with high data rate, extend the communication range between the source and destination by converting a long communication link to shorter multiple links, strengthen network connectivity, and provide a more accurate network localization scheme. These short distance links use either decode-and-forward (DF) or amplify-and-forward (AF) relaying [Jia *et al.* (2018), Saeed *et al.* (2018), Issaid *et al.* (2017)]. X Tang et al. proposed a multi-hop FSO system and analyzed the performance of the links using a heterodyne differential phase-shift keying (DPSK) modulation scheme operating over a turbulence induced fading channel. The closed-form expressions for the average symbol error rate (ASER) and the outage probability (OP) have been obtained for the channel effects, numerical results were provided to evaluate the performance of the system [Tang *et al.* (2014)].

In [Alathwary and Altubaishi (2019)], performance analysis of multi-hop hybrid FSO/RF System was presented with DF relaying using Gamma–Gamma (GG) turbulence channel with the pointing errors and path loss effects for FSO link and Nakagami-m distribution for RF link. The authors investigated the outage probability and ergodic capacity for different weather conditions. N Saeed et al. investigated the connectivity of UOWSN and its impacts on the network localization performance in

terms of connectivity, robustness, and the number of anchor nodes. And also the network connectivity probability has been derived as the function of communication range, network density, and optical transmitter's divergence angle [Saeed *et al.* (2018)]. In [Jamali *et al.* (2017)], the authors evaluated the end-to-end bit error rate (BER) of point-to-point multi-hop UWOC systems analytically with respect to all UWOC channel degrading effects.
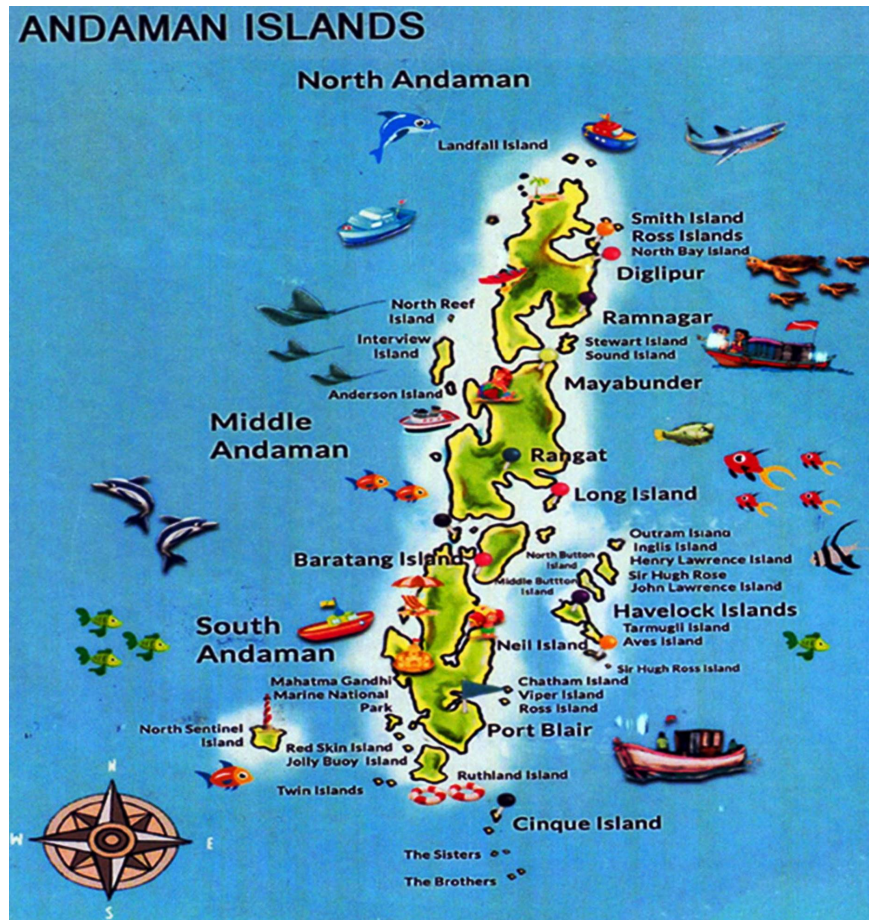
Figure 5.1: Islands in Andaman Nicobar map

The convergence of FSO and UWOC is an emerging and attractive one to solve the connectivity difficulties. Networks that require higher data transmission rate and improved spectral efficiency needs this kind of FSO-UWOC convergent communication systems. The average BER and OP performance of FSO-UWOC convergent system was investigated in [Jurado-Navas *et al.* (2019)] and [Christopoulou *et al.* (2019)] using DF and AF relaying, respectively.

In this chapter, we propose a multi-hop FSO-UWOC convergent system which can be applicable for communication between two lighthouse stations. We derive a closed form OP expression for DPSK modulation scheme using the cumulative distribution function (CDF). As DPSK has several advantages such as less bandwidth requirement, 3 dB sensitivity, simpler receiver circuitry, and long-haul applicability, one can make use of it for WOC systems [Gnauck and Winzer (2005)]. Malaga distribution is considered for modeling the FSO link as it is suitable for all turbulence regimes and because of its applicability to moderate and strong turbulence, GG distribution is considered for modeling the UWOC link [Krishnan (2018), Jurado-Navas *et al.* (2011*b*), Balaji and Prabu (2018*a*)]. Numerical results for OP are analyzed and presented for the proposed system.

The convergent FSO-UWOC-FSO system is essential where both the lighthouses need information/communication from the underwater sensors/vehicles. For example, India has many islands like Andaman, Nicobar, and Lakshadweep. These islands individually consist of many sub-islands and are located a few kilometers apart. Andaman and Nicobar islands itself comprises 572 islands, of which 37 are inhabited, and its map is shown in Fig. 5.1 [Online (2020)]. This kind of island having lighthouse can be communicated efficiently with the multi-hop convergent FSO-UWOC communication system.

The contributions of this chapter are as follows:

- We proposed a multi-hop convergent FSO - UWOC - FSO communication system and derived the expressions for outage probability.

- Closed-form expressions for the outage probability of the end-to-end system are derived using the cumulative distribution function (CDF).

- The performance of the proposed system is analyzed under different turbulence, and weather conditions, along with pointing error effects.

- The analysis is carried out with different oceanic conditions such as the clear ocean, coastal ocean, turbid harbor for the UWOC link, and various atmospheric effects such as very clear air, fog, rain, drizzle haze for the FSO link.

- A comparison was shown for the individual FSO system, UWOC system, and end-to-end system.

5.2   System and Channel Model

We consider a system model as shown in the Fig. 5.2, which consists of multi-hop FSO and UWOC links. The source and destination are connected through three relays with four links. FSO links are considered between lighthouse and ship, UWOC links are considered between the ship and UWAV. The FSO links are Malaga distributed, and UWOC links are gamma–gamma (GG) distributed.
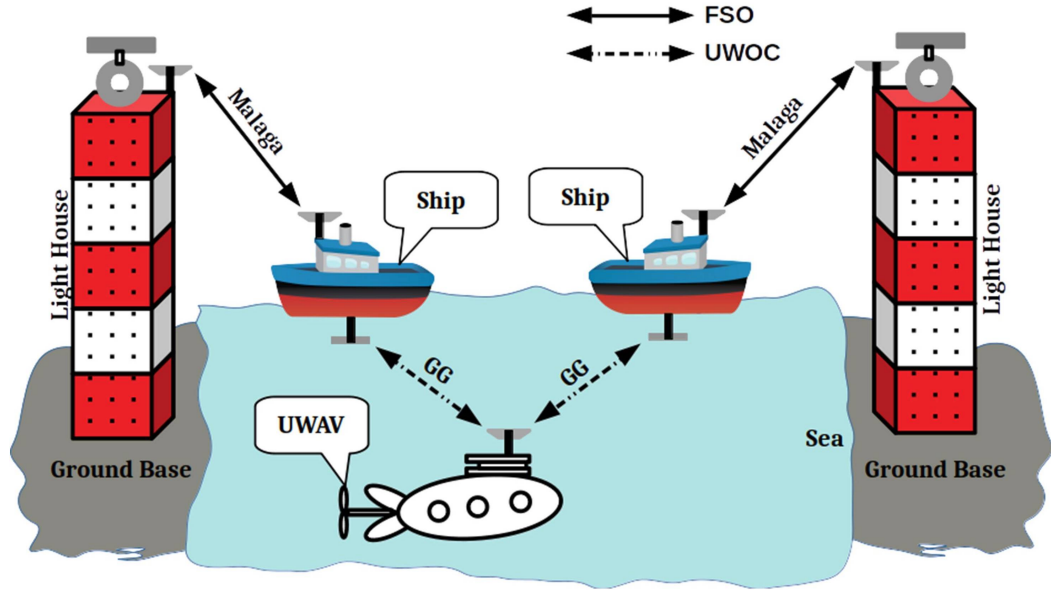
Figure 5.2: System Model

5.2.1   FSO Link

The FSO link is considered as M-distributed. The physical model formed by M-distributed channel contains three components: the first one is line-of-sight (LOS) component U_L and its average power is represented by $\Omega = E[|U_L|^2]$. The second one is coupled to LOS component U_S^C due to the eddies on propagation axis and the third one is independent scatter component U_S^G due to the eddies off the axis. The average power of U_S^C and U_S^G are represented by $E[|U_S^C|^2] = 2\rho b_0$ and $E[|U_S^G|^2] = 2(1-\rho)b_0$. The total average power of scattered components is $E[|U_S^C|^2 + |U_S^G|^2] = 2b_0$. The parameter $0 \leq \rho \leq 1$ related to the scattered components, it represents the amount of scattering power coupled to the LOS component [Jurado-Navas *et al.* (2011*b*)]. The probability distribution function (PDF) of the irradiance γ is given by [Balaji and Prabu (2018*a*)]

$$f_{\gamma_1}(\gamma) = \frac{g^2 A}{2\gamma} \sum_{m=1}^{\beta_1} a_m B^{-\left(\frac{\alpha_1+m}{2}\right)} G_{1,3}^{3,0}\left(C_1\gamma \,\middle|\, \begin{matrix} g^2+1 \\ X \end{matrix}\right) \tag{5.1}$$

where

$$C_1 = \frac{B}{A_0 P_{FSO}^l} \;\; ; \;\; B = \frac{\alpha_1\beta_1}{\xi\beta_1 + \Omega'}$$

$$X = g^2, \; \alpha_1, \; m$$

The path loss of FSO link P_{FSO}^l is determined by Beer-Lambert's law as

$$P_{FSO}^l = exp(-\sigma L)$$

The σ indicates attenuation coefficient and L is the link distance.

$$A \triangleq \frac{2\alpha_1^{\frac{\alpha_1}{2}}}{\xi^{1+\frac{\alpha_1}{2}}\Gamma(\alpha_1)} \left(\frac{\xi\beta_1}{\xi\beta_1+\Omega'}\right)^{\beta_1+\frac{\alpha_1}{2}}$$

$$a_m \triangleq \binom{\beta_1-1}{m-1} \frac{(\xi\beta_1+\Omega')^{1-\frac{m}{2}}}{(m-1)!} \left(\frac{\Omega'}{\xi}\right)^{m-1} \left(\frac{\alpha_1}{\beta_1}\right)^{\frac{m}{2}}$$

The parameter g in Eq. (5.1) indicates the pointing error due to weak earthquakes, building sway, and thermal expansion of the signal and is given as $g = \frac{w_{zeq}}{2\sigma}$, where $w_{zeq} = \left[\frac{\sqrt{\pi}erf(v)w_z^2}{2ve^{-v^2}}\right]^{\frac{1}{2}}$ and w_z in w_{zeq} is the beam width at link distance L.

The parameters α_1 and β_1 are related to the atmospheric turbulence of the channel. α_1 is related to the effective number of enlarged scattering cells in the atmosphere and is positive. Similarly, β_1 is taken as natural number, which represents the amount of fading parameter. The parameter $\Omega' = \Omega + 2\rho b_0 + 2\sqrt{2b_0\rho\Omega}cos(\phi_A-\phi_B)$ represents the average power from the consistent contributions. The angles ϕ_A and ϕ_B indicate the deterministic phases of the LOS and the coupled-to-LOS components. The parameter $\xi = E[|U_S^G|^2] = 2(1-\rho)b_0$. $\Gamma(.)$ is the Gamma function. The CDF of Eq. (5.1) is derived using [Adamchik and Marichev (1990), Eq. (26)]

$$F_{\gamma_1}(\gamma) = \frac{g^2 A}{2} \sum_{m=1}^{\beta_1} a_m B^{-\left(\frac{\alpha_1+m}{2}\right)} G_{2,4}^{3,1}\left(C_1\gamma \,\middle|\, \begin{matrix} g^2+1, \; 1 \\ X, \; 0 \end{matrix}\right) \tag{5.2}$$

5.2.2 UWOC Link

The UWOC sources use either laser diode (LD) or the light emitting diode (LED) to provide large bandwidth and small beam divergence. Light propagating under the water degrades by absorption, scattering, and turbulence effects. When the light signal is transmitted through the UWOC channel attenuation and fading are added to it. Then the received light signal intensity becomes $I_r = I_t \cdot P^l_{UWOC} \cdot \gamma$. Here I_t is the intensity of the transmitted signal, P^l_{UWOC} is the path loss which decreases the average irradiance of the light beam, caused by scattering/absorption effects and beam enlargement, and γ is the turbulence-induced fading of the normalized channel and satisfies a PDF.

The optical signal underwater experiences the absorption and scattering as it collides with the water molecules and particles, due to which there is intensity loss in the signal. As each photon loses its energy thermally, it is considered as absorption coefficient $a(\lambda)$. Similarly, because of the photon collision with the water particles, each photon changes its direction, it is considered as scattering coefficient $b(\lambda)$. The total attenuation underwater can be expressed as a beam extinction coefficient $c(\lambda) = a(\lambda) + b(\lambda)$ [Tang *et al.* (2013)]. Where λ is the transmitted optical signal wavelength. The coefficient values can vary with different types of water and source wavelength λ. Typical coefficient values are given in Table 3.1 [Hanson and Radic (2008)]. The propagation loss factor P^l_{UWOC} is expressed in terms of wavelength λ and link distance L as [Kaushal and Kaddoum (2016b)]

$$P^l_{UWOC}(\lambda, L) = exp(-c(\lambda)L)$$

In this chapter, as the underwater atmospheric optical turbulence caused by the random variations of the temperature and pressure of the channel, for UWOC link we considered the GG-distribution. Also, the GG-distribution can be used for UWOC link as the absorption and scattering effects not to affect the fading property of the optical signal [Liu *et al.* (2015)]. The irradiance PDF of GG-distribution is expressed as [Prabu *et al.* (2013)]

$$f_{\gamma_2}(\gamma) = C_3 \; G^{3,0}_{1,3} \left(C_2 \gamma \left| \begin{array}{c} g^2 \\ Y \end{array} \right. \right) \tag{5.3}$$

Where

$$C_2 = \frac{\alpha_2 \ \beta_2}{A_0 \ P_{UWOC}^l} \ ; \ C_3 = \frac{C_2 \ g^2}{\Gamma(\alpha_2) \ \Gamma(\beta_2)}$$

$$Y = g^2 - 1, \ \alpha_2 - 1, \ \beta_2 - 1$$

A_0 is the fraction of optical power received and is expressed as $[erf(v)]^2$ with $v = \frac{a_r}{w_z} \ \sqrt{(\frac{\pi}{2})}$. The parameter g represents misalignment between transmitter and receiver due to the floating nature of water and it is pointing error. The CDF of Eq. (5.3) is derived using [[Adamchik and Marichev (1990)], Eq. (26)] as

$$F_{\gamma_2}(\gamma) = C_3 \ \gamma \ \mathrm{G}_{2,4}^{3,1} \left(C_2\gamma \ \middle| \ \begin{matrix} g^2, \ 0 \\ Y, \ -1 \end{matrix} \right) \tag{5.4}$$

The P_{FSO}^l of 1Km link and P_{UWOC}^l of 10m link are given in Tables 5.1 and 5.2.

Table 5.1: Path loss of FSO link for link distance of 1km.

Weather condition	Attenuation coefficient, σ, dB/km	P_{FSO}^l
Very clear air	0.0647	0.9852
Drizzle	0.2208	0.9504
Haze	0.7360	0.8441
Mean rain (R=4)	0.7639	0.8387
Mean rain (R=5)	0.8793	0.8167
Strong rain (R=7)	0.5554	0.8800
Light Fog	4.2850	0.3728
Moderate fog	25.5160	0.0028

In Table 5.1, R represents the rate of rain fall in mm/hr. The path loss of FSO link during rain conditions depends on the rain drop size. The attenuation coefficient relationship for rain is given as in 3.4 [Soni (2018)].

Table 5.2: Path loss of UWOC link for link distance of 10m.

Type of water	$c(\lambda)(m^{-1})$	P_{UWOC}^l
Clear ocean	0.151	0.7063
Coastal ocean	0.399	0.3990
Turbid harbor	2.195	0.0064

5.3 Statistical Analysis

The overall PDF from source (light house) to UWAV can be expressed in terms of the equivalent signal-to-noise ratio (SNR), γ as [Vellakudiyan *et al.* (2019)]

$$f_\gamma(\gamma) = f_{\gamma_1}(\gamma) + f_{\gamma_2}(\gamma) - f_{\gamma_1}(\gamma)F_{\gamma_2}(\gamma) - F_{\gamma_1}(\gamma)f_{\gamma_2}(\gamma) \qquad (5.5)$$

The CDF for Eq. (5.5) is

$$F_\gamma(\gamma) = F_{\gamma_1}(\gamma) + F_{\gamma_2}(\gamma) - F_{\gamma_1}(\gamma)F_{\gamma_2}(\gamma) \qquad (5.6)$$

after substituting Eq. (5.2) and (5.4) in (5.6), the overall CDF from source to UWAV can be expressed as

$$F_\gamma(\gamma) = Z_1 + Z_2 - Z_1 Z_2 \qquad (5.7)$$

where

$$Z_1 = \frac{g^2 A}{2} \sum_{m=1}^{\beta_1} a_m B^{-\left(\frac{\alpha_1+m}{2}\right)} \mathrm{G}_{2,4}^{3,1}\left(C_1\gamma \left|\begin{array}{c} g^2 + 1,\ 1 \\ X,\ 0 \end{array}\right.\right)$$

and

$$Z_2 = C_3\ \gamma\ \mathrm{G}_{2,4}^{3,1}\left(C_2\gamma \left|\begin{array}{c} g^2,\ 0 \\ Y,\ -1 \end{array}\right.\right)$$

Similarly, the overll CDF from UWAV to destination (light house) is same as Eq. (5.7).

The end-to-end (lighthouse to lighthouse) CDF of the proposed system using the relays (ships, UWAV) is calculated using Eq. (5.6) by considering the CDFs of individual link i.e., Eq. (5.7) from source to UWAV as $F_{\gamma_1}(\gamma)$ and Eq. (5.7) from UWAV to destination as $F_{\gamma_2}(\gamma)$. As both the CDFs $F_{\gamma_1}(\gamma)$ and $F_{\gamma_2}(\gamma)$ are equal, the end-to-end CDF of the proposed system becomes

$$F_\gamma(\gamma) = (2 * F_{\gamma_1}(\gamma))\ -\ [F_{\gamma_1}(\gamma)]^2 \qquad (5.8)$$

The end-to-end CDF formed by substituting Eq. (5.7) in (5.8) is as follows,

$$F_\gamma(\gamma) = 2\ (Z_1\ +\ Z_2\ -\ Z_1\ Z_2)\ -\ [Z_1\ +\ Z_2\ -\ Z_1\ Z_2]^2 \qquad (5.9)$$

Eq. (5.9) has been given in detail as

$$
\begin{aligned}
F_\gamma(\gamma) = 2\,\Bigg(\frac{g^2 A}{2} &\sum_{m=1}^{\beta_1} a_m B^{-\left(\frac{\alpha_1+m}{2}\right)} \mathrm{G}_{2,4}^{3,1}\left(C_1\gamma\,\bigg|\,\begin{matrix} g^2+1,\ 1 \\ X,\ 0 \end{matrix}\right) + C_3\,\gamma\,\mathrm{G}_{2,4}^{3,1}\left(C_2\gamma\,\bigg|\,\begin{matrix} g^2,\ 0 \\ Y,\ -1 \end{matrix}\right) \\
&- \frac{g^2\,A\,C_3\,\gamma}{2}\sum_{m=1}^{\beta_1} a_m B^{-\left(\frac{\alpha_1+m}{2}\right)} \mathrm{G}_{2,4}^{3,1}\left(C_1\gamma\,\bigg|\,\begin{matrix} g^2+1,\ 1 \\ X,\ 0 \end{matrix}\right)\,\mathrm{G}_{2,4}^{3,1}\left(C_2\gamma\,\bigg|\,\begin{matrix} g^2,\ 0 \\ Y,\ -1 \end{matrix}\right)\Bigg) \\
&- \Bigg[\frac{g^2 A}{2}\sum_{m=1}^{\beta_1} a_m B^{-\left(\frac{\alpha_1+m}{2}\right)} \mathrm{G}_{2,4}^{3,1}\left(C_1\gamma\,\bigg|\,\begin{matrix} g^2+1,\ 1 \\ X,\ 0 \end{matrix}\right) + C_3\,\gamma\,\mathrm{G}_{2,4}^{3,1}\left(C_2\gamma\,\bigg|\,\begin{matrix} g^2,\ 0 \\ Y,\ -1 \end{matrix}\right) \\
&- \frac{g^2\,A\,C_3\,\gamma}{2}\sum_{m=1}^{\beta_1} a_m B^{-\left(\frac{\alpha_1+m}{2}\right)} \mathrm{G}_{2,4}^{3,1}\left(C_1\gamma\,\bigg|\,\begin{matrix} g^2+1,\ 1 \\ X,\ 0 \end{matrix}\right)\,\mathrm{G}_{2,4}^{3,1}\left(C_2\gamma\,\bigg|\,\begin{matrix} g^2,\ 0 \\ Y,\ -1 \end{matrix}\right)\Bigg]^2
\end{aligned}
\tag{5.10}
$$

5.4 Outage Probability Analysis

The probability that the end-to-end system output SNR falls below a specified threshold value is known as OP (P_{out}). The OP of the end-to-end system can be expressed as [Prabu $et\ al.$ (2014b)]

$$
P_{out} = P\left(SNR(\gamma) \le SNR_{TH}\right)
\tag{5.11}
$$

Where SNR_{TH} (γ_{th}) is the threshold SNR value below which the quality of service is not acceptable. The P_{out} for DPSK modulation technique is given by

$$
P_{out}(DPSK) = P\left(\gamma \le \frac{P\nu\,\gamma_{th}}{\eta A_d T}\right) = F_\gamma\left(\frac{SNR_{TH}}{C_4}\right)
\tag{5.12}
$$

Where $C_4 = \frac{\eta A_d T}{P\nu}$, P is the Planck's constant, ν is the received signal frequency in Hz, η denotes the quantum efficiency of the detector, T is the DPSK symbol duration rate in seconds, and A_d is the area of the detector in m^2.

5.5 Results and Discussions

In this section, OP of the proposed system is analyzed in terms of SNR and threshold SNR for different values of $\alpha, \beta, g, P_{FSO}^l$, and P_{UWOC}^l [Vellakudiyan $et\ al.$ (2019), Jurado-Navas $et\ al.$ (2011a)]. The parameters α and β are related to the turbulence

of the channel, higher values of these parameters indicate weak turbulence and vice versa. Always the relation $\alpha > \beta$ should be satisfied [Uysal *et al.* (2006), Popoola and Ghassemlooy (2009), Wang and Cheng (2010)]. In this chapter, we performed OP analysis by considering the FSO and UWOC link parameters α and β separately. The parameters $\alpha = 2$ and $\beta = 1$ are considered as strong turbulence (ST) case and $\alpha = 4.1$ and $\beta = 2$ is considered as moderate turbulence (MT) case. Similarly, by making the α and β as constant for both links P_{out} is analyzed for different values of g, considering different weather conditions with path loss. The values $\Omega = 0.5$ and $b_0 = 0.25$ and $\rho = 0.25$ makes the normalized transmitted power.
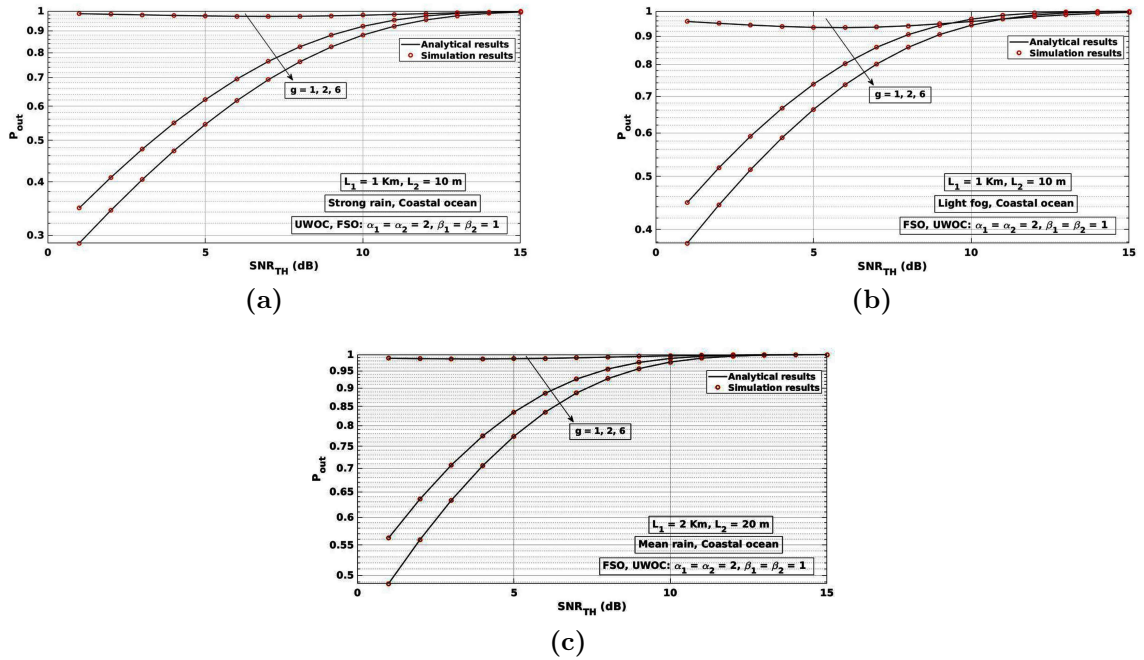
Figure 5.3: P_{out} Vs SNR_{TH} for different weather conditions based on pointing errors. (a) for strong rain and coastal ocean conditions (b) for light fog and coastal ocean conditions (c) for moderate rain and coastal ocean conditions.

Fig. 5.3a visualizes the OP of the end-to-end multi-hop system for strong rain and coastal ocean weather conditions with strong turbulence. We consider the FSO and UWOC channels' link distances 1 Km and 10 m, respectively. The path losses of FSO and UWOC links are 0.8800 (strong rain) and 0.3990 (coastal ocean water), respectively. We varied the pointing error parameter g from 1 to 6. The least value of g indicates a more pointing error, and the highest value indicates the least pointing error. As g increases, the outage value varies from 0.287 to 1.

Fig. 5.3b depicts P_{out} for the same link distances as mentioned in 5.3a. But the FSO link has light fog with a path loss value of 0.3728. The UWOC link has the same coastal water attenuation. Here we varied the pointing error parameter. When $g = 6$, the outage probability increases from 0.377 to 1 as the threshold SNR (SNR_{TH}) increases.

Fig. 5.3c shows the outage analysis for 2 Km of FSO link and 20 m of UWOC link with strong turbulence. The path loss for moderate rain is 0.6670, and the coastal ocean is 0.1592. In this case, as the threshold SNR increases, with variation in g, the outage also increases and becomes constant (1) from $SNR_{TH} = 15$dB.
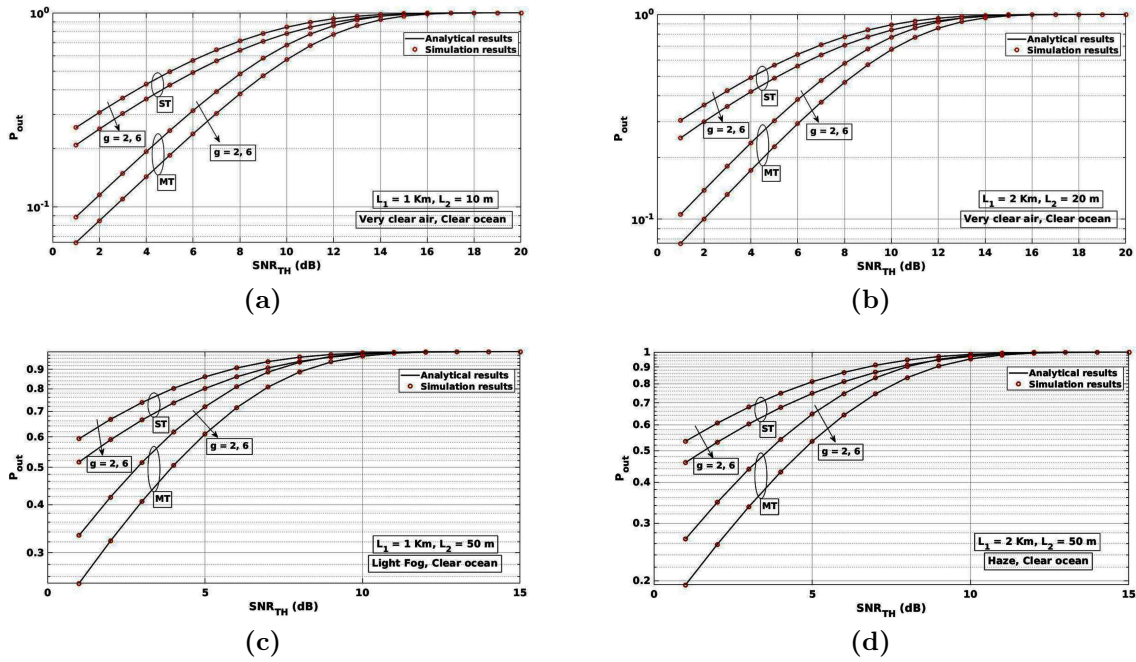
Figure 5.4: P_{out} Vs SNR_{TH} for different turbulence conditions along with pointing errors. (a) & (b) for very clear air and clear ocean conditions with different link distances (c) for light fog and clear ocean conditions (d) for haze and clear ocean conditions.

Fig. 5.4 shows outage performance analysis for different FSO weather conditions and fixed UWOC water (clear ocean) conditions. In this scenario, we varied the FSO and UWOC link lengths, turbulence, and pointing error parameters by making the SNR constant.

Fig. 5.4a depicts outage performance analysis for very clear air and clear ocean conditions. In this scenario for 1 Km FSO link $P_{FSO}^{l} = 0.9852$ and for 10 m UWOC link $P_{UWOC}^{l} = 0.7063$. We varied turbulence parameters α and β along with g. For

the same turbulence conditions, as g increases, outage performance decreases.

Fig. 5.4b visualizes the P_{out} for same weather conditions as shown in Fig. 5.4a. In this case, for 2 Km FSO link has $P_{FSO}^l = 0.9706$ and 10 m UWOC link has $P_{UWOC}^l = 0.4989$. For the two cases $g = 2, 6$ the outage performance decreases with the increase in the threshold SNR. For example, the outage becomes 1 at 20dB of threshold SNR for both the strong and moderate turbulence cases.

Fig. 5.4c presents P_{out} for 1 Km FSO link with light fog and 50 m clear ocean link. The path loss is 0.3728 (light fog) and 0.1758 (clear ocean) for FSO and UWOC links. For this case we considered strong and moderate turbulence conditions. P_{out} varies from 0.249 to 1 based on variation in the pointing error parameter, g.

Fig. 5.4d shows the outage analysis for 2 Km FSO link with haze and 50 m of clear ocean link conditions. As per the pointing error parameter, outage varies from 0.19 to 1 for strong and moderate turbulence conditions. $P_{FSO}^l = 0.7125$, $P_{UWOC}^l = 0.1758$.
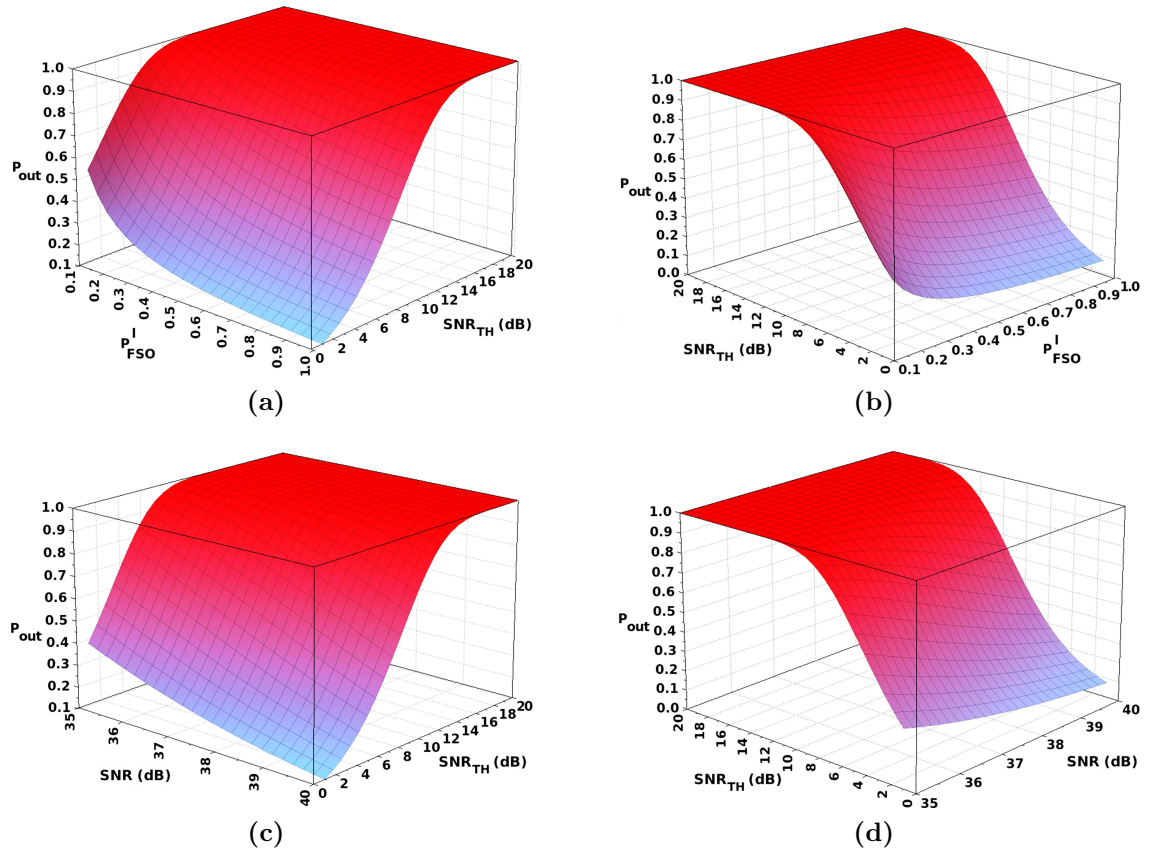
Figure 5.5: P_{out} Vs P_{FSO}^l Vs SNR_{TH} for clear ocean condition when (a) $g = 2$ and (b) $g = 6$. P_{out} Vs SNR Vs SNR_{TH} for very clear air and clear ocean conditions when (c) $g = 2$ and (d) $g = 6$.

71

Fig. 5.5a and 5.5b depicts three dimentional plots of P_{out} for varying FSO link distance with 20 m of clear oceanic link. P_{FSO}^l varies from 0 to 1 and SNR_{TH} varies from 1 to 20dB. We considered moderate turbulence case for both FSO and UWOC links. Fig. 5.5a shows the outage analysis for $g = 2$ and Fig. 5.5b shows the outage analysis for $g = 6$. As SNR_{TH} increases, OP increases and as P_{FSO}^l increases, OP decreases.

Fig. 5.5c and 5.5d gives outage probability analysis with variation in SNR and SNR_{TH} for $g = 2$ and $g = 6$. SNR is varied from 35-40dB and SNR_{TH} is varied from 1-20dB. In this case also we considered moderate turbulence for both FSO and UWOC links. When the path loss is low, as g value increases OP decreases. Increase in SNR results in decreasing OP.
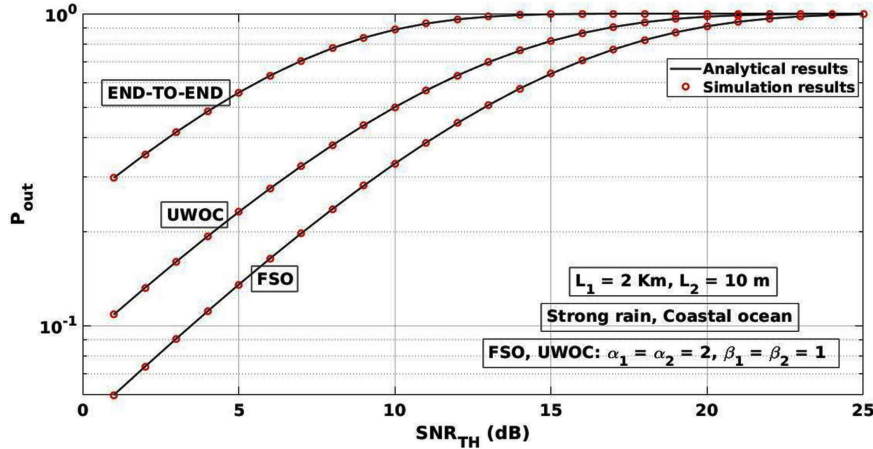
Figure 5.6: Outage versus SNR_{TH}(dB) for Strong rain and coastal ocean conditions

Fig. 5.6 portrays the outage performance of the individual FSO and UWOC links and the end-to-end multi-hop system over a weak pointing error scenario ($g = 6$). We consider a 2 Km FSO link with strong rain and a 10 m coastal oceanic link. We consider strong turbulence in both the FSO and UWOC channels. The path loss of the FSO link is 0.7743 (strong rain), and it is 0.3990 (coastal ocean water) for the UWOC link. The end-to-end system performance shows poor outage performance compared with the individual links because of the effects on the respective links.

5.6 Summary

This chapter presented the outage analysis of a multi-hop FSO-UWOC confluent system. Derived a closed-form expression for the outage probability of the end-to-end system by assuming the FSO link as M-distributed and UWOC link as GG-distributed.

Further, the results are demonstrated for the derived analytical expressions based on various parameters and different weather conditions. This convergent multi-hop FSO-UWOC system can be applicable for IoUT and UOWSN and other coastal operations such as lighthouse communications, port security, oceanography, weather monitoring, etc.

Chapter 6

Performance Analysis of Multi-hop FSO Convergent with UWOC System

6.1 Introduction

The high-speed online internet-based applications (virtual online meetings, live audio, video streaming with 4K and 8K resolutions, gaming boxes, etc.) are increasing exponentially, thus requiring access to high-speed wireless technologies to ensure connectivity and the quality of services. The proposed 5th generation (5G) wireless networks will offer new ultra-high-speed services with enormous device connectivity, ultra-low latency, ultra-high system capacity, and energy usage, tremendously high quality of experience (QoE) together with improved security. To deliver these, 5G and beyond will rely on multiple technologies including, cell densification, massive multiple-input multiple-output (MIMO), millimeter wave (mmW) communications, cognitive radio networks, TeraHertz, and optical communications [Al-Kinani *et al.* (2018), Chowdhury *et al.* (2020), Abaza *et al.* (2015)].

Radio frequency (RF) technology is well established and widely used in many indoor, outdoor and space communication systems. However, it faces a number of challenges, including increasing interference levels, spectrum congestion, inadequate channel capacity, higher costs, which need to be addressed [Liu *et al.* (2020)]. In order to address some of these issues, in particular spectrum congestion, one possible alternative complementary solution would be the adoption of wireless optical communication (WOC) technology in dedicated applications. WOC technology, which primarily covers the optical spectrum of infrared (IR), ultraviolet (UV) and visible light (VL) [Ghassemlooy *et al.* (2019)], offers several attractive and unique features,

such as: low development and installation costs, improved energy efficiency, high level of physical layer security, steering and tracking capabilities, license-free spectrum with unlimited bandwidth. Due to this attractive advantages of WOC, it is highly preferred in various applications and integrated with other wired and wireless communication technologies [Algamal *et al.* (2020), Djordjevic (2018), Uysal *et al.* (2014)].

The recent techniques introduced in wireless and optical domain such as wavelength division multiplexing (WDM), robust modulation techniques, advanced diversity techniques and simultaneous wireless/light information and power transfer (SWIPT/SLIPT) techniques are barrowed and implemented in WOC. Recently the mixed systems such as RF/FSO/mmw/VLC/UWOC in different combinations are highly attractive in next generation communication systems [Elsayed and Yousif (2020), Singh and Malhotra (2019), Krishnan (2018)].

In recent years, we have seen increasing research on ocean monitoring, shallow water monitoring, seabed geodesy, oil and gas exploration, seismic events, search and relocation, underwater and ship-to-ship communications, underwater wireless aerial vehicle (UWAV) communications, etc. [Raj and Majumder (2019)]. Underwater WOC (UWOC) has attracted a great deal of attention in underwater environments for real-time multimedia services between UWAVs and land vehicles and for coastal surveillance systems due to very low latency and high data transmission rates compared to existing RF and acoustic communication systems [Oubei *et al.* (2018), Vali *et al.* (2017)].

Currently, however, UWOC systems can communicate across ranges typically below 100 m, which interfere with their broad use. This hindrance is primarily due to the degrading effects on the UWOC channels, namely absorption, scattering, and turbulence, which cause loss and inter-symbol interference (ISI). Compared to traditional underwater acoustic communication systems, short, accessible UWOC connecting lengths are the main drawbacks [Jamali *et al.* (2017), Singh *et al.* (2020)]. Thus, in recent years, many researchers have focused mainly on the effects of the UWOC channel model (absorption, scattering and turbulence) and the development of intelligent UWOC systems and the development of efficient transmission and/or reception methods to extend the range of feasible communications towards ocean monitoring, underwater optical wireless sensor networks (UOWSNs), and internet of underwater things (IoUTs) applications etc. [Uppalapati *et al.* (2020), Ramavath *et al.* (2020)].

The literature shows that channel impairing effects like delay spread, loss, and

fading variance swiftly increases as the channel length increases [Tang *et al.* (2013), Korotkova *et al.* (2012), Anandkumar and Sangeetha (2021)]. The turbulence-induced irrational fluctuation becomes the major challenge in the free-space-optical (FSO) system, even in a clear weather condition with communication links over 1 km. In many FSO related literatures, this problem addressed with multi-hop transmission.

Tang et al. have proposed a multi-hop FSO communication system using the heterodyne (HD) differential phase-shift keying (DPSK) modulation scheme. The authors analyzed the performance of the proposed system with a modified statistical fading channel model for multi-hop FSO systems using channel-state-assisted information (CSIA) and fixed-gain relays incorporating path-loss, pointing errors and atmospheric turbulence effects. Authors derived the novel expressions for the outage probability and average symbol error rate (ASER). The results confirm that there will be a loss of performance as the number of hops increases [Tang *et al.* (2014)].

The performance analysis of the FSO communication system based on multi-hop decode-and-forward (DF) relaying IM/DD is presented in [Abaza *et al.* (2015)]. Multi-hop has been shown to be an efficient technique for alleviating turbulence, attenuation and geometric losses in FSO communication systems. A comparison was also made with the direct link system and the diversified system, taking into account the correlation effects of the transmitter. The results of the Bit Error Rate (BER) analysis show that multiple input single output multi-hop FSO systems are superior to their counterparts over high attenuation links.

This motivates a multi-hop UWOC system design to split the total communication distance into shorter ones, each with much reduced impairing effects to perform well with such distance limitation. Also, the main drawback of UWOC is the short-range communication compared to acoustic communication. The number of intermediate relay nodes can increase the total transmitted power by using multi-hop transmission to support longer distances considerably while maintaining the safe transmission power density.

A multi-relay/multi-hop communication system can extend the communication range between the source and the destination. Relays convert long communication links to multiple shorter links, enhance network connectivity. These short-distance links use either amplify-and-forward (AF) or DF relays. A multi-hop communication system can provide a more accurate network localization scheme; enhance the reliability of the communication link with a high data rate [Jia *et al.* (2018), Saeed *et al.*

(2018), Issaid *et al.* (2017)].

The authors present a unified dual-hop UWOC system with fixed-gain AF relays in [Zedini *et al.* (2020)]. The authors analyzed the performance of the system in the presence of temperature gradients and air bubbles operating either under HD or IM/DD. Closed-form expressions are derived using the Fox bivariate H function for performance metrics such as the average BER and the probability of interruption for different modulation schemes and ergodic capacity. Moreover, the results show that the dual-hop UWOC system can effectively reduce short-range and temperature gradients and air bubble-induced turbulences compared to a single UWOC link. The effects of the underwater channel on the BER performance of the UWOC system are studied and enhanced by multi-hop transmission in [Jamali *et al.* (2017)]. The authors analyzed the BER performance of the UWOC multi-hop system with respect to all underwater channel degrading effects, namely scattering, absorption and turbulence-induced fading. Numerical results show that multi-hop transmission can extend the UWOC system over longer distances and significantly improve system performance [Jamali *et al.* (2017)].

The end to end average BER and outage performance of multi-hop AF-based UWOC communication system is studied over mixture EG distribution fading model in [Yue *et al.* (2020)]. In [Tabeshnezhad and Pourmina (2017)], the authors studied the outage probability of on-off keying modulation and the DF relay based UWOC system, taking into account both serial relaying (multi-hop transmission) and parallel relaying (cooperative communications). The integration of two or more wireless technologies such as RF/FSO/UWOC offers enhanced features and capabilities that will lead to improved system performance in terms of reliability, load balancing, throughput and energy efficiency of individual networks.

Amirabadi et al. proposed a multi-hop hybrid FSO/RF communication system to avoid disruption of long-range RF communications. The authors proposed a two-part structure. The first part links the mobile users to the source base station; the second part is the link between the source and the destination base stations. Multiple mobile users connect to the source base station via a long-range AF relay connection using the first part. The source and destination base stations are connected to the DF relay using the second part via a multi-hop hybrid parallel FSO/RF link. New closed-form asymptotic expressions are derived for BER and Outage Probability of the proposed system [Amirabadi and Vakili (2019, 2020)].

In [Tokgoz *et al.*], the authors proposed a hybrid FSO-mmW system as an emerging and promising system for high data rate applications and authors have proposed a new selection mechanism to select appropriate communication link among FSO and mmW links without need of feedback. The activation of each link is obtained using index modulation and the performance is analyzed in terms of average BER, spectral efficiency, ergodic capacity, and probability of failure.

The combination of FSO and UWOC is becoming an attractive alternative to connectivity snags. In order to meet the high data rate expectations of OWC systems, a high-transmission FSO-UWOC convergence system is needed. Due to the rapid evolution of FSO-UWOC converging systems, the emerging market is increasing the need for high-speed OWC systems [Tsai *et al.* (2019), Jurado-Navas *et al.* (2019)].

Outage probability and BER performance of the RF-UWOC system presented in [Naik *et al.* (2020)], where the oceanic turbulence channels was modeled using the hyperbolic tangential log-normal (HTLN) density function. In [Christopoulou *et al.* (2019)], the authors proposed a multi-sensor mixed UWOC-FSO system and verified the performance of the underwater sensor networks (UWSN) in terms of the outage probability. A converging UWOC-FSO system for internet of underwater things and UWSN applications has recently been proposed. Bhargava et al. proposed the DPSK-based FSO-UWOC dual-hop system for underwater wireless sensor networks and multi-hop communication system to enable the communication between the islands [Kumar and Krishnan (2020)]. Using the DF-based closed-form expressions, the authors performed ABER analysis for dual-hop system and outage analysis for the multi-hop system [Kumar and Krishnan (2020), Levidala and Krishnan (2020)].

FSO and UWOC convergent systems serve a number of applications, such as: Navy (Security and Surveillance), Safe transport. In marine applications, anti-submarine warfare (ASW) is a more challenging and fascinating form of warfare and controls autonomous underwater vehicles (AUVs) like torpedo. Torpedo can be used to detect or protect ships from attack. The survival capability of a ship is greater if the torpedo can be detected early and in a range greater than the escape range of the platform. Whereas multiple ships carry heavy goods, they need a safer route (less risk and safe from enemy attacks) to reach their destination. AUV-based torpedo can be used to navigate a safer ship path. As a result, current maritime warfare requires reliable early warning torpedo detection and counter-measurement systems that can directly engage the attacking torpedo. In this chapter, we considered a high-speed optical

link between the ships/ASWs and the ship/ASW to torpedo. Namely, the FSO link between ships/ASWs and the UWOC link between ship/ASW and torpedo.

The chapter's contributions are as follows:

- We proposed a novel multi-hop FSO - UWOC convergent system and derived the outage probability and ABER expressions.

- The outage and ABER performance of the proposed system is evaluated in the presence of different weather conditions, turbulence regimes and pointing error effects.

- The outage and ABER performance of the proposed system is analyzed in order to vary the number of hops of the convergence systems.

- A case study was done for the proposed system with real-time values of Arabian Sea (GPS coordinates: N 13° 0'38.0988', E 74° 47'17.4876') near Surathkal located at Mangalore, Karnataka, India.

The remaining part of the chapter is organized as follows. The proposed system model is presented in Section 6.2. Section 6.3 discusses the statistical channel models of the proposed system. The expressions for the bit error rate and outage probability of the proposed end-to-end system is evaluated in Section 6.4. Outage probability and ABER results are discussed for different FSO and UWOC conditions in Section 6.5 and finally chapter concluded in Section 6.6.

6.2   System Model

We consider a system model, which consists of multi-hop FSO and UWOC links as shown in Fig. 6.1. The first (n-1) links between the relays above the sea surface are considered as connected with FSO links. Similarly, the communication link between $(n-1)^{th}$ relay on the sea surface and UWAV inside the seawater are connected using UWOC link. The source and destination are connected through relays with 'n' number of links. The data received at UWAV is given as [Naik $et\ al.$ (2021), Tang $et\ al.$ (2013)],

$$Y = h\ s + n, \tag{6.1}$$

where $\gamma = \frac{h^2 P}{\sigma^2}$ is the signal to noise ratio (SNR), $P = \mathbb{E}\left(|s|^2\right)$, $\mathbb{E}(\cdot)$ is expected value, $h = h_l h_t h_p$ is channel coefficient parameter due to turbulence (h_t), attenuation due to path loss (h_l) and pointing errors (h_p) [Farid and Hranilovic (2007)], s is transmitted
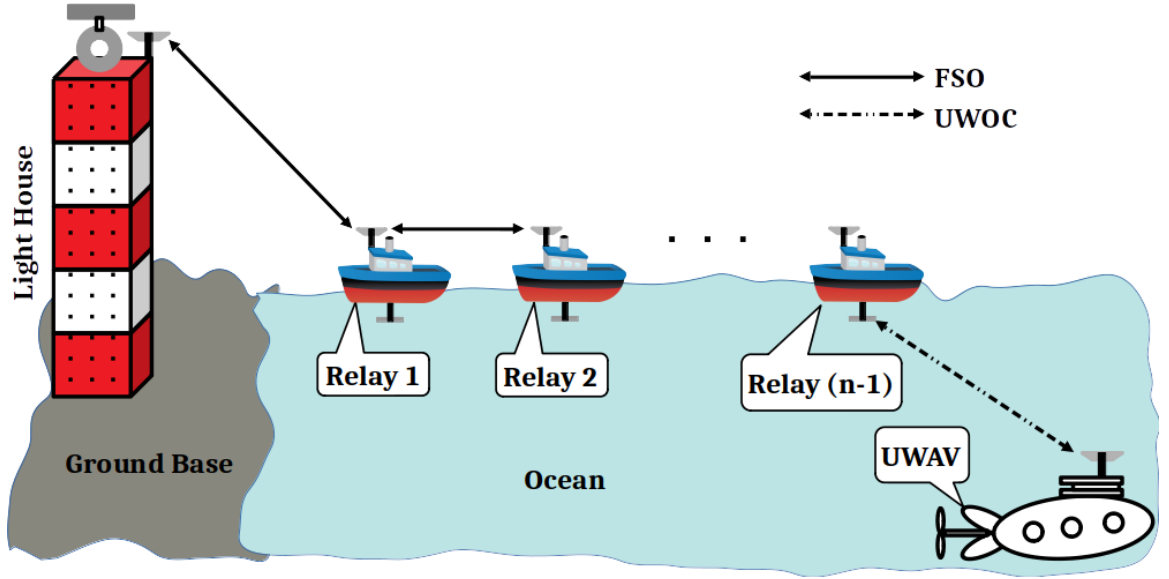
Figure 6.1: Generalized multi-hop system model.

data and n is additive white Gaussian noise with zero mean and σ^2 variance. Here, we have assumed the source of noise variance to be shot noise and have ignored the noise variance arising from background noise (due to smaller than other noise sources). Thus, noise variance is specified as $\sigma^2 = 2qi_dB$, where B is electronic band-width, $q = 1.602 \times 10^{-19}\ C$ is charge of electron, i_d is dark current of photo-detector (in nA).

As part of the multi-hop FSO-UWOC convergent system analysis, for simplicity, a triple-hop convergent communication system is shown in Fig. 6.2 is considered.The FSO and UWOC links are modelled using Gamma-Gamma (GG) and HTLN distributions respectively.

6.3 Statistical Characteristics

6.3.1 FSO channel model

The generalized turbulence perturbing to FSO system under the influence of pointing error is obtained using GG distribution, and its cumulative distribution function (CDF) is given in [Sandalidis *et al.* (2009)], is considered and modified in terms of average SNR as follows.

$$F_{\gamma_1}(\gamma_1) = \frac{g^2}{\Gamma(\alpha)\Gamma(\beta)} \mathrm{G}_{2,4}^{3,1}\left({}^{1,g^2+1}_{g^2,\alpha,\beta,0} \left| \frac{\alpha\beta g^2}{h_{l_1}\bar{\gamma}_f(g^2+1)}\gamma_1 \right. \right) \tag{6.2}$$
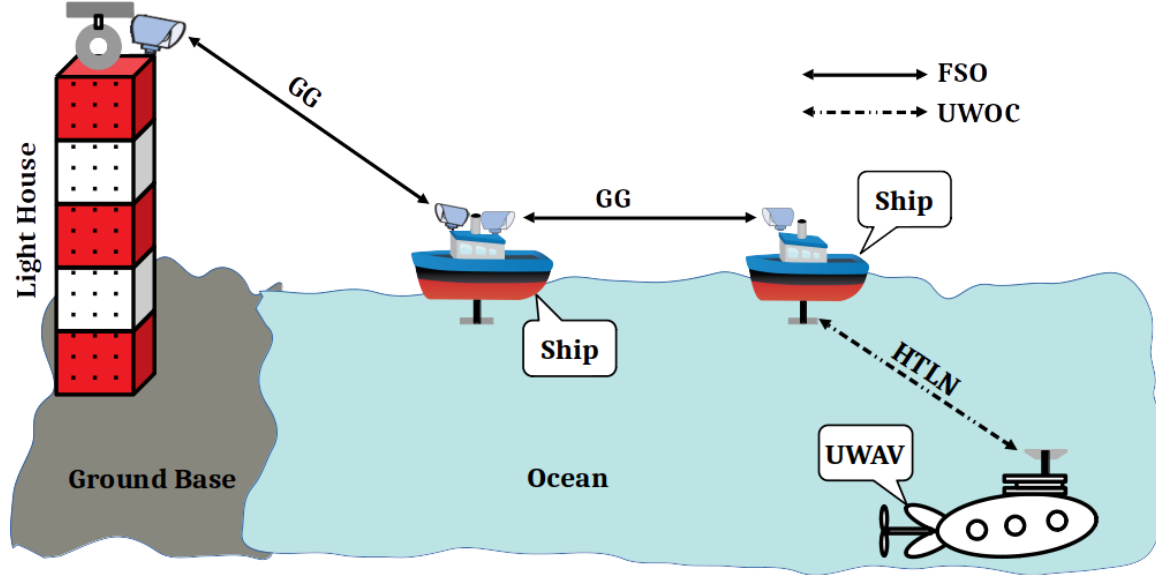
Figure 6.2: Triple-hop system model.

where, α corresponds to the effective number of large scale turbulence, β is a natural number and it represents the fading parameter are expressed in Eqs. (6.19) and (6.20) of Section 6.5.1, g is related to pointing error and is given as $g = \frac{W_{Z_{eq}}}{\sigma_s}$, $W_{Z_{eq}}$ is the beam-width, σ_s is the standard deviation of jitter and $\bar{\gamma}_f$ is the average SNR of the FSO link.

6.3.2 UWOC channel model

The UWOC channel is characterized by the weak turbulent oceanic medium in the presence of pointing errors, and is modeled using the HTLN distribution function, its CDF is given as [Naik *et al.* (2020)],

$$F_{\gamma_n}(\gamma_n) = \frac{e^{2a} g^2 \gamma_n^b}{b \left(A_0 h_{l_2} \bar{\gamma}_u\right)^b} G_{1+2b,1+2b}^{1+b,1+b} \left(\left. \begin{matrix} \frac{i-b}{b}, -1, \frac{i-b+g^2}{b} \\ \frac{i-b+g^2-1}{b}, 0, \frac{i-b-1}{b} \end{matrix} \right| e^{2a} \left(\frac{\gamma_n}{A_0 h_{l_2} \bar{\gamma}_u} \right)^b \right) \tag{6.3}$$

where a and b are shaping and scaling parameters of HTLN distribution function, $i = 1, 2, \ldots, b$, $A_0 = [erf(v)]^2$ is the fractional power at centre of the detector, $v = \frac{a_r}{w_z} \sqrt{\left(\frac{\pi}{2}\right)}$. a_r is the radius of the receiver and w_z is the beam width. γ_n is SNR of UWOC link, $\bar{\gamma}_u$ is the average SNR, and h_l^u is the path loss of the UWOC link.

The path loss of the FSO and UWOC links are obtained using Beer Lambert's law

and is given as [Pham *et al.* (2014), Levidala *et al.* (2021)],

$$h_{l_1} = \exp\left(-\sigma\ L_1\right),$$
$$h_{l_2} = \exp\left(-c(\lambda)\ L_2\right) \tag{6.4}$$

where σ and $c(\lambda)$ are the attenuation coefficients of the FSO and UWOC links, respectively, L_1 and L_2 are the link ranges of FSO and UWOC links, respectively.

6.3.3 CDF of end-to-end system

The SNR associated with the n DF relays is the minimum SNR required to decode the source message correctly at the destination node. Hence, the CDF of the end-to-end system using the n DF relay is defined as [Miridakis *et al.* (2014)],

$$F_{\gamma_{e2e}}\left(\gamma\right) = 1 - \left(1 - F_{\gamma_1}\left(\gamma\right)\right)\left(1 - F_{\gamma_2}\left(\gamma\right)\right) \cdots \left(1 - F_{\gamma_n}\left(\gamma\right)\right). \tag{6.5}$$

For ease of analysis, we have considered the CDFs associated with the FSO system (*i.e*, first $n-1$ relayed links) are similar $\left(i.e,\ F_{\gamma_1}\left(\gamma\right) = F_{\gamma_2}\left(\gamma\right) = \cdots = F_{\gamma_{n-1}}\left(\gamma\right)\right)$ and the nth relayed link is associated to UWOC link. Hence the end-to-end CDF can be obtained as,

$$F_{\gamma_{e2e}}\left(\gamma\right) = 1 - \left(1 - F_{\gamma_1}\left(\gamma\right)\right)^{n-1}\left(1 - F_{\gamma_n}\left(\gamma\right)\right). \tag{6.6}$$

Make use of binomial distribution to Eq. (6.6), obtained end-to-end CDF is given as,

$$F_{\gamma_{e2e}}\left(\gamma\right) = 1 + \sum_{k=0}^{n-1}(-1)^{n-k}\binom{n-1}{k}\left(F_{\gamma_1}\left(\gamma\right)\right)^{n-k-1}\left(1 - F_{\gamma_n}\left(\gamma\right)\right). \tag{6.7}$$

CDF of the end-to-end system presented in Fig. 6.2 (triple-hop system) is given as,

$$F_{\gamma_{e2e}}\left(\gamma\right) = F_{\gamma_1}\left(\gamma\right)\left(1 - F_{\gamma_n}\left(\gamma\right)\right)\left(2 - F_{\gamma_1}\left(\gamma\right)\right) + F_{\gamma_n}\left(\gamma\right) \tag{6.8}$$

6.4 Performance analysis

The performance analysis in terms of average BER and outage probability obtained in this section.

6.4.1 Average bit error rate

The average BER of the proposed end-to-end system is given as,

$$P_e = P_1 P_2 \cdots p_{n-1} \left(1 - P_n\right) + P_1 P_2 \cdots p_{n-2} \left(1 - P_{n-1}\right) P_n + \cdots + \left(1 - P_1\right) P_2 \cdots P_{n-1} P_n. \tag{6.9}$$

First $n-1$ links are similar FSO links $i.e.$, $P_1 = P_2 = \cdots P_{n-1}$ then

$$P_e = P_1^{(n-1)} \left(1 - P_n\right) + (n-1)P_1^{(n-2)} \left(1 - P_1\right) P_2 \tag{6.10}$$

where P_1 is BER for the FSO link, P_2 is BER of UWOC link. P_1 and P_2 for different modulations are calculated using,

$$P_1 = \frac{q^p}{2 \, \Gamma(p)} \int_0^\infty \gamma^{p-1} \exp\left(-q\gamma\right) F_{\gamma_1}\left(\gamma\right) d\gamma. \tag{6.11}$$

where p and q decides the type of detection and modulation schemes, respectively, which are shown in Table 6.1. Substituting Eq.(6.2) in Eq.(6.11), and using the Eq.(11) of [Adamchik and Marichev (1990)], the Eq.(6.11) rewritten as

$$P_1 = \frac{q^p g^2}{2 \, \Gamma(p)\Gamma(\alpha)\Gamma(\beta)} \int_0^\infty \gamma^{p-1} \mathrm{G}_{0,1}^{1,0}\left(q\gamma \,\middle|\, \begin{matrix} - \\ 0 \end{matrix}\right) \mathrm{G}_{2,4}^{3,1}\left(\frac{\alpha\beta g^2}{h_{l_1}\bar{\gamma}(g^2+1)}\gamma \,\middle|\, \begin{matrix} 1, g^2+1 \\ g^2, \alpha, \beta, 0 \end{matrix}\right) d\gamma. \tag{6.12}$$

After performing integration and some mathematical manipulations, the ABER of the FSO link can be given as

$$P_1 = \frac{g^2}{2 \, \Gamma(p)\Gamma(\alpha)\Gamma(\beta)} \, \mathrm{G}_{3,4}^{3,2}\left(\frac{\alpha\beta g^2}{h_{l_1}\bar{\gamma}q(g^2+1)} \,\middle|\, \begin{matrix} 1, g^2+1, 1-p \\ g^2, \alpha, \beta, 0 \end{matrix}\right) \tag{6.13}$$

Similarly, P_n can be calculated as,

$$P_n = \frac{q^p}{2 \, \Gamma(p)} \int_0^\infty \gamma^{p-1} \exp\left(-q\gamma\right) F_{\gamma_n}\left(\gamma\right) d\gamma. \tag{6.14}$$

Substituting Eq. (6.3) in (6.14), and using the Eq.(11) of [Adamchik and Marichev (1990)], the Eq.(6.14) rewritten as,

$$P_n = \frac{e^{2a} g^2 q^p}{2b \left(A_0 h_{l_2}\bar{\gamma}\right)^b \Gamma(p)} \int_0^\infty \gamma^{b+p-1} \mathrm{G}_{0,1}^{1,0}\left(q\gamma \,\middle|\, \begin{matrix} - \\ 0 \end{matrix}\right) \mathrm{G}_{1+2b,1+2b}^{1+b,1+b}\left(\frac{e^{2a}}{\left(A_0 h_{l_2}\bar{\gamma}\right)^b}\gamma^b \,\middle|\, \begin{matrix} \frac{i-b}{b}, -1, \frac{i-b+g^2}{b} \\ \frac{i-b+g^2-1}{b}, 0, \frac{i-b-1}{b} \end{matrix}\right) d\gamma. \tag{6.15}$$

Integrating the above equation, obtained ABER expression is given as,

$$P_n = \frac{e^{2a}g^2 b^{b+p-0.5}}{2b\Gamma(p)\,(2\pi)^{0.5(b-1)}\,(A_0 h_{l_2} q\bar{\gamma})^b} \mathrm{G}_{1+3b,1+2b}^{1+b,1+2b} \left(e^{2a} \left(\frac{b}{A_0 h_{l_2} q\bar{\gamma}} \right)^b \left| \begin{matrix} \frac{i-b}{b}, -1, \frac{i-b-p}{b}, \frac{i-b+g^2}{b} \\ \frac{i-b+g^2-1}{b}, 0, \frac{i-b-1}{b} \end{matrix} \right. \right).$$

$$(6.16)$$

Table 6.1: BER parameters for different modulation schemes.

p	q	Modulation
0.5	0.5	Coherent Binary Frequency Shift Keying (CBFSK)
0.5	1	Coherent Binary Phase Shift Keying (CBPSK)
1	0.5	Non-Coherent Binary Frequency Shift Keying (NBFSK)
1	1	Differential Binary Phase Shift Keying (DBPSK)

6.4.2 Outage probability

The outage probability is defined as the probability that the SNR of DF relay falls below a given threshold SNR $(i.e, \gamma_{th})$ which is given as,

$$P_{out} = P\left(\min\{\gamma_1, \gamma_2, \cdots, \gamma_n\} \le \gamma_{th}\right) = F_{\gamma_{e2e}}\left(\gamma_{th}\right)$$

$$= 1 + \sum_{k=0}^{n-1} (-1)^{n-k} \binom{n-1}{k} \left(F_{\gamma_1}\left(\gamma_{th}\right)\right)^{n-k-1} \left(1 - F_{\gamma_n}\left(\gamma_{th}\right)\right). \qquad (6.17)$$

The outage probability for the proposed triple-hop system shown in Fig. 6.2 is derived from the multi-hop expression Eq. (6.17) as follows,

The outage performance of the proposed system is analyzed for different weather conditions, turbulent regimes, number of hops of FSO link and different pointing error scenario of both FSO and UWOC links. The different system and channel parameters considered for the analysis are tabulated in Tables 6.2, 6.3, 5.1 and 6.4.

6.5   Results and Discussions

In this section, we analyze the performance of the proposed system in terms of outage probability, ABER, and channel capacity. We consider different weather conditions (clear air, moderate rain, and light fog) and turbulence (strong turbulence -ST,

$$
\begin{aligned}
P_{out} \; = \;\; & \frac{g^2}{\Gamma\left(\alpha\right)\Gamma\left(\beta\right)} \mathrm{G}_{2,4}^{3,1}\left(\left.{}_{g^2,\alpha,\beta,0}^{1,g^2+1} \right| \frac{\alpha\beta g^2 \gamma_{th}}{h_{l_1}\bar{\gamma}_f\left(g^2+1\right)} \right) \\
\times \;\; & \left(1 - \frac{e^{2a}g^2\gamma_{th}^b}{b\left(A_0 h_{l_2}\bar{\gamma}_u\right)^b} \mathrm{G}_{1+2b,1+2b}^{1+b,1+b}\left(\left.{}_{\frac{i-b+g^2-1}{b},0,\frac{i-b-1}{b}}^{\frac{i-b}{b},-1,\frac{i-b+g^2}{b}} \right| e^{2a}\left(\frac{\gamma_{th}}{A_0 h_{l_2}\bar{\gamma}_u} \right)^b \right) \right) \\
\times \;\; & \left(2 - \frac{g^2}{\Gamma\left(\alpha\right)\Gamma\left(\beta\right)} \mathrm{G}_{2,4}^{3,1}\left(\left.{}_{g^2,\alpha,\beta,0}^{1,g^2+1} \right| \frac{\alpha\beta g^2 \gamma_{th}}{h_{l_1}\bar{\gamma}_f\left(g^2+1\right)} \right) \right) \\
+ \;\; & \frac{e^{2a}g^2\gamma_{th}^b}{b\left(A_0 h_{l_2}\bar{\gamma}_u\right)^b} \mathrm{G}_{1+2b,1+2b}^{1+b,1+b}\left(\left.{}_{\frac{i-b+g^2-1}{b},0,\frac{i-b-1}{b}}^{\frac{i-b}{b},-1,\frac{i-b+g^2}{b}} \right| e^{2a}\left(\frac{\gamma_{th}}{A_0 h_{l_2}\bar{\gamma}_u} \right)^b \right). \qquad (6.18)
\end{aligned}
$$

Table 6.2: Turbulence parameters of FSO link.

Turbulence parameters	Description
$\alpha = 2.75, \beta = 2.25$	Moderate turbulence
$\alpha = 2, \beta = 1$	Strong turbulence

Table 6.3: Pointing error conditions.

Pointing error parameter	Description
$g = 3$	Weak pointing error (WPE)
$g = 1.25$	Moderate pointing error (MPE)
$g = 1$	Strong pointing error (SPE)

Table 6.4: Path loss of 50 m UWOC link.

Water type	$c(\lambda)(m^{-1})$	h_{l_2} (dB)
Clear ocean	0.151	0.1758
Coastal ocean	0.399	0.0101
Turbid harbor	2.195	1.0593×10^{-11}

moderate turbulence - MT) for all FSO links. Since we consider the HTLN channel model for the UWOC link, it is assumed to have weak turbulence. Attenuation/path loss is considered (including absorption and scattering) and obtained the results for different oceanic conditions such as the clear ocean, coastal ocean, and turbid harbor. We consider the same pointing error value for both the FSO and UWOC links. In the case of all FSO links, we consider 1 km of link distance. Similarly, all UWOC links have a 50 m link distance. Figures 6.3 to 6.5 provide the end-to-end outage performance of the system for different FSO and UWOC link parameters.
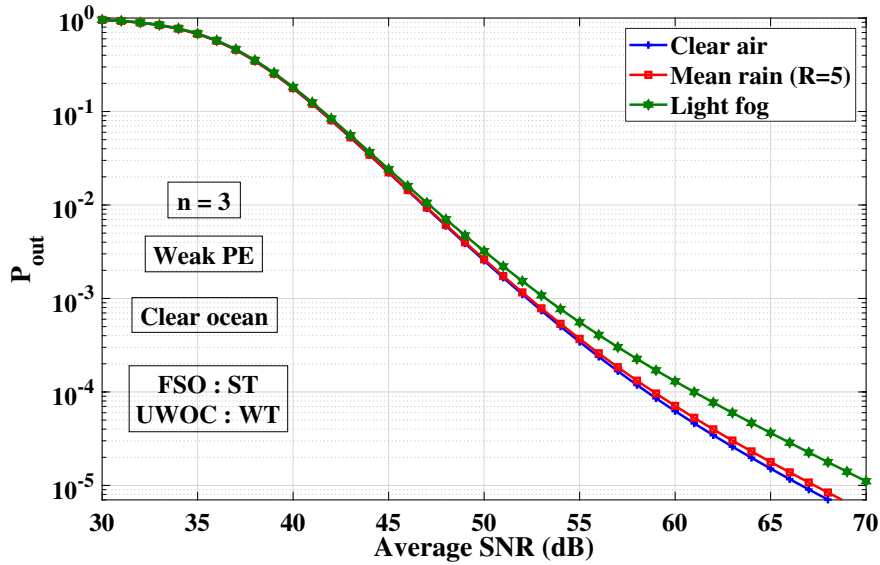
Figure 6.3: Outage performance of the end-to-end system under the influence of various FSO weather conditions.

Figures 6.3 to 6.8 provide the end-to-end outage performance of the system for different FSO and UWOC link parameters. Fig. 6.3 visualizes the outage analysis of the triple-hop converging system under different FSO weather conditions. The weak pointing error and strong turbulence condition is considered for FSO link in this analysis. As the average SNR increases, it is observed that the outage decreases. Similarly, the performance of the outage decreases with the change in weather conditions. Compared to clear air, the light fog condition reduces the performance of the end-to-end system.

Fig. 6.4 depicts the outage probability performance of the triple-hop end to end system for the strong turbulence, clear air FSO and varying underwater scenarios such as, clear ocean, coastal ocean and turbid harbor ocean. Weak pointing error is
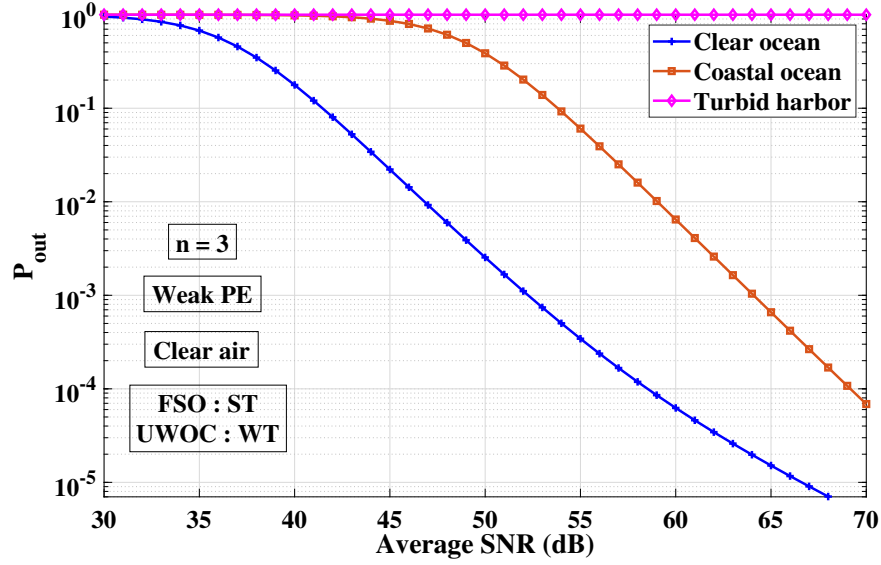
Figure 6.4: Outage performance of the triple-hop system under the influence of strong turbulence and clear air FSO with varying oceanic water conditions.

Table 6.5: Physical parameters used in the calculations.

Variable	Range
C_n^2	10^{-8} to 10^{-14} $m^{-2/3}$
h_{l_1}	Refer Table 5.1
h_{l_2}	Refer Table 6.4
L_1	1 Km
L_2	50 m
λ	530 nm UWOC 1550 nm FSO
k	$2\pi/\lambda$
a_r	0.1 m
w_z	1 m
a	0.349
b	2

considered for both FSO and UWOC links. Variation in performance can be observed from different oceanic water. Compared to clear ocean, to achieve 10^{-2} outage performance, for coastal ocean case, it requires additional 12 dB of average SNR. Where as the performance in turbid harbor water is highly influenced by errors due to the higher amount of attenuation compared with the clear and coastal ocean and hence communication is not possible under turbid harbor water.
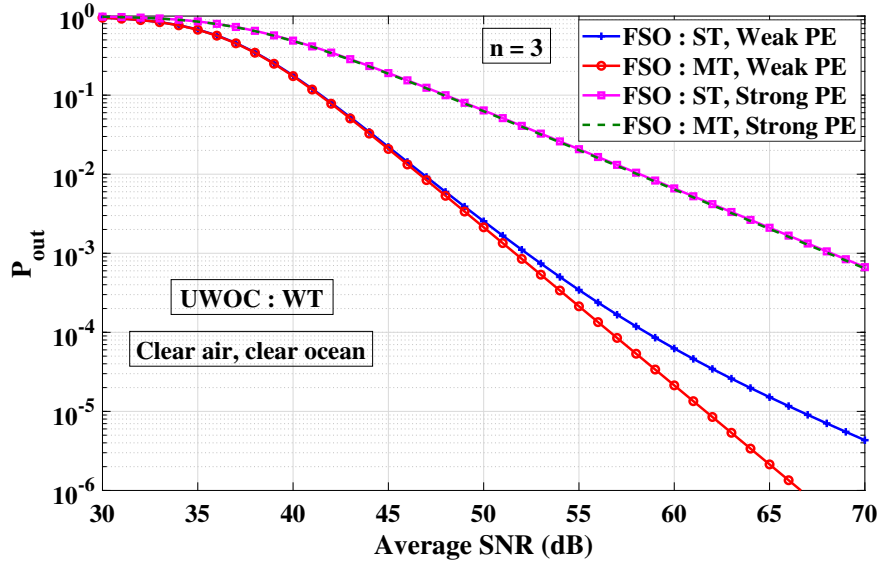
Figure 6.5: Outage performance of the end-to-end system under the influence of various strengths of turbulence and varying pointing errors.

Fig. 6.5 shows the performance of the triple-hop communication system under different FSO turbulence conditions, such as moderate and strong. Similar to the previous case, here a weak and strong pointing error conditions are assumed for this analysis. Clear weather and clear ocean conditions are considered for the FSO and UWOC links, respectively. The plot shows that the outage decreases due to an increase in the average SNR. There is also deterioration in the performance of the proposed system from moderate to strong turbulence.

Fig. 6.6 shows the performance of the end-to-end triple-hop system with varying pointing error values, such as $g = 3$, 1.25 and 1 for weak, moderate, and strong pointing error respectively. In this case, clear weather conditions are considered for both the FSO and UWOC links. Strong turbulence condition is applied over the FSO link. There is a significant loss in the received signal when the pointing error is high. With the decrease in the pointing error value, the performance of the proposed system
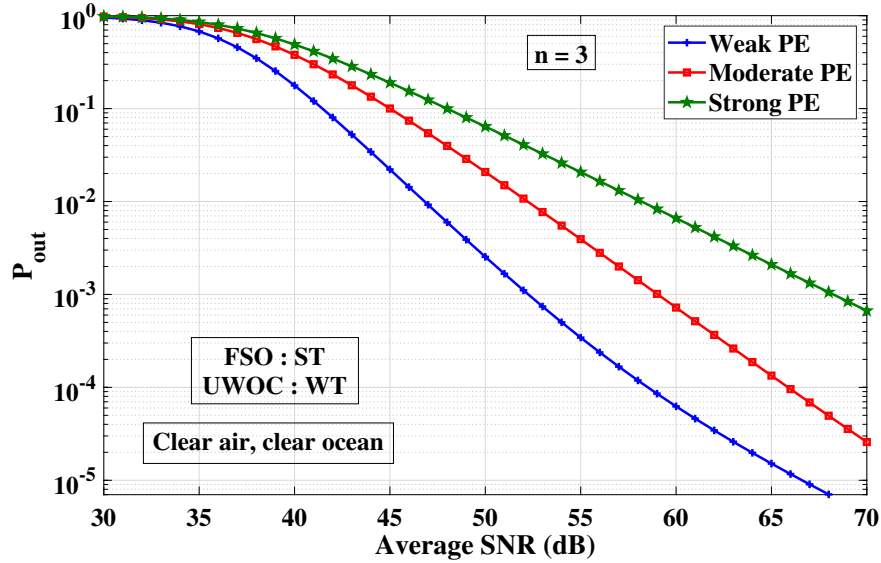
Figure 6.6: Outage performance of the end-to-end system under the influence of various strengths of pointing errors.

is reduced from weak to strong pointing error.

Fig. 6.7 visualizes the outage probability analysis of the proposed generalized multi-hop communication system. The number links 'n' varied by considering the weak pointing error and ST for FSO link. In clear FSO and UWOC weather conditions, it is observed that there is deterioration in the performance of the end-to-end system with the increase in the number of connections/hops.

Fig. 6.8 shows the outage analysis of the proposed triple-hop communication system; and the individual FSO and UWOC links. Weak pointing error conditions are assumed for both FSO and UWOC links. Strong FSO turbulence is considered for this analysis. Clear weather conditions are considered for both the FSO and UWOC links. The result shows that the end-to-end triple-hop system depends on the UWOC link.

Fig. 6.9 depicts the outage probability analysis for a triple-hop system for different pointing error values from one link to another. Moderate turbulence is considered for FSO link along with clear air and clear oceanic conditions. As shown in Table 6.3, WPE, SPE represents weak and strong pointing error values, respectively. The UWOC link under strong pointing error shows more effect compared with the weak pointing error on the end-to-end triple-hop system. From the figure it can be observed that the outage probability of 10^{-2} is achieved at 40 dB of average SNR for strong UWOC
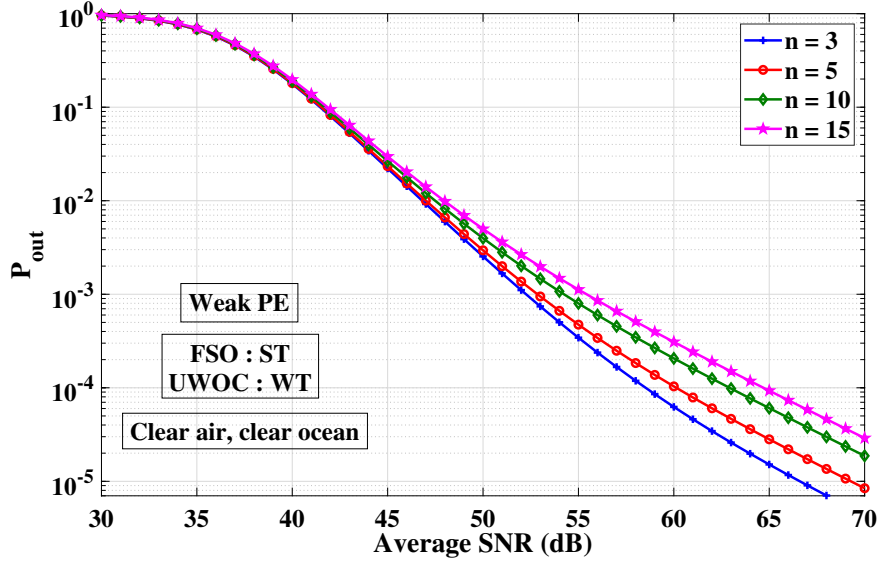
Figure 6.7: Outage performance of the proposed system with varying number of hops n.
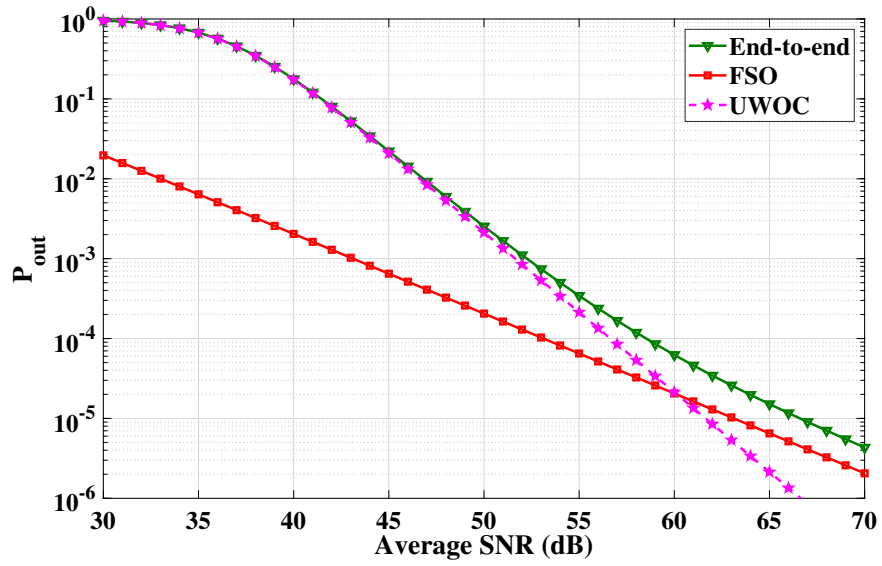
Figure 6.8: Outage performance of the proposed and individual systems.

Figure 6.9: Outage performance of a triple-hop system for different pointing error values from one link to other links.

pointing error conditions. For weak UWOC pointing error condition, the outage of approximately 10^{-1} is achieved for the same average SNR of 40 dB.

Figures 6.10 to 6.15 provide the ABER performance of the proposed end-to-end system for different FSO and UWOC link parameters. Fig. 6.10 visualizes the ABER analysis of the triple-hop converging system under different modulation schemes. The weak pointing error and strong turbulence condition is considered for FSO link in this analysis. It is observed that the ABER decreases, with the increase in average SNR. Under clear FSO and oceanic conditions, the CBPSK scheme shows the better performance compared to other modulation schemes.

Fig. 6.11 shows the ABER performance for the triple-hop end-to-end system. Clear air and clear ocean conditions are considered for the FSO and UWOC links. FSO turbulence and pointing error conditions are varied by considering the CBPSK modulation scheme. Both turbulence and pointing error shows the effect on the end-to-end system. Under moderate turbulence, to achieve the ABER of 10^{-4}, it requires 21 dB of average SNR at weak pointing error. For strong pointing error, it requires an additional 10 dB of average SNR to achieve the same ABER. In fig. 6.11 it is also observed that, moderate turbulence and weak pointing error outperforms the end-to-end system.

Fig. 6.12 depicts the ABER analysis for the triple-hop convergent system for

Figure 6.10: ABER performance of the proposed system for varying modulation schemes.
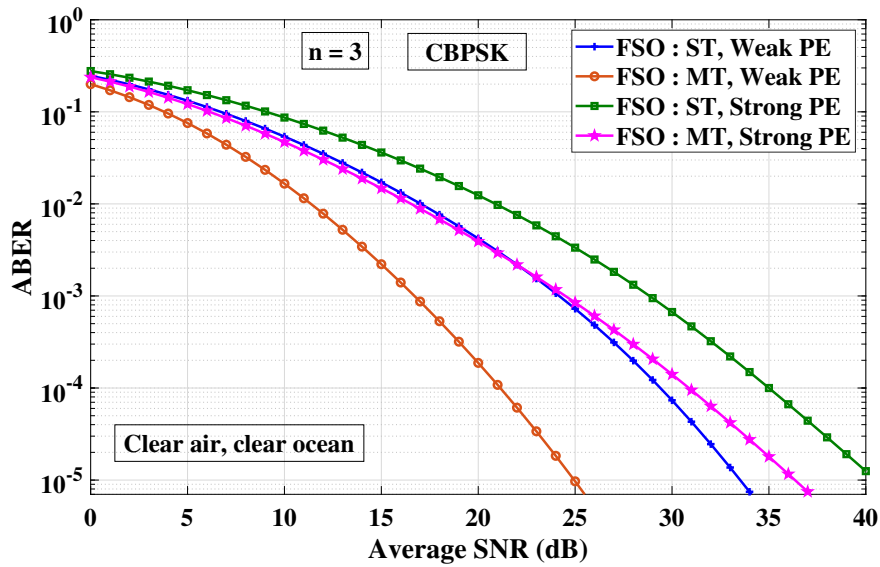
Figure 6.11: ABER performance of the proposed system for varying pointing error and FSO turbulence.

CBPSK scheme and varying pointing error cases. We consider clear weather conditions for both FSO and UWOC links. We also consider strong turbulence for FSO link. There is a considerable ABER variation from the weak to strong pointing error. With strong pointing error there is degradation in the performance of end-to-end system.
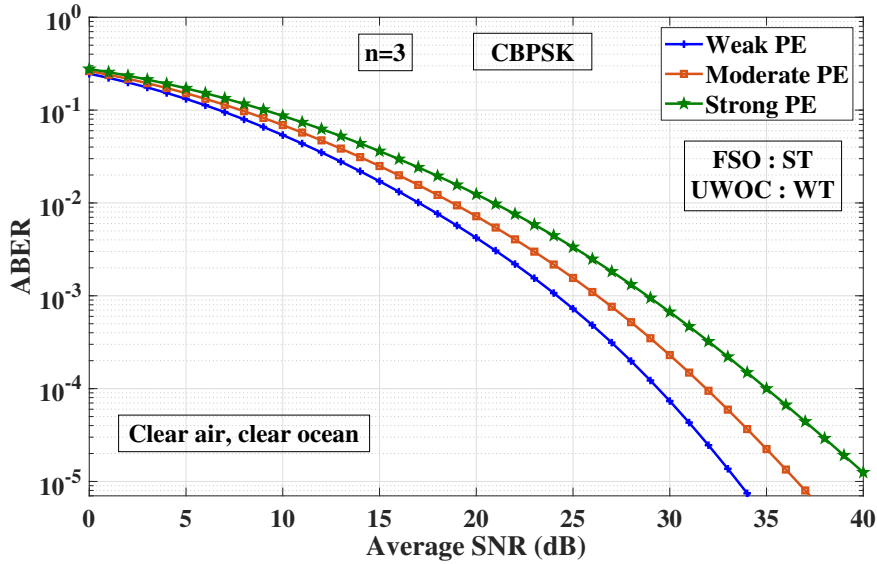
Figure 6.12: ABER performance of the proposed system for varying pointing errors.

Figs. 6.13 & 6.14 presents the ABER performance of the triple-hop system for the varying FSO and UWOC weather conditions, respectively. We consider the strong FSO turbulence for both the cases. For fig. 6.13, we consider the clear ocean water, and for fig. 6.14, we consider the clear FSO link. Compared to clear air, light fog weather degrades the system performance. Similarly, compared to clear water, turbid water degraded the system performance.

Fig. 6.15 exhibits the end-to-end system's performance for varying number of hops 'n' over clear FSO and UWOC weather conditions. We consider weak pointing error, strong FSO turbulence, CBPSK modulation scheme for the analysis. As the number of hops increase, the performance also increase. To achieve the ABER of 10^{-4}, with 5 hops it takes 11 dB of average SNR, and it requires additional 19 dB of average SNR is to achieve the same ABER value.

Fig. 6.16 depicts the ABER analysis of a triple-hop communication system over clear air and oceanic weather conditions, under the influence of different pointing error from one link to another link. To analyze the ABER, moderate turbulence and CBPSK modulation schemes are considered. The results show that the weak pointing error
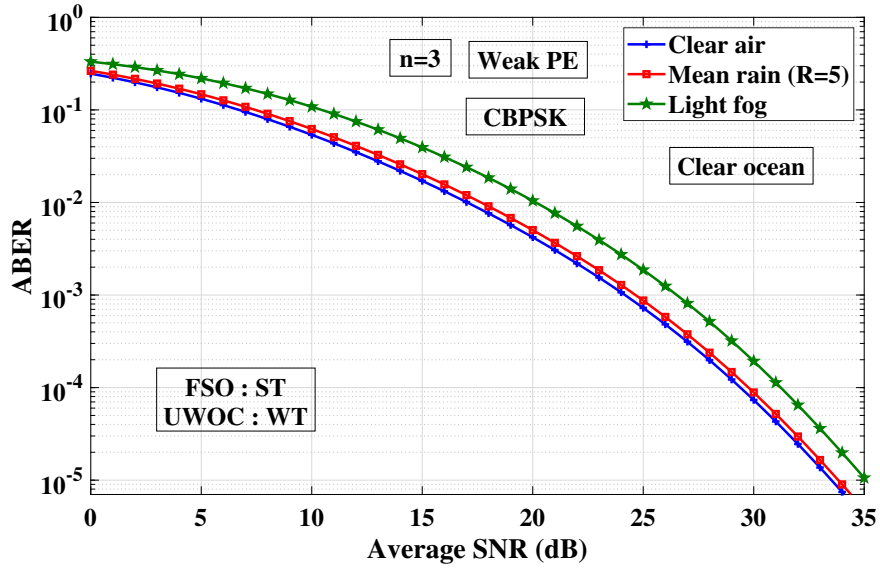
Figure 6.13: ABER performance of the proposed system for varying FSO path loss.
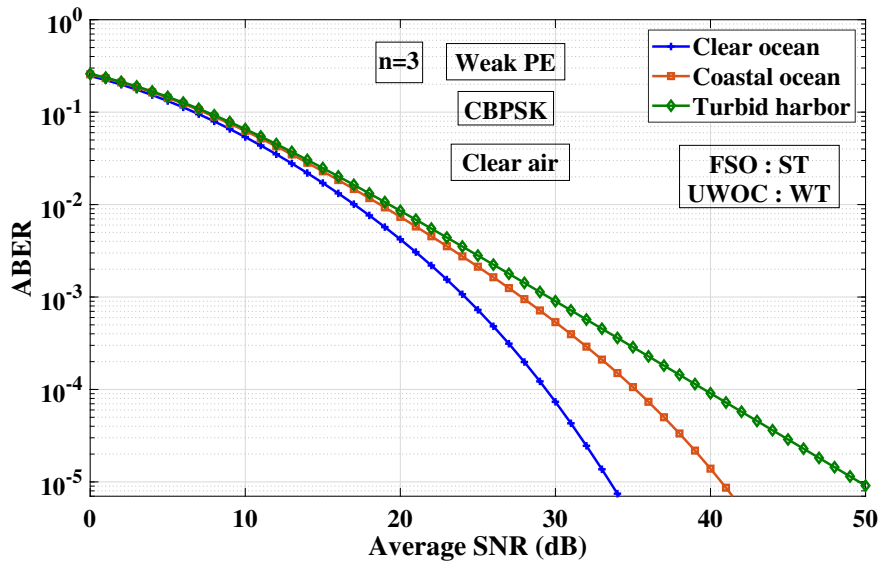
Figure 6.14: ABER performance of the proposed system for varying UWOC path loss.

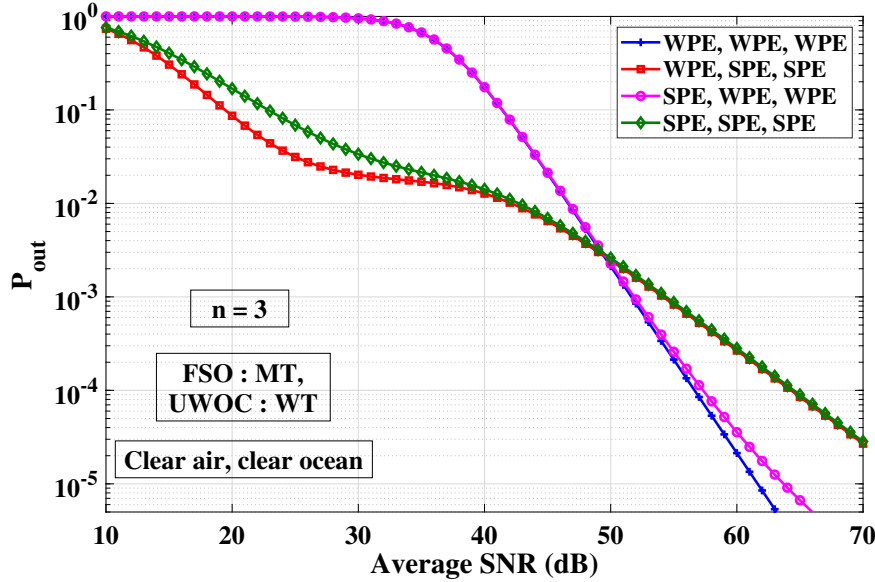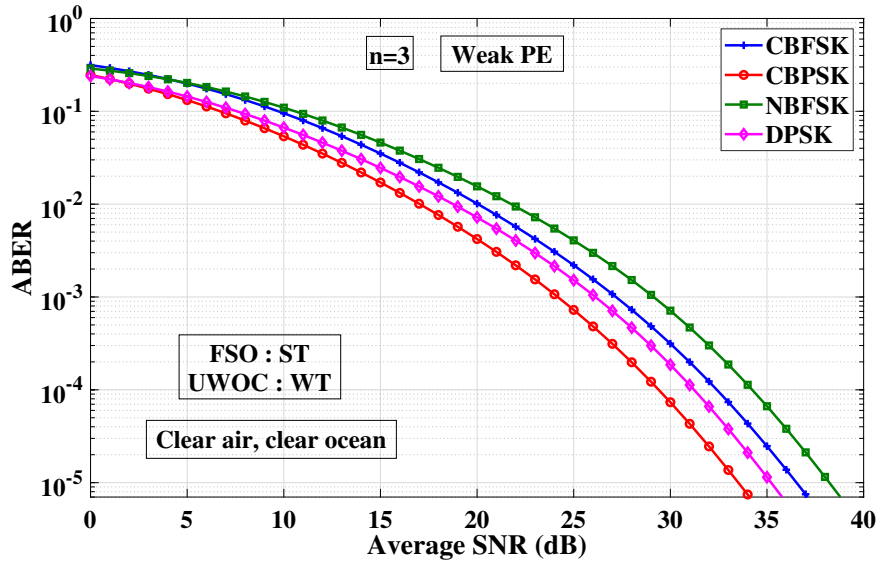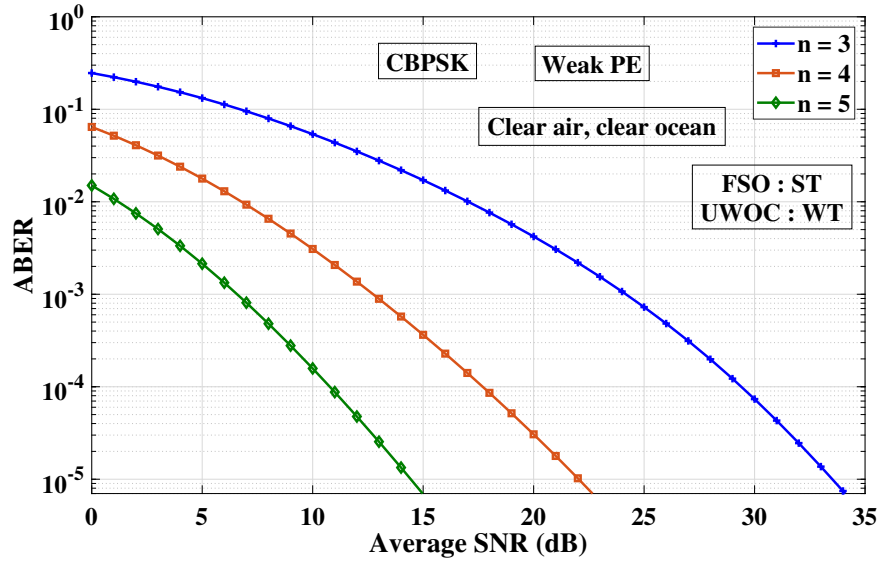**Figure 6.15:** ABER performance of the proposed system for varying number of hops $'n'$.
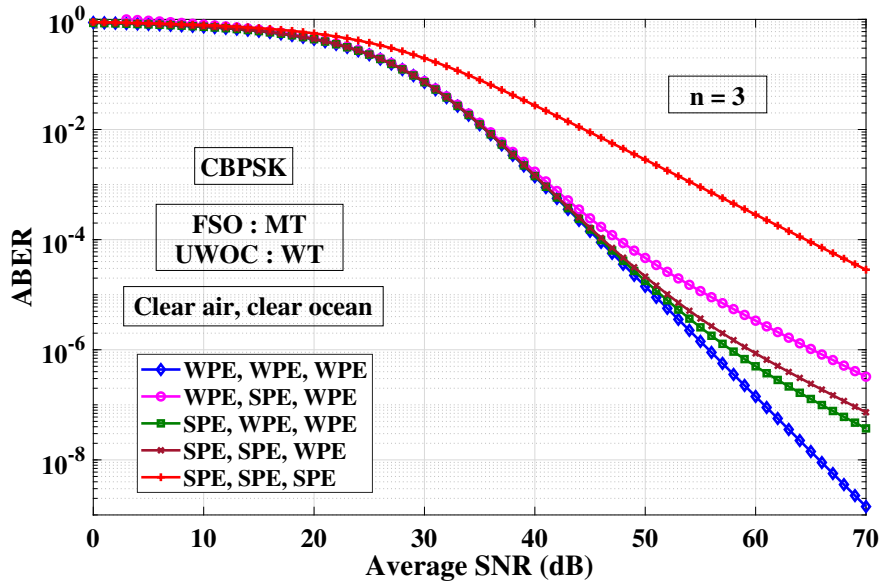
Figure 6.16: ABER performance of a triple-hop system for different pointing error values from one link to other links.

gives a better performance compared with the strong pointing error. Strong pointing error over UWOC link requires an additional 17 dB of average SNR to achieve the ABER of 10^{-4}.

6.5.1 Case study

A case study on how the speed of the ship, the height of the ship (turbulence level with respect to that altitude), the speed of the wind, and the variation of the link between the ships (hops) interfere with the transmission of light to free space has been tested in this section. Wind power is one of the most crucial parameter to introduce changes in the received energy. It is the most prominent factor in the attenuation of the signal that propagates through free space [Tang *et al.* (2014)]. Due to the turbulence associated with the non-homogeneity refractive index of the particles present in the atmosphere, the optical signal fades as the atmospheric visibility decreases. This study was carried out in Surathkal, located 20 km north of Mangalore. In this case study, we assumed that the ships are located in the Arabian Sea near Surathkal (GPS coordinates: N 13° 0' 38.0988", E 74° 47' 17.4876"), Karnataka, India. Wind turbulence causes drastic changes in the refractivity index of the atmosphere, redistributing the FSO link optical beam. Due to the re-distribution of optical energy, the change in refractive index structure parameter is taken into account in order to investigate the wind effect on FSO.

This section gives a brief overview of the multi-hop FSO converging with the UWOC system design by considering the triple-hop communication system and evaluating its outage performance versus the link distance. We assume that both the transmitter and the receiver are aligned with a weak point error and time-synchronized. In addition to the default system parameters set out in the previous section, we also consider very clear air and clear ocean cases. Notably, the wind speed (15 m/s) above the ocean, the average speed of the ship (20 knots/h), and the refractive index structure parameter (3.033×10^{-12}) are taken into account for FSO links. Fig. 6.17 shows the details of the case study. Although the ships are moving at a constant speed, the fluctuations result in a change in the location of the received beam at the receiver's aperture due to the direction of the ship. As the link range increases, the outage also increases.

The wind speed during 22nd January to 4th February 2021 at Surathkal, India is illustrated in Fig. 6.18. The minimum and maximum wind speed recorded in this
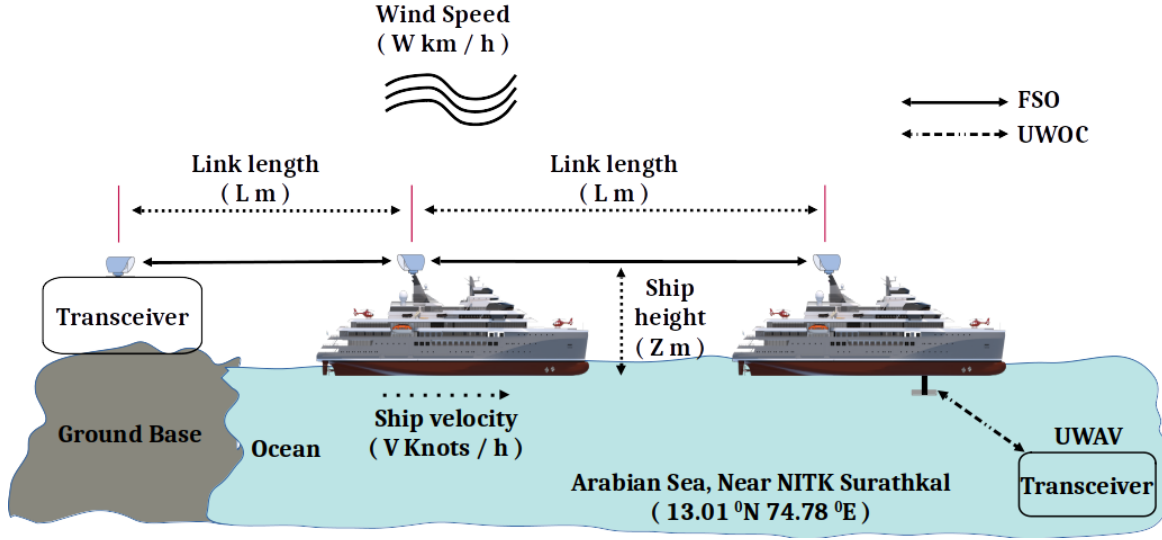
Figure 6.17: Case study of the proposed triple-hop system with various parameters.

duration is 0.36 Km/h and 28.7 Km/h respectively. The outage performance of the proposed system is analyzed in case study based on the recorded values of this wind speed at a height of 80m.

The performance of the end-to-end system depends on the height of the ship as well as link length. The turbulence related parameters, α and β given in Eqs. (6.19) and (6.20) depends on the refractive index structure parameter $C_n^2(Z)$, and link length L. Variations in $C_n^2(Z)$ are obtained according to wind speed and height of the ship.

$$\alpha = \left(\exp\left(\frac{0.17 \ \sigma_R^2}{\left(1 + 0.167 \ \sigma_R^{12/5}\right)^{7/6}} \right) - 1 \right)^{-1} \tag{6.19}$$

$$\beta = \left(\exp\left(\frac{0.225 \ \sigma_R^2}{\left(1 + 0.259 \ \sigma_R^{12/5}\right)^{5/6}} \right) - 1 \right)^{-1}. \tag{6.20}$$

The Rytov variance σ_R^2 is given as,

$$\sigma_R^2 = 0.5 \ C_n^2(Z) \ k^{7/6} \ L^{11/6} \tag{6.21}$$

where L is the link length in meters, $k = 2\pi/\lambda$, λ is the optical wavelength, and $C_n^2(Z)$ is [Khallaf and Uysal (2019)] the refractive index structure constant and is given as,
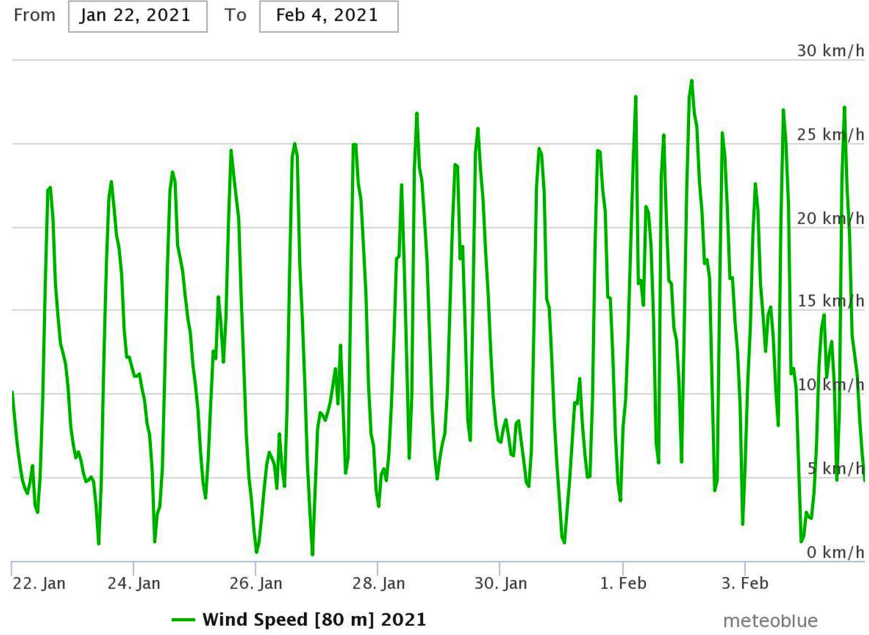
Figure 6.18: Wind Speed and direction during 22nd January to 4th February 2021 at Surathkal, India [Online (2021*b*)].

$$
\begin{aligned}
C_n^2(Z) \ = \ & 0.00594 \left(\frac{W}{27} \right)^2 \left(10^{-5} Z \right)^{10} \exp \left(-\frac{Z}{1000} \right) \\
+ \ & 2.7 \times 10^{-16} \exp \left(-\frac{Z}{1500} \right) + A \exp \left(-\frac{Z}{100} \right).
\end{aligned}
\tag{6.22}
$$

Fig. 6.19 depicts the end-to-end system's performance with the change in link length. Fig. 6.19a shows the outage analysis for different heights of the ships. Similarly, Fig. 6.19b gives the overall system performance with the change in time of a day. During the day time, the sunlight will add a background noise to the transmitted light signal. During night time, there will not be such a background noise. As the link range increases, the outage also increases. Also, with the decrease in the height and link length, there are considerable performance changes in the end-to-end system.
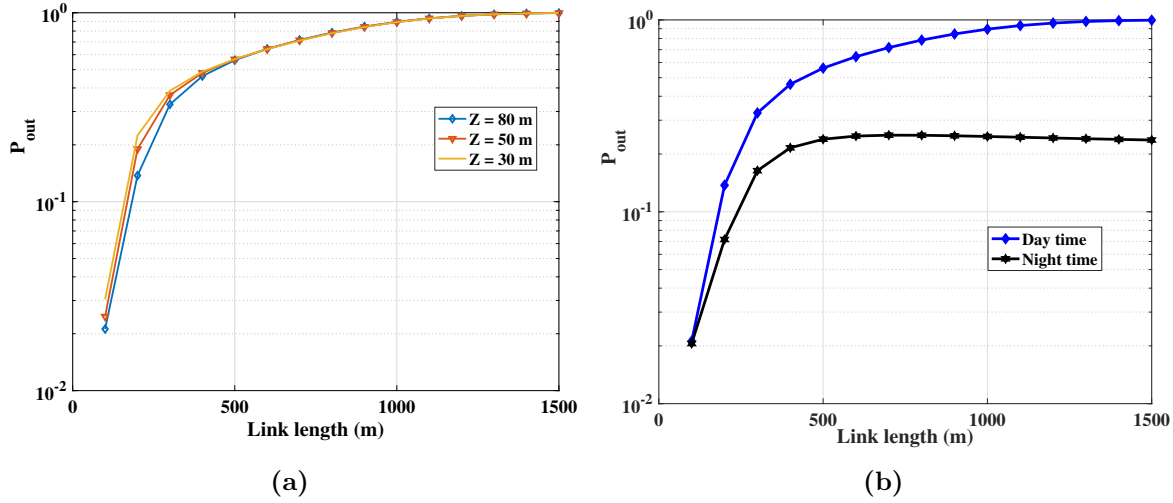
Figure 6.19: P_{out} Vs Link length in clear ocean and very clear air conditions (a) for varying ship height (b) for change in time of the day.

6.5.2 Complexity analysis

The turbulence analysis of FSO and UWOC channel using the CDF of Málaga distribution is given as [Ansari *et al.* (2015)],

$$F_{\gamma_{HD}}(\gamma) = \frac{g^2 A}{2} \sum_{m=1}^{\beta} b_m \; \mathrm{G}_{2,4}^{3,1} \left[B\frac{\gamma}{\bar{\gamma}} \;\middle|\; \begin{array}{c} 1, g^2+1 \\ g^2, \alpha, m, 0 \end{array} \right], \tag{6.23}$$

where $A \triangleq \frac{2\,\alpha^{\alpha/2}}{\xi^{1+\alpha/2}\Gamma(\alpha)} \left(\frac{\xi\,\beta}{\xi\,\beta+\Omega'} \right)^{\beta+\alpha/2}$, $a_m \triangleq \left(\begin{array}{c} \beta-1 \\ m-1 \end{array} \right) \frac{(\xi\,\beta+\Omega')^{1-m/2}}{(m-1)!} \left(\frac{\Omega'}{\xi} \right)^{m-1} \left(\frac{\alpha}{\beta} \right)^{m/2}$,

$b_m = a_m \left[\frac{\alpha\beta}{\xi\beta+\Omega'} \right]^{-\frac{\alpha+m}{2}}$, $B = \frac{g^2\alpha\beta\;(\xi+\Omega')}{[(g^2+1)(\xi\beta+\Omega')]}$, and $\Omega' = \Omega+2\left(b_0\rho + \sqrt{2}b_0\rho\Omega\cos(\phi_A-\phi_B)\right)$.

Number of unknowns in Málaga distribution are $2\beta+13$, which are $\alpha, \beta, \xi, \Omega'$, $g, A, B, b_0, \Omega, \rho, \phi_A, \phi_B, \bar{\gamma}, a_1, a_2, \cdots, a_m, b_1, b_2, \cdots, b_\beta$, where as Gamma-Gamma has 5 unknowns, which are $\alpha, \beta, g, h_l, \bar{\gamma}$.

From Fig. 6.20, the computational complexity of HTLN and GG CDF's are very less compared with the other CDF obtained using the Málaga CDF.

6.5.3 Cost analysis

The expected cost analysis for RF and FSO systems given in [Dahrouj *et al.* (2015), Naik *et al.* (2020)]. Deploying the UWOC link requires higher installation and main-
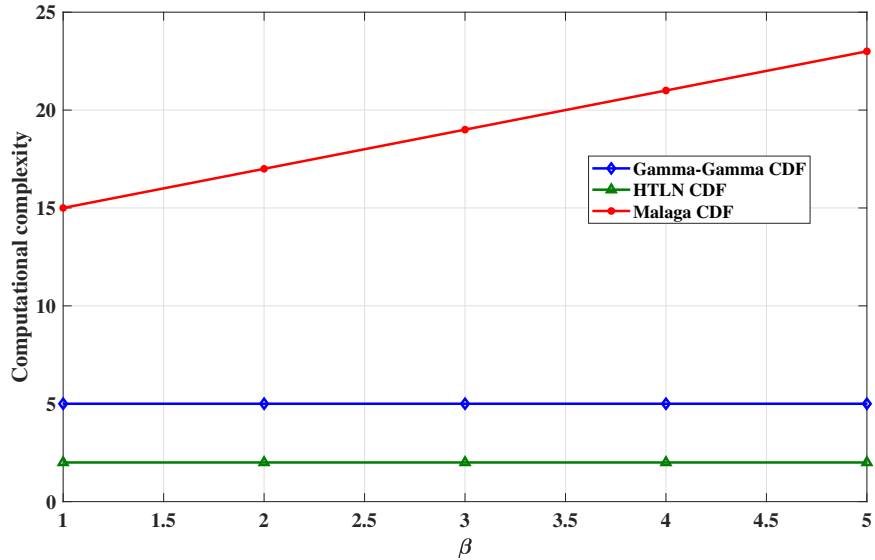
Figure 6.20: CDF complexity comparison of Gamma-Gamma, HTLN and Málaga.
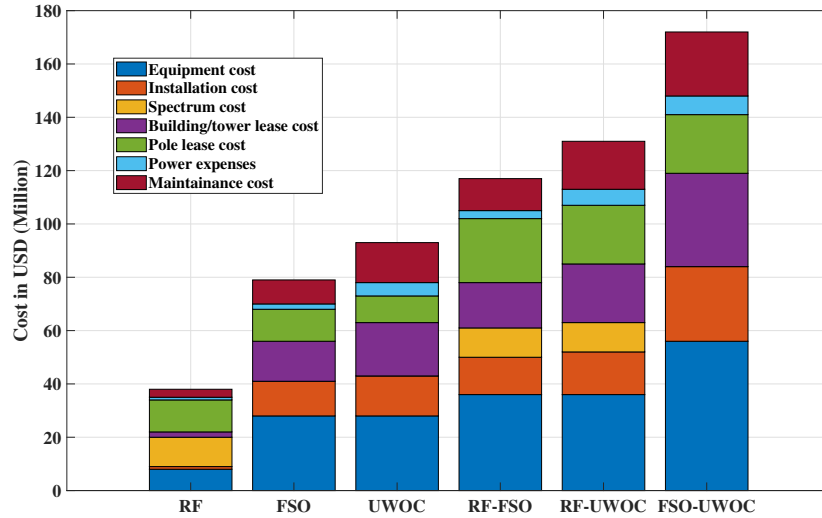
Figure 6.21: Cost analysis of various communication schemes.

tenance costs than the FSO link. Fig. 6.21 shows the cost analysis to establish RF, FSO, and UWOC links. The RF systems alone take the less overall cost for terrestrial communication. Due to the high equipment cost and installation costs for FSO, UWOC, and convergent UWOC systems, they seem to be expensive. But there is no spectrum cost in both FSO or UWOC systems. There is a trade off between convergent systems' cost and data transfer rate.

6.6　Summary

A multi-hop FSO-UWOC convergence system for tracking and security applications is proposed in this chapter. The performance of the proposed system is studied for different FSO weather conditions, underwater conditions, turbulence regimes, and pointing error scenarios. In comparison to the clear ocean, the coastal ocean situation requires an additional 12 dB of average SNR to achieve 10^{-2} outage performance. In contrast, due to the higher attenuation in turbid harbor water compared to the clear and coastal ocean, performance is heavily influenced by errors, and hence communication is impossible. To attain the ABER of 10^{-4} in moderate turbulence, 21 dB of average SNR at weak pointing error is required. To obtain the same ABER with a strong pointing error, an additional 10 dB of average SNR is required. The results show that the proposed system provides reliable high-speed connectivity for the mentioned applications.

Chapter 7

Performance Analysis of Multi-hop UWOC Convergent with FSO System

7.1 Introduction

Life on planet earth depends on the water available from different sources like rivers, lakes, wells, and oceans. These sources provide different types of water for various purposes such as agriculture, industrial and domestic use. For every living being and plant, there is a need for water in the direct form or oxygen; no water - no life. Oceans' impact is more on the earth's surface, and human life depends heavily on the ocean. Humans explored only very small amount of the whole ocean, and a massive volume of waters are yet there to investigate. In human life, the oceans play more essential roles such as climate regulation, transportation, recreation, nourishment, and medication. Due to several hazards (erosion, harmful algal blooms, hurricanes, flooding, tsunamis, depleted oxygen regions, marine debris, oil and chemical spills, and sea-level rise), discovering new oceanic waters become critical. Hence, advanced technologies like underwater optical wireless sensor networks (UOWSNs) and the Internet of underwater things (IoUT) have recently attracted significant attention and are becoming a promising alternative to explore the underwater environment [Zhou *et al.* (2015), Online (2021*a*)]. Research on the Internet of things (IoT) started three decades ago and remarkable progress over the last decade. IoT spread its branches to several fields. In 2010s, the IoUT concept came into the world [Kao *et al.* (2017*b*)]. IoUT is a new subdivision of IoT, and its definition is "the network of smart interconnected underwater objects" [Domingo (2012), Berlian *et al.* (2016)]. IoUT is applicable in defense, home security, industrial, scientific, etc. Fig. 7.1 shows several

underwater applications, objects used in UOWSNs and IoUT.

The marine applications require high-speed wireless communication systems such as underwater wireless optical communication (UWOC) and free-space optical (FSO) systems to develop a network of all-optical internet of underwater things (O-IoUT). The O-IoUT is useful in studying marine antiquity, navigating submarines, communicating off-shore ships, tracking the marine species, and searching and rescue operations. The O-IoUT networks collect the data autonomously and share it with the nearby monitoring base stations on the shore. This data is helpful in monitoring, exploring the underwater environment [Khalil *et al.* (2020)]. In [Ramavath *et al.* (2020)], a high-speed and reliable UWOC system for IoUT applications was investigated using multiple-input multiple-output (MIMO) and channel coding techniques. Ajay et al. proposed an M-ary quadrature amplitude modulation (QAM) based UWOC system for reconfigurable UOWSNs employed in river meets ocean scenario. The authors analyzed the ABER performance of the system for different varying parameters [Uppalapati *et al.* (2020)].

Research on converging one type of communications system with other types is increasing every day. Similarly, investigations on the multi-hop approach are also gaining more attraction. In [Anees and Bhatnagar (2015*b*,*a*)], the authors investigated the performance of asymmetric amplify and forward (AF); decode and forward (DF) based dual-hop radio frequency (RF) - FSO communication system. A 500-Gb/s convergent FSO-UWOC system was established and analyzed with four-level pulse amplitude modulation (PAM4) over 100 m FSO link with either 5 m turbid water link or 10 m piped water link in [Tsai *et al.* (2020)]. The authors demonstrated a five-wavelength polarization-multiplexing scheme employing a red/green/blue (R/G/B). The authors analyzed the end-to-end system performance and achieved an aggregate data rate of 500 Gb/s channel capacity for the convergent FSO-UWOC system [Tsai *et al.* (2020)].

Zedini et al. investigated a multi-hop heterodyne FSO system's performance with AF channel state information (CSI), considering the pointing errors. The authors also performed an analysis of dual-hop UWOC systems over exponential-generalized gamma (EGG) turbulence channels [Zedini and Alouini (2015), Zedini *et al.* (2020)]. In [Prabu and Kumar (2016)], the authors proposed and analyzed the outage performance of polarization shift keying (PolSK) based multi-hop parallel relay-assisted FSO system over a strong atmospheric turbulence channel, taking misalignment fad-

ing into consideration. The average bit error rate (ABER) performance of a DF-based multi-hop radio on free-space optics (ROFSO) system was examined using orthogonal frequency division multiplexing(OFDM) scheme with phase shift keying (PSK) modulation in [Balaji and Prabu (2018a)].

Baruah et al. performed a study on the outage analysis of a DF-based multi-hop mixed hybrid RF/FSO-FSO-UWOC co-operative system [Baruah and Sarma (2020)]. In [Li et al. (2021)], authors investigated the performance of a reconfigurable intelligent surface (RIS)-assisted dual-hop mixed RF-UWOC system. The performance (outage, ABER, and average capacity) of a hybrid FSO/(FSO-FSO)/(RF-FSO) system was studied in [Bag et al. (2020)] using a DF relay. The study shows an improvement in the performance with an additional millimeter-wave (mmWave) RF backup link between source and relay.

A convergent FSO-UWOC system's outage analysis has been evaluated using lognormal channel model in [Christopoulou et al. (2019)]. A RF-UWOC co-operative system's performance was investigated in [Naik et al. (2020)] over a hyperbolic tangent log-normal (HTLN) distributed channel with pointing errors. In [Levidala and Krishnan (2020)], the authors analyzed the asymptotic BER performance of a dual-hop convergent UWOC-FSO communication system. Kumar et al. performed outage analysis of a multi-hop UWOC-FSO system in [Kumar and Krishnan (2020)].

The contributions of this chapter are as follows:

- We proposed a novel multi-hop UWOC - convergent with FSO system and derived the outage probability expressions.

- The outage performance of the proposed system is evaluated in the presence of different turbulence regimes and pointing error effects.

- The outage performance of the proposed system is analyzed in terms of varying number of underwater hops of the convergence systems.

The rest of the chapter is configured as follows. The multi-hop UWOC convergent with the FSO system is introduced in Section 7.2. In Section 7.3, the end-to-end statistical channel models of the proposed system are discussed. The outage probability expressions for the proposed end-to-end system are presented in Section 7.4. The outage results and their corresponding discussions for different UWOC and FSO turbulent parameters, path loss, and misalignment fading are provided in Section 7.5. Finally, the chapter concludes in Section 7.6.

7.2   System Model
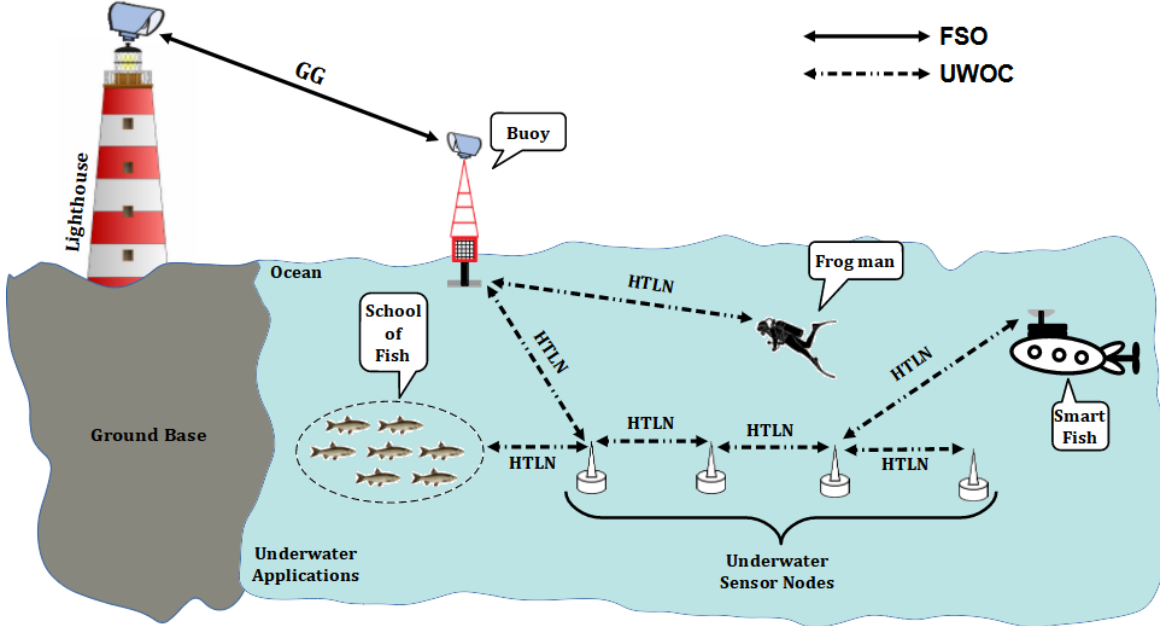
Figure 7.1: Generalized multi-hop system model.

We propose a system model consisting of multi-hop UWOC and FSO links as shown in Fig. 7.1. The first (n-1) links between the relays are considered underwater as UWOC links. Similarly, the communication link between $(n-1)^{th}$ relay on the sea surface and lighthouse is connected using the FSO link. The source and destination are communicated through (n-1) relays with an 'n' number of links. The UWOC and FSO links are modeled using Hyper Tangent Log-Normal (HTLN) and Gamma-Gamma (GG) distributions.

7.3   Statistical Characteristics

The statistical channel characteristics of UWOC and FSO systems are defined using the cumulative distribution function (CDF), which are discussed below.

7.3.1   UWOC statistical channel model

The optical signal in the underwater channel is influenced due to the turbulence effect, misalignment errors (also known as pointing errors), and beam attenuation. The turbid underwater channel can be modelled with various distribution functions given in [Sharifzadeh and Ahmadirad (2018)]. In this chapter, we have modelled the turbulence channel with a novel distribution function, which is named as HTLN distribution

106

function for modelling the weak oceanic turbulence by taking the pointing errors into account. The CDF is of HTLN distribution is given as [Naik *et al.* (2020)],

$$F_{\gamma_1}(\gamma_1) = \frac{g^2 \exp(2a)}{b} \left(\frac{\gamma_1}{A_0 \ h_l^u \bar{\gamma}_u} \right)^b \ G_{1+2b,1+2b}^{1+b,1+b} \left(\frac{\frac{i-b}{b}, -1, \frac{i-b+g^2}{b}}{\frac{i-b+g^2-1}{b}, 0, \frac{i-b-1}{b}} \left| \left(\frac{e^{\frac{2a}{b}} \gamma_1}{A_0 \ h_l^u \bar{\gamma}_u} \right)^b \right. \right) \quad (7.1)$$

where $i = 1, 2, \ldots, b$. A_0 is the amount of fractional power at the detector. h_l^u & $\bar{\gamma}_u$ are the path loss and the average signal to noise ratio (SNR) of the UWOC link.

7.3.2 FSO statistical channel model

The FSO system is GG distributed under the influence of turbulence and pointing errors. The CDF given in [Sandalidis *et al.* (2009)], is considered for the FSO channel link and modified/rewritten in terms of average SNR.

$$F_{\gamma_n}(\gamma_n) = \frac{g^2}{\Gamma(\alpha)\Gamma(\beta)} G_{2,4}^{3,1} \left(\frac{1,g^2+1}{g^2,\alpha,\beta,0} \left| \frac{g^2 \alpha \beta}{h_l^f \bar{\gamma}_f (g^2+1)} \gamma_n \right. \right) \quad (7.2)$$

Where, α and β corresponds to the effective number of large and small scale turbulent eddies. h_l^f is the free-space path loss, $\Gamma(.)$ is the gamma function and $\bar{\gamma}_f$ is the average SNR of the FSO link. The misalignment fading parameter g is given as $g = \frac{W_{Z_{eq}}}{\sigma_s}$, $W_{Z_{eq}}$ is the beam-width, σ_s is the standard deviation of jitter.

7.3.3 CDF of end-to-end system

The minimum SNR required to decode the source message correctly at the destination node is the SNR associated with the n DF relays. Hence, the end-to-end system's CDF using the n DF relay is given as [Miridakis *et al.* (2014)],

$$F_{\gamma_{e2e}}(\gamma) = 1 - \left(1 - F_{\gamma_1}(\gamma)\right)\left(1 - F_{\gamma_2}(\gamma)\right) \cdots \left(1 - F_{\gamma_n}(\gamma)\right) \quad (7.3)$$

We have considered the CDFs associated with the UWOC system (*i.e,* for the first $n-1$ relayed links) as similar for ease of analysis. $\left(i.e, \ F_{\gamma_1}(\gamma) = F_{\gamma_2}(\gamma) = \cdots = F_{\gamma_{n-1}}(\gamma)\right)$ and the FSO channel link is associated with the nth relay. Hence the obtained end-to-end CDF is as follows,

$$F_{\gamma_{e2e}}(\gamma) = 1 - \left(1 - F_{\gamma_1}(\gamma)\right)^{n-1} \left(1 - F_{\gamma_n}(\gamma)\right). \quad (7.4)$$

The end-to-end CDF is obtained making use of binomial distribution to Eq. (7.4), and is given as,

$$F_{\gamma_{e2e}}(\gamma) = 1 + \sum_{k=0}^{n-1} (-1)^{n-k} \binom{n-1}{k} \left(F_{\gamma_1}(\gamma)\right)^{n-k-1} \left(1 - F_{\gamma_n}(\gamma)\right) \qquad (7.5)$$

The end-to-end system's CDF presented in Fig. 7.1 is given as,

$$F_{\gamma_{e2e}}(\gamma) = F_{\gamma_1}(\gamma)\left(1 - F_{\gamma_n}(\gamma)\right)\left(2 - F_{\gamma_1}(\gamma)\right) + F_{\gamma_n}(\gamma) \qquad (7.6)$$

7.4 Outage performance

The outage probability is the probability that the DF relay SNR falls below a given threshold SNR (*i.e.*, γ_{th}), which is shown as,

$$P_{out} = P\left(\min\{\gamma_1, \gamma_2, \cdots, \gamma_n\} \leq \gamma_{th}\right) = F_{\gamma_{e2e}}(\gamma_{th})$$

$$= 1 + \sum_{k=0}^{n-1} (-1)^{n-k} \binom{n-1}{k} \left(F_{\gamma_1}(\gamma_{th})\right)^{n-k-1} \left(1 - F_{\gamma_n}(\gamma_{th})\right) \qquad (7.7)$$

The outage probability for the multi-hop UWOC convergent with FSO system shown in Fig. 7.1 is derived from the Eq. 7.7 and is given in Eq. 7.8.

$$
\begin{aligned}
P_{out} &= \frac{g^2 \exp(2a)}{b} \left(\frac{\gamma_{th}}{A_0\, h_l^u \bar{\gamma}_u}\right)^b \\
&\times \left(2 - \frac{g^2 \exp(2a)}{b}\left(\frac{\gamma_{th}}{A_0\, h_l^u \bar{\gamma}_u}\right)^b \mathrm{G}_{1+2b,1+2b}^{1+b,1+b}\left(\left.\begin{smallmatrix}\frac{i-b}{b},-1,\frac{i-b+g^2}{b}\\ \frac{i-b+g^2-1}{b},0,\frac{i-b-1}{b}\end{smallmatrix}\right| \left(\frac{e^{\frac{2a}{b}}\gamma_{th}}{A_0\, h_l^u \bar{\gamma}_u}\right)^b\right)\right) \\
&\times \mathrm{G}_{1+2b,1+2b}^{1+b,1+b}\left(\left.\begin{smallmatrix}\frac{i-b}{b},-1,\frac{i-b+g^2}{b}\\ \frac{i-b+g^2-1}{b},0,\frac{i-b-1}{b}\end{smallmatrix}\right| \left(\frac{e^{\frac{2a}{b}}\gamma_{th}}{A_0\, h_l^u \bar{\gamma}_u}\right)^b\right) \\
&\times \left(1 - \frac{g^2}{\Gamma(\alpha)\Gamma(\beta)}\mathrm{G}_{2,4}^{3,1}\left(\left.\begin{smallmatrix}1,g^2+1\\ g^2,\alpha,\beta,0\end{smallmatrix}\right| \frac{g^2\alpha\beta\gamma_{th}}{h_l^f \bar{\gamma}_f (g^2+1)}\right)\right) \\
&+ \frac{g^2}{\Gamma(\alpha)\Gamma(\beta)}\mathrm{G}_{2,4}^{3,1}\left(\left.\begin{smallmatrix}1,g^2+1\\ g^2,\alpha,\beta,0\end{smallmatrix}\right| \frac{g^2\alpha\beta\gamma_{th}}{h_l^f \bar{\gamma}_f (g^2+1)}\right) \qquad (7.8)
\end{aligned}
$$

The proposed system's outage performance is analyzed for different weather conditions, turbulent regimes, number of hops of UWOC link, and different pointing error scenarios of both FSO and UWOC links. Tables 7.1, 7.2, and 7.3 shows various system and channel parameters considered for the analysis. The path loss of the 2 Km FSO link is considered from the Table III of [Levidala and Krishnan (2020)]. The path loss for the varying UWOC link lengths is calculated from the Table I of [Kumar and Krishnan (2020)].

Table 7.1: Turbulence parameters of FSO link [Levidala and Krishnan (2020)].

Turbulence parameters	Description
$\alpha_f = 10, \beta_f = 5$	Moderate turbulence
$\alpha_f = 2, \beta_f = 1$	Strong turbulence

Table 7.2: Turbulence parameters of UWOC link.

Turbulence parameters	Description
$\alpha_u = 0.349, \beta_u = 2$	Weak turbulence set 1 (WT1)
$\alpha_u = 2, \beta_u = 2$	Weak turbulence set 2 (WT2)

Table 7.3: Pointing error conditions.

Pointing error parameter	Description
$g = 4$	Weak pointing error
$g = 1.25$	Moderate pointing error
$g = 1$	Strong pointing error

7.5 Results and Discussions

This section analyzes the outage probability versus average SNR of the proposed system with the 10 dB of constant threshold SNR. The weather and turbulence conditions are the same for all underwater links. Similarly, the pointing error parameter is equal in both FSO and UWOC links. The UWOC links lengths vary according to the type of water (clear ocean - 50 m; coastal ocean - 30 m; turbid harbor - 10 m). To obtain all the results, we consider the 2 Km FSO link. Figures 7.2 to 7.5 provide the outage performance of the end-to-end system for different UWOC and

FSO link parameters, such as weather conditions (clear air, haze, drizzle, and light fog); turbulence (strong, moderate, and weak) and pointing error (strong, moderate, and weak).
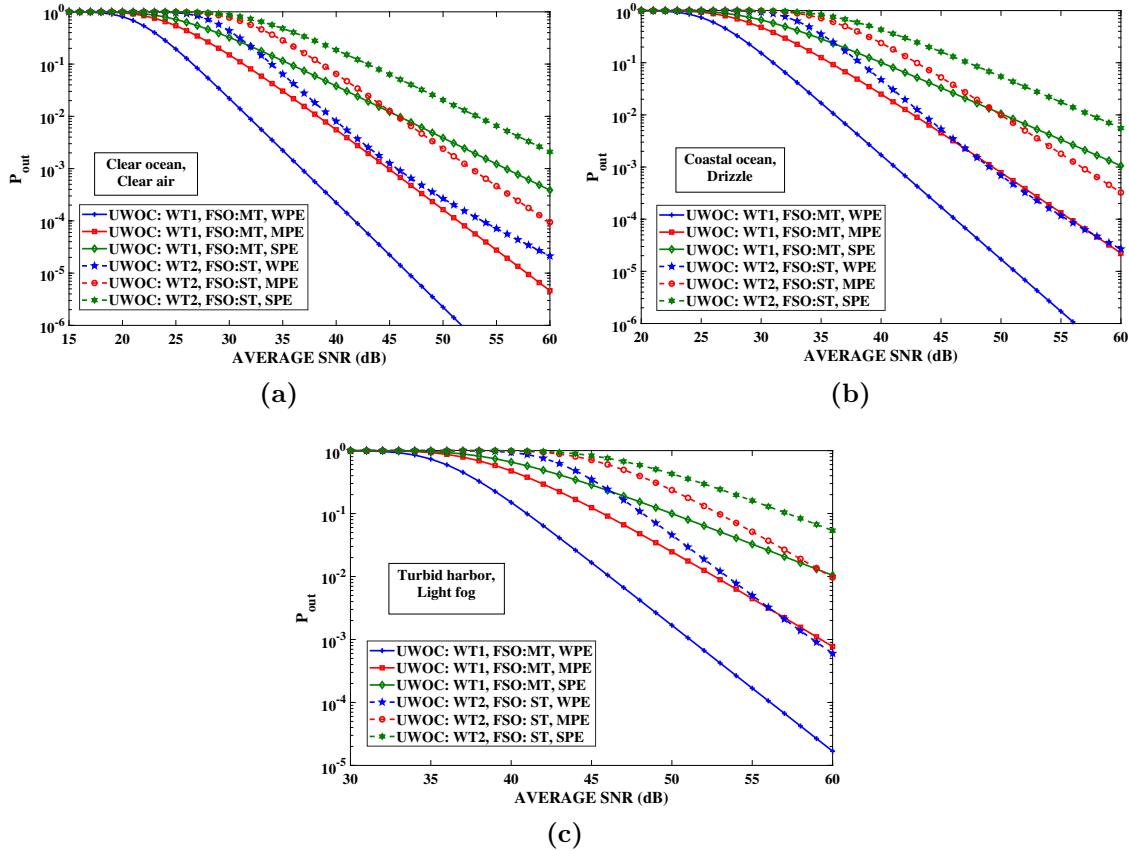
Figure 7.2: Outage Vs Average SNR for varying turbulence conditions and pointing errors. (a) for clear ocean and clear air (b) for coastal ocean and drizzle weather (c) for turbid harbor and light fog conditions.

Fig. 7.2 visualizes the quad-hop converging system's outage analysis under pointing error conditions (weak - WPE; moderate - MPE, and strong pointing error - SPE). The pointing error parameter has been varied by considering strong and weak turbulence in both the UWOC and FSO links. It is observed that the outage decreases as the average SNR increases. Similarly, the outage decreases with the decrease in pointing error. Under the weak turbulence and weak pointing error scenario, there is a decrease in the end-to-end system's outage performance from clear water to turbid water.

Fig. 7.3 shows the quad-hop communication system's performance under varying
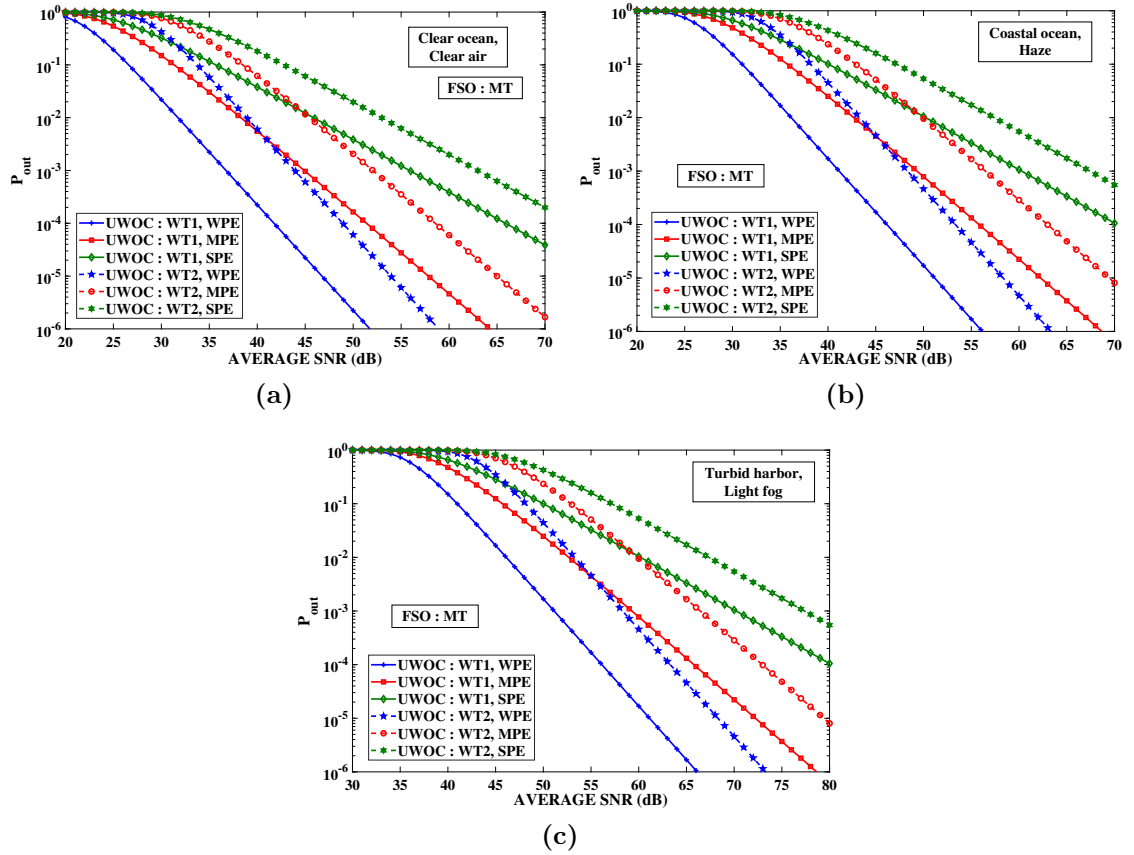
Figure 7.3: Outage Vs Average SNR for varying pointing errors when FSO has weak turbulence. (a) for clear ocean and very clear air (b) for coastal ocean and haze weather (c) for turbid harbor and light fog conditions.

pointing error parameter g when the FSO link has weak turbulence. Similar to the previous case, the end-to-end system outage analysis is shown for weak, moderate, and strong pointing errors. For the UWOC link, weak and strong turbulence conditions are applied. Clear weather conditions are considered for the FSO link. The plot shows the decrease in outage due to an increase in the average SNR. The deterioration can also be observed in the proposed system's performance from weak to strong turbulence of the UWOC link.

Fig. 7.4 shows the end-to-end quad-hop system's outage performance with varying pointing error values when the UWOC link has weak turbulence. For the FSO links, weak and strong turbulence are considered. A significant loss in the received signal can be observed when there is strong turbulence with a strong pointing error. With the decrease in the pointing error value, the proposed system's performance is reduced
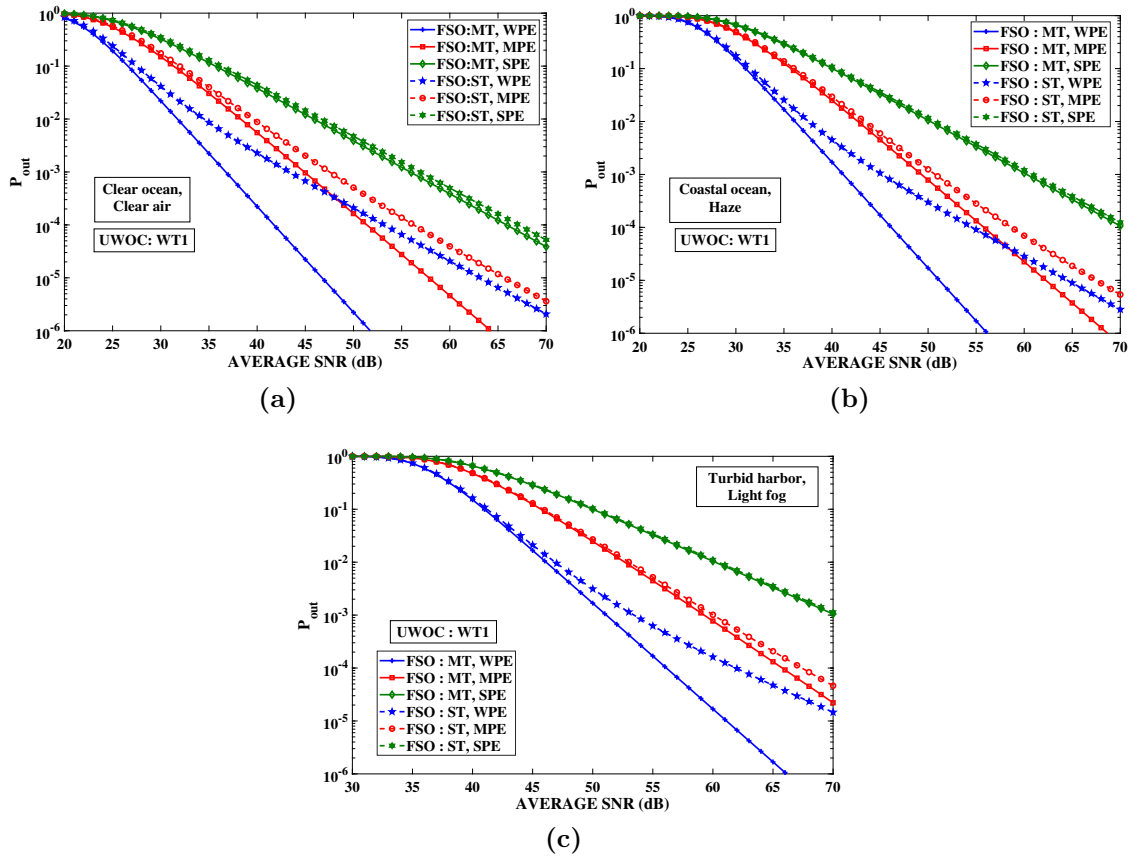
Figure 7.4: Outage Vs Average SNR for varying pointing errors when UWOC has weak turbulence. (a) for clear ocean and very clear air (b) for coastal ocean and haze weather (c) for turbid harbor and light fog conditions.
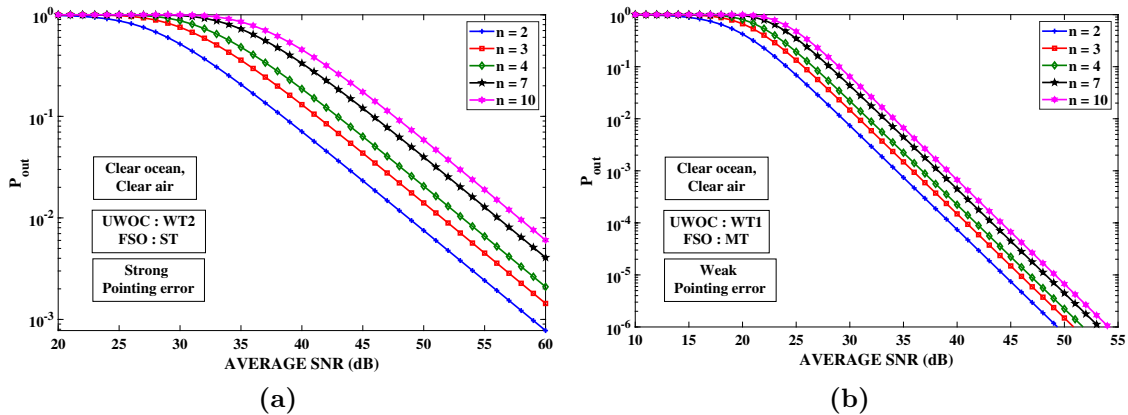
Figure 7.5: Outage Vs Average SNR for varying number of hops. (a) for strong turbulence and strong pointing errors (b) weak turbulence and weak pointing errors.

from clear ocean to turbid harbor waters.

Fig. 7.5 visualizes the outage performance analysis of the proposed multi-hop convergent communication system for the clear ocean and clear air conditions. Fig. 7.5a shows the outage analysis for the strong pointing error and strong turbulence parameters. Fig. 7.5b depicts the end-to-end system performance for the weak pointing error and weak turbulence scenario. The results show that the end-to-end multi-hop system performance degrades as the number of hops 'n' increases.

7.6   Summary

A multi-hop UWOC convergent with the FSO system for O-IoUT and UOWSN applications is proposed in this chapter. The proposed system's outage performance is studied for different FSO and UWOC weather conditions, turbulence regimes, and pointing error scenarios. The results show that the proposed system provides a better and more reliable high-speed connectivity for the applications mentioned above.

Chapter 8

Conclusions and Future Directions

8.1 Conclusions

This research mainly focuses on the performance analysis of convergent FSO - UWOC systems. We considered the challenges and limitations of FSO and UWOC systems. We derived the analytical channels models under the effects of turbulence, attenuation, and the pointing errors of both the FSO and UWOC systems. We considered different weather conditions for the FSO communication system, such as haze, fog, rain, and clear air. Similarly, we considered different types of water, such as the clear ocean, coastal ocean, and turbid harbor, for the UWOC system. We used the MIMO technique to improve the dual-hop system performance.

Chapter-3 uses a novel closed-form ABER expression for the proposed convergent UWOC-FSO system. The simulation results are plotted and analyzed for weak, moderate, and ST regimes with the various levels of scatterings for both UWOC and FSO links. The results were further analyzed for different environments of UWOC and FSO links with the different levels of pointing errors. The results also show the performance degradation of the system in the case of turbid harbors compared to clear and coastal ocean scenarios. The proposed convergent UWOC-FSO system can be helpful in UWSN, oceanography, disaster precaution, and military applications.

Chapter-4 proposes a MIMO-based convergent UWOC-FSO system. A Novel closed-form ABER expression is derived for the end-to-end system. We have analyzed the proposed system ABER performance under various turbulence and pointing error regimes (weak and strong) for various oceanic and free space weather conditions of both UWOC and FSO links. The results show that 35 dB performance enhancement of the end-to-end system from SISO to 2×3 MIMO system for the clear ocean

and clear air conditions under weak turbulence case at ABER of 10^{-5}. In a turbid harbor environment, a higher average SNR is required due to high attenuation. Hence, an additional 17.5 dB of average SNR is required to achieve better performance in the case of turbid harbor compared to clear and coastal ocean scenarios. The results also depict the more ABER values with the increase in correlation coefficient ρ. The proposed MIMO-based dual-hop convergent UWOC-FSO system gives improved performance compared to the SISO system. This study will be helpful for design engineers to establish reliable high-speed connectivity in ocean monitoring applications.

Chapter-5 presented the outage analysis of a multi-hop FSO-UWOC confluent system. Derived a closed-form expression for the outage probability of the end-to-end system by assuming the FSO link as M-distributed and UWOC link as GG-distributed. Further, the results are demonstrated for the derived analytical expressions based on various parameters and different weather conditions. This convergent multi-hop FSO-UWOC system can be applicable for IoUT and UOWSN and other coastal operations such as lighthouse communications, port security, oceanography, weather monitoring, etc.

A multi-hop FSO-UWOC convergence system for tracking and security applications is proposed in this chapter-6. The performance of the proposed system is studied for different FSO weather conditions, underwater conditions, turbulence regimes, and pointing error scenarios. In comparison to the clear ocean, the coastal ocean situation requires an additional 12 dB of average SNR to achieve 10^{-2} outage performance. In contrast, due to the higher attenuation in turbid harbor water compared to the clear and coastal ocean, performance is heavily influenced by errors, and hence communication is impossible. To attain the ABER of 10^{-4} in moderate turbulence, 21 dB of average SNR at weak pointing error is required. To obtain the same ABER with a strong pointing error, an additional 10 dB of average SNR is required. The results show that the proposed system provides reliable high-speed connectivity for the mentioned applications.

A multi-hop UWOC convergent with the FSO system for O-IoUT and UOWSN applications is proposed in this chapter-7. The proposed system's outage performance is studied for different FSO and UWOC weather conditions, turbulence regimes, and pointing error scenarios. The results show that the proposed system provides a better and more reliable high-speed connectivity for the applications mentioned above.

8.2 Future Directions

We have achieved the objective and the aims listed in Chapter One through this research work. WOC has different fields to pursue research, and further, this research work has the following future scopes.

The end-to-end system performance can be analyzed using the exponential generalized gamma (EGG) distribution for the underwater link. The performance of the end-to-end system can be analyzed using the error control coding techniques such as BCH, RS, LDPC and turbo codes. The concept of reconfigurable intelligent surface (RIS) can be used in WOC systems to overcome the light of sight (LOS) issues. When the LOS transmission is not possible, using the RIS devices signal makes the transmission between the source and destination possible. The energy harvesting concept called simultaneous light information and power transfer (SLIPT) can also be introduced in the UWSN and IoUT devices to increase their operating times or extend their services for a few more minutes to hours.

Bibliography

Abaza, M., **R. Mesleh**, **A. Mansour**, *et al.* (2015). Performance analysis of miso multi-hop fso links over log-normal channels with fog and beam divergence attenuations. *Optics Communications*, **334**, 247–252.

Adamchik, V. and **O. Marichev**, The algorithm for calculating integrals of hypergeometric type functions and its realization in REDUCE system. *In Proceedings of the international symposium on Symbolic and algebraic computation*. 1990.

Al-Kinani, A., **C.-X. Wang**, **L. Zhou**, and **W. Zhang** (2018). Optical wireless communication channel measurements and models. *IEEE Communications Surveys & Tutorials*, **20**(3), 1939–1962.

Alathwary, W. A. and **E. S. Altubaishi** (2019). On the performance analysis of decode-and-forward multi-hop hybrid fso/rf systems with hard-switching configuration. *IEEE Photonics Journal*, **11**(6), 1–12.

Algamal, A. A., **H. A. Fayed**, **M. Mahmoud**, and **M. H. Aly** (2020). Reliable fso system performance matching multi-level customer needs in alexandria city, egypt, climate: sandstorm impact with pointing error. *Optical and Quantum Electronics*, **52**(7), 1–18.

Amirabadi, M. A. and **V. T. Vakili** (2019). On the performance of a multi-user multi-hop hybrid fso/rf communication system. *Optics Communications*, **444**, 172–183.

Amirabadi, M. A. and **V. T. Vakili** (2020). On the performance of a novel multi-hop relay-assisted hybrid fso/rf communication system with receive diversity. *Optik*, 165883.

Anandkumar, D. and **R. Sangeetha** (2021). A survey on performance enhancement in free space optical communication system through channel models and modulation techniques. *Optical and Quantum Electronics*, **53**(1), 1–39.

Andrews, L. C. and **R. L. Phillips** (2005). Laser beam propagation through random media. *Laser Beam Propagation Through Random Media: Second Edition*.

Anees, S. and **M. R. Bhatnagar** (2015*a*). Performance evaluation of decode-and-forward dual-hop asymmetric radio frequency-free space optical communication system. *IET Optoelectronics*, **9**(5), 232–240.

Anees, S. and **M. R. Bhatnagar** (2015*b*). Performance of an amplify-and-forward dual-hop asymmetric rf–fso communication system. *Journal of Optical Communications and Networking*, **7**(2), 124–135.

Anees, S. and **R. Deka**, On the performance of DF based dual-hop mixed RF/UWOC system. *In 2019 IEEE 89th Vehicular Technology Conference (VTC2019-Spring)*. IEEE, 2019.

Ansari, I. S., **F. Yilmaz**, and **M.-S. Alouini** (2015). Performance analysis of free-space optical links over málaga ($\mathcal{M}$) turbulence channels with pointing errors. *IEEE Transactions on Wireless Communications*, **15**(1), 91–102.

Bag, B., **A. Das**, **C. Bose**, and **A. Chandra** (2020). Improving the performance of a df relay-aided fso system with an additional source–relay mmwave rf backup. *Journal of Optical Communications and Networking*, **12**(12), 390–402.

Balaji, K. and **K. Prabu** (2018*a*). Ber analysis of relay assisted psk with ofdm rofso system over malaga distribution including pointing errors under various weather conditions. *Optics Communications*, **426**, 187–193.

Balaji, K. and **K. Prabu** (2018*b*). Performance evaluation of fso system using wavelength and time diversity over malaga turbulence channel with pointing errors. *Optics Communications*, **410**, 643–651.

Baruah, S. R. and **P. Sarma**, Outage analysis of df based mixed hybrid multi-hop cooperative system. *In 2020 IEEE 17th India Council International Conference (INDICON)*. IEEE, 2020.

Berlian, M. H., **T. E. R. Sahputra**, **B. J. W. Ardi**, **L. W. Dzatmika**, **A. R. A. Besari**, **R. W. Sudibyo**, and **S. Sukaridhoto**, Design and implementation of smart environment monitoring and analytics in real-time system framework based on internet of underwater things and big data. *In 2016 International Electronics Symposium (IES)*. IEEE, 2016.

Callaham, M. (1981). Submarine commmunications. *IEEE Communications Magazine*, **19**, 16–25.

Chan, V. W. (2006). Free-space optical communications. *Journal of Lightwave technology*, **24**(12), 4750–4762.

Chowdhury, M. Z., **M. K. Hasan**, **M. Shahjalal**, **M. T. Hossan**, and **Y. M. Jang** (2020). Optical wireless hybrid networks: Trends, opportunities, challenges, and research directions. *IEEE Communications Surveys & Tutorials*, **22**(2), 930–966.

Chowdhury, M. Z., **M. T. Hossan**, **A. Islam**, and **Y. M. Jang** (2018). A comparative survey of optical wireless technologies: Architectures and applications. *ieee Access*, **6**, 9819–9840.

Christopoulou, C., **H. G. Sandalidis**, and **I. S. Ansari** (2019). Outage probability of a multisensor mixed uowc–fso setup. *IEEE Sensors Letters*, **3**(8), 1–4.

Cisco (2020). Cisco annual internet report (2018–2023). *Online*. URL https://www.cisco.com/c/en/us/solutions/collateral/executive-perspectives/annual-internet-report/white-paper-c11-741490.html.

Dahrouj, H., **A. Douik**, **F. Rayal**, **T. Y. Al-Naffouri**, and **M.-S. Alouini** (2015). Cost-effective hybrid rf/fso backhaul solution for next generation wireless systems. *IEEE Wireless Communications*, **22**(5), 98–104.

Diamant, R., **F. Campagnaro**, **M. D. F. De Grazia**, **P. Casari**, **A. Testolin**, **V. S. Calzado**, and **M. Zorzi** (2017). On the relationship between the underwater acoustic and optical channels. *IEEE Transactions on Wireless Communications*, **16**(12), 8037–8051.

Djordjevic, I. B., *Advanced optical and wireless communications systems*. Springer, 2018.

DLR (2018). Dlr researchers set world record in free-space optical communications. *Online*. URL https://www.dlr.de/content/en/articles/news/2018/2/20180510_dlr-and-adva-set-a-new-world-record-in-optical-free-space-data-transmission_27323.html.

D.Messier (2016). Dlr researchers set world record in free-space optical communications. *Online*. URL http://www.parabolicarc.com/2016/11/05/dlrresearchers-set-world-record-freespace-optical-communications/.

Domingo, M. C. (2012). An overview of the internet of underwater things. *Journal of Network and Computer Applications*, **35**(6), 1879–1890.

Duncan, K. J., Laser based power transmission: Component selection and laser hazard analysis. *In 2016 IEEE PELS Workshop on Emerging Technologies: Wireless Power Transfer (WoW)*. IEEE, 2016.

Elsayed, E. E. and **B. B. Yousif** (2020). Performance evaluation and enhancement of the modified ook based im/dd techniques for hybrid fiber/fso communication over wdm-pon systems. *Optical and Quantum Electronics*, **52**(9), 1–27.

Fakidis, J., **S. Videv**, **S. Kucera**, **H. Claussen**, and **H. Haas** (2016). Indoor optical wireless power transfer to small cells at nighttime. *Journal of Lightwave Technology*, **34**(13), 3236–3258.

Farid, A. A. and **S. Hranilovic** (2007). Outage capacity optimization for free-space optical links with pointing errors. *Journal of Lightwave technology*, **25**(7), 1702–1710.

Fei, C., **J. Zhang**, **G. Zhang**, **Y. Wu**, **X. Hong**, and **S. He** (2018). Demonstration of 15-m 7.33-gb/s 450-nm underwater wireless optical discrete multitone transmission using post nonlinear equalization. *Journal of Lightwave Technology*, **36**(3), 728–734.

Fu, Y. and **Y. Du** (2018). Performance of heterodyne differential phase-shift-keying underwater wireless optical communication systems in gamma-gamma-distributed turbulence. *Applied optics*, **57**(9), 2057–2063.

Gappmair, W. (2011). Further results on the capacity of free-space optical channels in turbulent atmosphere. *IET communications*, **5**(9), 1262–1267.

Ghassemlooy, Z., **W. Popoola**, and **S. Rajbhandari**, *Optical wireless communications: system and channel modelling with Matlab®*. CRC press, 2019.

Ghassemlooy, Z., **M. Uysal**, **M. A. Khalighi**, **V. Ribeiro**, **F. Moll**, **S. Zvanovec**, and **A. Belmonte** (2016). An overview of optical wireless communications. *Optical Wireless Communications*, 1–23.

Gnauck, A. H. and **P. J. Winzer** (2005). Optical phase-shift-keyed transmission. *Journal of lightwave technology*, **23**(1), 115–130.

Goodwin, F. E. (1970). A review of operational laser communication systems. *Proceedings of the IEEE*, **58**(10), 1746–1752.

Hanson, F. and **S. Radic** (2008). High bandwidth underwater optical communication. *Applied optics*, **47**(2), 277–283.

Issaid, C. B., **K.-H. Park**, and **M.-S. Alouini** (2017). A generic simulation approach for the fast and accurate estimation of the outage probability of single hop and multihop fso links subject to generalized pointing errors. *IEEE Transactions on Wireless Communications*, **16**(10), 6822–6837.

Jaiswal, A., **M. R. Bhatnagar**, **P. Soni**, and **V. K. Jain** (2019). Differential optical spatial modulation over atmospheric turbulence. *IEEE Journal of Selected Topics in Signal Processing*, **13**(6), 1417–1432.

Jamali, M. V., **A. Chizari**, and **J. A. Salehi** (2017). Performance analysis of multi-hop underwater wireless optical communication systems. *IEEE Photonics Technology Letters*, **29**(5), 462–465.

Jamali, M. V., **P. Khorramshahi**, **A. Tashakori**, **A. Chizari**, **S. Shahsavari**, **S. AbdollahRamezani**, **M. Fazelian**, **S. Bahrani**, and **J. A. Salehi**, Statistical distribution of intensity fluctuations for underwater wireless optical channels in the presence of air bubbles. *In 2016 Iran Workshop on Communication and Information Theory (IWCIT)*. IEEE, 2016a.

Jamali, M. V., **P. Nabavi**, and **J. A. Salehi** (2018). MIMO underwater visible light communications: Comprehensive channel study, performance analysis, and multiple-symbol detection. *IEEE Transactions on Vehicular Technology*, **67**(9), 8223–8237.

Jamali, M. V., **J. A. Salehi**, and **F. Akhoundi** (2016*b*). Performance studies of underwater wireless optical communication systems with spatial diversity: MIMO scheme. *IEEE Transactions on Communications*, **65**(3), 1176–1192.

Jeffrey, A. and **D. Zwillinger**, *Table of integrals, series, and products*. Elsevier, 2007.

Jia, C., **P. Wang**, **Y. Li**, **C. Huang**, **H. Fu**, and **W. Pang** (2018). Abers of ldpc-coded multi-hop fso over double gg fading channels with pointing error and path loss. *IEEE Photonics Technology Letters*, **30**(15), 1357–1360.

Jurado-Navas, A., **J. M. G. Balsells**, **J. F. Paris**, **M. Castillo-Vázquez**, and **A. Puerta-Notario** (2011*a*). General analytical expressions for the bit error rate of atmospheric optical communication systems. *Optics letters*, **36**(20), 4095–4097.

Jurado-Navas, A., **J. M. Garrido-Balsells**, **M. Castillo-Vazquez**, **A. García-Zambrana**, and **A. Puerta-Notario**, Converging underwater and fso ground communication links. *In 2019 Optical Fiber Communications Conference and Exhibition (OFC)*. IEEE, 2019.

Jurado-Navas, A., **J. M. Garrido-Balsells**, **J. F. Paris**, **M. Castillo-Vázquez**, and **A. Puerta-Notario** (2012). Impact of pointing errors on the performance of generalized atmospheric optical channels. *Optics Express*, **20**(11), 12550–12562.

Jurado-Navas, A., **J. M. Garrido-Balsells**, **J. F. Paris**, **A. Puerta-Notario**, and **J. Awrejcewicz** (2011*b*). A unifying statistical model for atmospheric optical scintillation. *Numerical simulations of physical and engineering processes*, **181**(8), 181–205.

Kao, C.-C., **Y.-S. Lin**, **G.-D. Wu**, and **C.-J. Huang** (2017*a*). A comprehensive study on the internet of underwater things: applications, challenges, and channel models. *Sensors*, **17**(7), 1477.

Kao, C.-C., **Y.-S. Lin**, **G.-D. Wu**, and **C.-J. Huang**, A study of applications, challenges, and channel models on the internet of underwater things. *In 2017 International Conference on Applied System Innovation (ICASI)*. IEEE, 2017b.

Karp, S. (1976). Optical communications between underwater and above surface (satellite) terminals. *IEEE Transactions on Communications*, **24**(1), 66–81.

Kaushal, H. and **G. Kaddoum** (2016a). Optical communication in space: Challenges and mitigation techniques. *IEEE communications surveys & tutorials*, **19**(1), 57–96.

Kaushal, H. and **G. Kaddoum** (2016b). Underwater optical wireless communication. *IEEE access*, **4**, 1518–1547.

Kaymak, Y., **R. Rojas-Cessa**, **J. Feng**, **N. Ansari**, **M. Zhou**, and **T. Zhang** (2018). A survey on acquisition, tracking, and pointing mechanisms for mobile free-space optical communications. *IEEE Communications Surveys & Tutorials*, **20**(2), 1104–1123.

Khalighi, M.-A., **C. Gabriel**, **T. Hamza**, **S. Bourennane**, **P. Leon**, and **V. Rigaud**, Underwater wireless optical communication; recent advances and remaining challenges. *In 2014 16th International Conference on Transparent Optical Networks (ICTON)*. IEEE, 2014.

Khalighi, M. A. and **M. Uysal** (2014). Survey on free space optical communication: A communication theory perspective. *IEEE communications surveys & tutorials*, **16**(4), 2231–2258.

Khalil, R. A., **M. I. Babar**, **N. Saeed**, **T. Jan**, and **H.-S. Cho** (2020). Effect of link misalignment in the optical-internet of underwater things. *Electronics*, **9**(4), 646.

Khallaf, H. S. and **M. Uysal**, Uav-based fso communications for high speed train backhauling. *In 2019 IEEE Wireless Communications and Networking Conference (WCNC)*. IEEE, 2019.

Kiasaleh, K. (2006). Performance of coherent dpsk free-space optical communication systems in k-distributed turbulence. *IEEE transactions on communications*, **54**(4), 604–607.

Killinger, D. (2002). Free space optics for laser communication through the air. *Optics and photonics news*, **13**(10), 36–42.

Korotkova, O., **N. Farwell**, and **E. Shchepakina** (2012). Light scintillation in oceanic turbulence. *Waves in Random and Complex Media*, **22**(2), 260–266.

Krishnan, P. (2018). Performance analysis of hybrid RF/FSO system using BPSK-SIM and DPSK-SIM over gamma-gamma turbulence channel with pointing errors for smart city applications. *IEEE Access*, **6**, 75025–75032.

Kumar, L. B. and **P. Krishnan** (2020). Multi-hop convergent fso-uwoc system to establish a reliable communication link between the islands. *Optics Communications*, 126107.

Levidala, B. K. and **P. Krishnan** (2020). Asymptotic bit error rate analysis of convergent underwater wireless optical communication-free-space optical system over combined channel model for different turbulence and weather conditions with pointing errors. *Optical Engineering*, **59**(11), 116102.

Levidala, B. K., **P. N. Ramavath**, and **P. Krishnan** (2021). Performance enhancement using multiple input multiple output in dual-hop convergent underwater wireless optical communication–free-space optical communication system under strong turbulence with pointing errors. *Optical Engineering*, **60**(10), 106106.

Li, C.-Y., **X.-H. Huang**, **H.-H. Lu**, **Y.-C. Huang**, **Q.-P. Huang**, and **S.-C. Tu** (2020*a*). A wdm pam4 fso–uwoc integrated system with a channel capacity of 100 gb/s. *Journal of Lightwave Technology*, **38**(7), 1766–1776.

Li, C.-Y., **H.-H. Lu**, **Y.-C. Wang**, **Z.-H. Wang**, **C.-W. Su**, **Y.-F. Lu**, and **W.-S. Tsai** (2019). An 82-m 9 gb/s PAM4 FSO-POf-UWOC convergent system. *IEEE Photonics Journal*, **11**(1), 1–9.

Li, S., **L. Yang**, **D. B. da Costa**, **M. Di Renzo**, and **M.-S. Alouini** (2021). On the performance of ris-assisted dual-hop mixed rf-uwoc systems. *IEEE Transactions on Cognitive Communications and Networking*.

Li, S., **L. Yang**, **D. B. da Costa**, **J. Zhang**, and **M.-S. Alouini** (2020*b*). Performance analysis of mixed RF-UWOC dual-hop transmission systems. *IEEE Transactions on Vehicular Technology*, **69**(11), 14043–14048.

Liu, W., **J. Ding**, **J. Zheng**, **X. Chen**, and **I. Chih-Lin** (2020). Relay-assisted technology in optical wireless communications: A survey. *IEEE Access*.

Liu, W., **Z. Xu**, and **L. Yang** (2015). Simo detection schemes for underwater optical wireless communication under turbulence. *Photonics Research*, **3**(3), 48–53.

Lu, M., **M. Bagheri**, **A. P. James**, and **T. Phung** (2018). Wireless charging techniques for UAVs: A review, reconceptualization, and extension. *IEEE Access*, **6**, 29865–29884.

Mahdy, A. and **J. S. Deogun**, Wireless optical communications: a survey. *In 2004 IEEE wireless communications and networking conference (IEEE Cat. No. 04TH8733)*, volume 4. IEEE, 2004.

Miridakis, N. I., **M. Matthaiou**, and **G. K. Karagiannidis** (2014). Multiuser relaying over mixed rf/fso links. *IEEE Transactions on Communications*, **62**(5), 1634–1645.

Naik, R. P., **U. S. Acharya**, and **P. Krishnan** (2020). Co-operative RF-UWOC link performance over hyperbolic tangent log-normal distribution channel with pointing errors. *Optics Communications*, 125774.

Naik, R. P., **G. G. Simha**, and **P. Krishnan** (2021). Wireless-optical-communication-based cooperative iot and iout system for ocean monitoring applications. *Applied Optics*, **60**(29), 9067–9073.

Nezamalhosseini, S. A. and **L. R. Chen** (2020). Optimal power allocation for MIMO underwater wireless optical communication systems using channel state information at the transmitter. *IEEE Journal of Oceanic Engineering*, **46**(1), 319–325.

Niu, M., **J. Cheng**, and **J. F. Holzman** (2013). MIMO architecture for coherent optical wireless communication: System design and performance. *Journal of Optical Communications and Networking*, **5**(5), 411–420.

Online (-). Sonardyne website. *https://www.sonardyne.com/application/ocean-science/*, **-**.

Online (2020). Map. *Online*. URL https://www.experienceandamans.com/andaman_map.php.

Online (2021*a*). Online. *Online*. URL https://oceanservice.noaa.gov/facts/exploration.html.

Online (2021*b*). Wind speed recorded - online. *Online*. URL https://www.meteoblue.com/en/weather/forecast/week/surathkal_india_11184404.

Oubei, H. M., **C. Shen**, **A. Kammoun**, **E. Zedini**, **K.-H. Park**, **X. Sun**, **G. Liu**, **C. H. Kang**, **T. K. Ng**, **M.-S. Alouini**, *et al.* (2018). Light based underwater wireless communications. *Japanese Journal of applied physics*, **57**(8S2), 08PA06.

Pham, H. T., **N. T. Dang**, and **A. T. Pham** (2014). Effects of atmospheric turbulence and misalignment fading on performance of serial-relaying m-ary pulse-position modulation free-space optical systems with partially coherent gaussian beam. *IET communications*, **8**(10), 1762–1768.

Pham, T. V., **T. C. Thang**, and **A. T. Pham** (2018). Average achievable rate of spatial diversity MIMO-FSO over correlated gamma–gamma fading channels. *Journal of Optical Communications and Networking*, **10**(8), 662–674.

Popoola, W. O., *Subcarrier intensity modulated free-space optical communication systems*. University of Northumbria at Newcastle (United Kingdom), 2009.

Popoola, W. O. and **Z. Ghassemlooy** (2009). Bpsk subcarrier intensity modulated free-space optical communications in atmospheric turbulence. *Journal of Lightwave technology*, **27**(8), 967–973.

Prabu, K. (2014). Performance analysis of free space optical systems over strong atmospheric channel with pointing errors. *Ph.D. Thesis*.

Prabu, K. (2019). Analysis of FSO systems with SISO and MIMO techniques. *Wireless Personal Communications*, **105**(3), 1133–1141.

Prabu, K., **S. Bose**, and **D. S. Kumar** (2013). Bpsk based subcarrier intensity modulated free space optical system in combined strong atmospheric turbulence. *Optics Communications*, **305**, 185–189.

Prabu, K. and **D. S. Kumar** (2014). BER analysis of DPSK–SIM over MIMO free space optical links with misalignment. *Optik*, **125**(18), 5176–5180.

Prabu, K. and **D. S. Kumar** (2015). MIMO free-space optical communication employing coherent BPOLSK modulation in atmospheric optical turbulence channel with pointing errors. *Optics Communications*, **343**, 188–194.

Prabu, K. and **D. S. Kumar** (2016). Polarization shift keying based relay-assisted free space optical communication over strong turbulence with misalignment. *Optics & Laser Technology*, **76**, 58–63.

Prabu, K., **D. S. Kumar**, and **R. Malekian** (2014*a*). BER analysis of BPSK-SIM-based SISO and MIMO FSO systems in strong turbulence with pointing errors. *Optik*, **125**(21), 6413–6417.

Prabu, K., **D. S. Kumar**, and **T. Srinivas** (2014*b*). Performance analysis of fso links under strong atmospheric turbulence conditions using various modulation schemes. *Optik*, **125**(19), 5573–5581.

Raj, A. B. and **A. K. Majumder** (2019). Historical perspective of free space optical communications: from the early dates to today's developments. *IET Communications*, **13**(16), 2405–2419.

Ramavath, P. N., **S. A. Udupi**, and **P. Krishnan** (2020). High-speed and reliable underwater wireless optical communication system using multiple-input multiple-output and channel coding techniques for IoUT applications. *Optics Communications*, **461**, 125229.

Research, O.-W. (2021). Wolfram website. *https://functions.wolfram.com/HypergeometricFunctions/MeijerG/21/02/07/0002/*, -.

Saeed, N., **A. Celik**, **M.-S. Alouini**, and **T. Y. Al-Naffouri** (2018). Performance analysis of connectivity and localization in multi-hop underwater optical wireless sensor networks. *IEEE Transactions on Mobile Computing*, **18**(11), 2604–2615.

Sandalidis, H. G., **T. A. Tsiftsis**, and **G. K. Karagiannidis** (2009). Optical wireless communications with heterodyne detection over turbulence channels with pointing errors. *Journal of lightwave technology*, **27**(20), 4440–4445.

Sarma, P., **R. Deka**, and **S. Anees**, Performance analysis of df based mixed triple hop rf-fso-uwoc cooperative system. *In 2020 IEEE 92nd Vehicular Technology Conference (VTC2020-Fall)*. IEEE, 2020.

Sharifzadeh, M. and **M. Ahmadirad** (2018). Performance analysis of underwater wireless optical communication systems over a wide range of optical turbulence. *Optics Communications*, **427**, 609–616.

Singh, M. and **J. Malhotra** (2019). Performance comparison of high-speed long-reach mode division multiplexing-based radio over free space optics transmission system using different modulation formats under the effect of atmospheric turbulence. *Optical Engineering*, **58**(4), 046112.

Singh, M., **M. L. Singh**, **G. Singh**, **H. Kaur**, **S. Kaur**, *et al.* (2020). Modeling and performance evaluation of underwater wireless optical communication system in the presence of different sized air bubbles. *Optical and Quantum Electronics*, **52**(12), 1–15.

Smyth, P. P., **D. Wood**, **S. Ritchie**, and **S. Cassidy**, Optical wireless: New enabling transmitter technologies. *In Proceedings of ICC'93-IEEE International Conference on Communications*, volume 1. IEEE, 1993.

Son, I. K. and **S. Mao** (2017). A survey of free space optical networks. *Digital communications and networks*, **3**(2), 67–77.

Song, Y., **W. Lu**, **B. Sun**, **Y. Hong**, **F. Qu**, **J. Han**, **W. Zhang**, and **J. Xu** (2017). Experimental demonstration of MIMO-OFDM underwater wireless optical communication. *Optics Communications*, **403**, 205–210.

Soni, G. (2018). Performance analysis of free space optical link under various attenuation effects. *Science Journal of Circuits, Systems and Signal Processing*, **7**(2), 43–47.

Tabeshnezhad, A. and **M. A. Pourmina** (2017). Outage analysis of relay-assisted underwater wireless optical communication systems. *Optics Communications*, **405**, 297–305.

Tang, S., **Y. Dong**, and **X. Zhang** (2013). Impulse response modeling for underwater wireless optical communication links. *IEEE transactions on communications*, **62**(1), 226–234.

Tang, X., **Z. Wang**, **Z. Xu**, and **Z. Ghassemlooy** (2014). Multihop free-space optical communications over turbulence channels with pointing errors using heterodyne detection. *Journal of Lightwave Technology*, **32**(15), 2597–2604.

Tokgoz, S. C., **S. Althunibat**, **S. L. Miller**, and **K. A. Qaraqe** (). Performance analysis of index modulation based link-selection mechanism for hybrid fso-mmwave systems. *Optics Communications*, **479**, 126305.

Tsai, W.-S., **C.-Y. Li**, **H.-H. Lu**, **Y.-F. Lu**, **S.-C. Tu**, and **Y.-C. Huang** (2019). 256 gb/s four-channel SDM-based PAM4 FSO-UWOC convergent system. *IEEE Photonics Journal*, **11**(2), 1–8.

Tsai, W.-S., **H.-H. Lu**, **H.-W. Wu**, **S.-C. Tu**, **Y.-C. Huang**, **J.-Y. Xie**, **Q.-P. Huang**, and **S.-E. Tsai** (2020). 500 gb/s pam4 fso-uwoc convergent system with a r/g/b five-wavelength polarization-multiplexing scheme. *IEEE Access*, **8**, 16913–16921.

Uppalapati, A., **R. P. Naik**, and **P. Krishnan** (2020). Analysis of m-qam modulated underwater wireless optical communication system for reconfigurable uowsns employed in river meets ocean scenario. *IEEE Transactions on Vehicular Technology*, **69**(12), 15244–15252.

Uysal, M., **C. Capsoni**, **Z. Ghassemlooy**, **A. Boucouvalas**, and **E. Udvary**, Optical wireless communications—an emerging technology. *In Optical wireless communications—An emerging technology (COST-IC1101)*. IEEE, 2014.

Uysal, M., **J. Li**, and **M. Yu** (2006). Error rate performance analysis of coded free-space optical links over gamma-gamma atmospheric turbulence channels. *IEEE Transactions on wireless communications*, **5**(6), 1229–1233.

Vali, Z., **A. Gholami**, **D. G. Michelson**, **Z. Ghassemlooy**, **M. Omoomi**, and **H. Noori** (2017). Use of gaussian beam divergence to compensate for misalignment of underwater wireless optical communication links. *IET Optoelectronics*, **11**(5), 171–175.

Varshney, N. and **A. K. Jagannatham** (2017). Cognitive decode-and-forward MIMO-RF/FSO cooperative relay networks. *IEEE Communications Letters*, **21**(4), 893–896.

Varshney, N., **A. K. Jagannatham**, and **P. K. Varshney** (2018). Cognitive MIMO-RF/FSO cooperative relay communication with mobile nodes and imperfect channel state information. *IEEE Transactions on Cognitive Communications and Networking*, **4**(3), 544–555.

Varshney, N. and **P. Puri** (2017). Performance analysis of decode-and-forward-based mixed MIMO-RF/FSO cooperative systems with source mobility and imperfect csi. *Journal of Lightwave Technology*, **35**(11), 2070–2077.

Vellakudiyan, J., **I. S. Ansari**, **V. Palliyembil**, **P. Muthuchidambaranathan**, and **K. A. Qaraqe** (2016). Channel capacity analysis of a mixed dual-hop radio-frequency–free space optical transmission system with málaga distribution. *IET Communications*, **10**(16), 2119–2124.

Vellakudiyan, J., **V. Palliyembil**, **I. S. Ansari**, **P. Muthuchidambaranathan**, and **K. A. Qaraqe** (2019). Performance analysis of the decode-and-forward relay-based rf-fso communication system in the presence of pointing errors. *IET Signal Processing*, **13**(4), 480–485.

Wang, N. and **J. Cheng** (2010). Moment-based estimation for the shape parameters of the gamma-gamma atmospheric turbulence model. *Optics express*, **18**(12), 12824–12831.

Xu, J., **X. Yu**, **M. Kong**, **B. Sun**, **J. Han**, and **N. Deng**, Towards broadband long-reach underwater wireless optical communication. *In Asia Communications and Photonics Conference*. Optical Society of America, 2016.

Yang, L., **Q. Zhu**, **S. Li**, **I. S. Ansari**, and **S. Yu** (2021). On the performance of mixed fso-uwoc dual-hop transmission systems. *IEEE Wireless Communications Letters*, **10**(9), 2041–2045.

Yue, P., **P. Zhao**, **X. Yi**, **Y. Wang**, **C. Shen**, and **Q. Ao** (2020). Performance analysis for multi-hop uowc system over mixture exponential–gamma with two im-dd fading channels. *Optics Communications*, **459**, 125012.

Zedini, E. and **M.-S. Alouini** (2015). On the performance of multihop heterodyne fso systems with pointing errors. *IEEE Photonics Journal*, **7**(2), 1–10.

Zedini, E., **A. Kammoun**, **H. Soury**, **M. Hamdi**, and **M.-S. Alouini** (2020). Performance analysis of dual-hop underwater wireless optical communication systems over mixture exponential-generalized gamma turbulence channels. *IEEE Transactions on Communications*, **68**(9), 5718–5731.

Zeng, Z., **S. Fu**, **H. Zhang**, **Y. Dong**, and **J. Cheng** (2016). A survey of underwater optical wireless communications. *IEEE communications surveys & tutorials*, **19**(1), 204–238.

Zhou, Z., **B. Yao**, **R. Xing**, **L. Shu**, and **S. Bu** (2015). E-carp: An energy efficient routing protocol for uwsns in the internet of underwater things. *IEEE Sensors Journal*, **16**(11), 4072–4082.

Publications Based on the Thesis

Journals:

1. **L Bhargava Kumar**, and Prabu Krishnan. "Asymptotic bit error rate analysis of convergent underwater wireless optical communication-free-space optical system over combined channel model for different turbulence and weather conditions with pointing errors." Optical Engineering 59, no. 11 (2020): 116102. https://doi.org/10.1117/1.OE.59.11.116102

2. **L Bhargava Kumar**, Prasad N. Ramavath, and Prabu Krishnan. "Performance enhancement using multiple input multiple output in dual-hop convergent underwater wireless optical communication–free-space optical communication system under strong turbulence with pointing errors." Optical Engineering 60, no. 10 (2021): 106106. https://doi.org/10.1117/1.OE.60.10.106106

3. **L Bhargava Kumar**, and Prabu Krishnan. "Multi-hop convergent FSO-UWOC system to establish a reliable communication link between the islands." Optics Communications 474 (2020): 126107. https://doi.org/10.1016/j.optcom.2020.126107

4. **L Bhargava Kumar**, Prasad Naik Ramavath, and Prabu Krishnan. "Performance analysis of multi-hop FSO convergent with UWOC system for security and tracking in navy applications." Optical and Quantum Electronics 54, no. 6 (2022): 1-26. https://doi.org/10.1007/s11082-022-03712-w

5. **L Bhargava Kumar**, Prasad Naik Ramavath, and Prabu Krishnan. " High-speed long-range multihop underwater wireless optical communication convergent with free-space optical system for optical internet of underwater things and underwater optical wireless sensor network applications." Optical Engineering 61, no. 7 (2022): 076107. https://doi.org/10.1117/1.OE.61.7.076107.

CURRICULUM VITAE

L Bhargava Kumar

C/O Dr. Prabu K, Assistant Professor, NITK,

D.No. 19-164/5(3), 1st Cross, Subhasitha Nagar, Kambla,

Surathkal, Mangalore - 575014.

☎ : +91 8500008785

✉ : l.bhargavkumar@gmail.com

EDUCATIONAL QUALIFICATIONS

Doctor of Philosophy (Ph.D.)

National Institute of Technology Karnataka, Surathkal   2018–Till date

Master of Technology (M.Tech)

Annamacharya Institute of Technology and Sciences, Rajampet.   2007–2010

Branch : VLSI System Design

Bachelor of Technology (B.Tech)

Narayana Engineering College, Gudur.   2004–2007

Branch : Electronics and Communication Engineering

Diploma

Government Polytechnic, Anantapur.   2001–2004

Branch : Electronics and Communication Engineering

Research Interests:

Free Space Optical (FSO), Underwater wireless optical communication (UWOC), Visible light communication (VLC), Unmanned aerial vehicle (UAV).

Publications:

Number of International Journal publications: 9

Number of International Conference publications: 2

Number of National Conference publications: 1